An Acoustic Study of Airways: Healthy and Pathological Models

BY

LORENZO ALIBONI
Laurea, Politecnico di Milano, Milan, Italy, 2015

THESIS

Submitted as partial fulfillment of the requirements
for the degree of Master of Science in Bioengineering in
the Graduate College of the
University of Illinois at Chicago, 2017

Chicago, Illinois

Defense Committee:

        Thomas J. Royston, Chair and Advisor
        Dieter Klatt
        Andrea Aliverti, Politecnico di Milano

To my parents Simonetta and Maurizio,
I will never be able to express enough gratitude for everything you did for me.
Thanks for this opportunity, for your support and your advice.
Thanks for always being there for me.
Without you I will not be who I am. I am proud of being your son.

Love You

ACKNOWLEDGMENTS

I express sincere appreciation and thankfulness to my advisor Professor Thomas Royston for his supervision and patience throughout this research. Also, I would like to thank Brian Henry for his support and guidance. To him must be acknowledged all the merits for the analytical codes I used as well as the patience and kindness while helping me in my everyday work with his experience, precious advice and friendship.

I am grateful to the other members of the dissertation committee, Professor Dieter Klatt and Professor Andrea Aliverti for their valuable comments and suggestions.

I would like to thank my friends Andrea and Cecilia who made Chicago feel like home.

Last, but not least, I would like to thank my family, my mother Simonetta, my father Maurizio and my sister Camilla for their love, support and encouragement.

<div align="right">LA</div>

TABLE OF CONTENTS

TABLE OF CONTENTS (continued)

LIST OF TABLES

LIST OF FIGURES

LIST OF FIGURES (continued)

LIST OF ABBREVIATIONS

AHP   Audible Human Project

ATS   American Thoracic Society

CDC   Center for Disease Control and Prevention

COPD   Chronic Obstructive Pulmonary Disease

CT   Computed Tomography

ECM   Extra Cellular Matrix

IDW   Initial Deflection Width

GUI   Graphic User Interface

i.e.   id est

LLL   Lower Left Lobe

MRE   Magnetic Resonance Elastography

PI   Pulmonary Infiltration

SI   International System of Units

SLDV   Scanning Laser Doppler Vibrometry

TCL   Tool Command Language

2CD   Two Cycle Duration

SUMMARY

Auscultation has been used qualitatively by clinicians for hundreds of years to diagnose and monitor the progression of pulmonary pathologies. Auscultation technique is based on the clinical evidence that the morphological and functional alterations of the respiratory system determined by diseases and injuries result in measurable changes in lung sounds generation and propagation. Centuries of clinical practice have led to an extensive cataloging of respiratory sounds and their alterations resulting from pathological conditions. However, the information collected over these years suffer from a lack of quantitative rigor as well as in a proper understanding and description of the phenomena involved. The effect of the pathology-induced structural and mechanical modifications on the sound transmission in the respiratory system has received arguably even less attention. A better understanding of sound propagation and of its alterations by pathological conditions or injuries might not only be valuable in terms of clinical interpretation and significance, but also pave the way for emerging imaging techniques such as magnetic resonance elastography.

The long-term objective of this project is the creation of a computational model able to precisely mimic the creation, propagation and noninvasive measurement of naturally-occurring sounds associated airway physiology as well as the alterations induced by airways pathology. In this thesis, fitting within the general scope mentioned above, an analytical code was validated that can provide accurate and quantitative information about the sound propagation in the lower respiratory tract. The same model was modified to account for the morphometrical and mechanical alterations induced by specific pathologies allowing a comparison with the physiological condition.

CHAPTER 1

INTRODUCTION

1.1   <u>Background & Motivation</u>

The basic principle of auscultation is the knowledge that pulmonary pathologies generally lead to morphological and functional alterations in the lungs and airways which eventually result in measurable changes in breath sound generation and propagation. Auscultation performed with stethoscopes has been used for hundreds of years and still today represents the most common and immediate way for diagnosis purposes based on the changes of breath sounds. However, this technique presents some limitations related to the fact that it is highly skill dependent and subjected to inter and intra observer variability. Furthermore, it can only provide qualitative information and only at a single location. Over the last few decades an increasing interest in a quantitative characterization of the sound generation and propagation in the respiratory system has led to a constant effort towards the generation of proper mechano-acoustical models. The first challenge to be faced was the natural geometrical complexity of the dichotomic branching system that characterizes the human tracheobronchial tree. Both Strahler et al. and Horsefield et al. [1] proposed a model able to properly quantify the complexity and asymmetry of the branching pattern of the bronchial tree, with the latter being able to represent a higher order branching system. Wodicka et al. [2] elaborated a model of sound propagation from inside the respiratory tract to the thorax surface caused by wall motion in large airways. To model the wall structure and dynamics, the analogy with an electrical distributed parameters model (transmission line) was used and the system was simplified to account for the first five generations of the bronchial tree. Jackson et al.

[3], [4] studied the frequency dependency of the acoustic impedance of the subglottal respiratory tract, Habib et al. [5] managed to identify the constituent relations to relate the alterations of the acoustic impedance to the airway geometry and the airway wall mechanical properties. In Royston et al. [6] sound propagation from trachea to thorax surface in healthy and pneumothorax conditions was simulated. Dai et al. [7], [8] studied both numerically and experimentally the sound transmission in the lungs.

In this work an analytical model of the sound propagation based on the considerations of Royston et al. [6] will be to applied to the an airway tree generated by anatomical images collected at different phases of the respiratory cycle. The model assumes to input a known pressure at the inlet of the trachea: what is evaluated is the response of the system to the inlet pressure in term of propagation of the acoustic waves over different frequencies. The beginning of both the inspiratory and expiratory phases will be analyzed. In the first instance, the analytical model, developed in MATLAB (r2016a, The MathWorks Inc., Natick, MA, 2016) by Brian Henry [9] in the context of the "Audible Human Project" (AHP), will be validated via numerical simulations in COMSOL Multiphysics® (COMSOL Multiphysics® v. 5.2a, www.comsol.com, Stockholm, Sweden) in the physiological conditions for both the phases mentioned above. This procedure will also allow a comparison, in terms of acoustic pressure propagation, between the two different phases taken into consideration. Successively, the morphometry of the trees and the mechanical properties of the airways will be modified to simulate some pathology-induced alterations of the architecture of the airways and the sound propagation will be analyzed under those circumstances. The effect of the pathology of asthma and the conditions of a generalized fibrosis and pulmonary infiltrate will be presented.

The long-term objective of this project is the creation of a computational model able to precisely mimic the creation, propagation and noninvasive measurement of naturally-occurring sounds associated airway physiology as well as the alterations induced by airways pathology. Such a comprehensive computational model would have a significant impact on medical education and research. From a research-oriented point of view, the enhanced understanding of waves propagation within the airways will allow to couple this computational approach to new emerging imaging techniques and, specifically, to magnetic resonance elastography (MRE).

1.2 <u>Anatomy of the Human Respiratory System</u>

The respiratory system supplies the body with the oxygen necessary for its physiological activity and expels the byproducts of this activity in form of carbon dioxide. In the term respiration four distinct and fundamental processes are involved [10]:

- Pulmonary ventilation, consisting in the addition to or removal from lungs of the volume of gas;

- External respiration, a process taking place in lungs by which blood is recharged with oxygen and discharged with carbon dioxide;

- Transport in which oxygen is moved from lungs to tissues and carbon dioxide from tissue to lungs;

- Internal respiration which consists in the gas exchange between systemic blood vessels and tissues at a peripheral level.

From an anatomical point of view, the respiratory system is generally categorized into two main parts: the upper and the lower tract. The upper respiratory system (identified also as supra-glottal region) includes the nose with its nasal cavity, the paranasal sinuses, the pharynx and the larynx.

This portion of the ventilatory tract has the main aim of filtering out foreign materials from the inhaled air, warming it to body temperature and finally humidifying it [11]. These steps are fundamental for the proper functioning of the whole system and to prevent any damage to the lower respiratory tract. The lower respiratory tract (also known as thoracic portion) includes the trachea, the lungs, the bronchi and the alveoli. Because of its importance in sound propagation the lower respiratory tract will be the object of further detailed descriptions (see Section 1.2.1) In addition to those components, the muscles and bones of the thorax (or chest cavity) will be briefly described in Section 1.2.3.

1.2.1   The Lower Respiratory Tract

As mentioned above, the lower respiratory tract is made up of trachea, the lungs, the bronchi and the alveoli. The trachea is a conduit with length approximately ranging between 12–14 cm, descending from the larynx through neck into mediastinum which is space in the thoracic chest surrounded by the lungs (sides), the spine column (rear) and the sternum (front). The trachea wall is supported and reinforced by sixteen to twenty U-shaped rings of hyaline cartilage joined by fibro-elastic connective tissue as well as by bands of smooth muscles. The anterolateral wall with the cartilaginous rings and the posterior fibromuscular membrane compose the two main regions of the tracheal wall. Despite its structure, the tracheal conduit remains flexible allowing the tracheal size and shape to vary in accordance with neck and head motions. The walls are lined internally by mucosa [12]. The dimensions and configuration of the trachea are also modified by the respiration, especially when ample thoracic displacements occur. The tracheal anatomy is also subjected to a great inter-subject variability. In adult males, the tracheal external diameter is around

1.3-2.5 cm and 1.3-2.7 cm in the in the coronal and sagittal plane respectively [13] [14] whereas in adult females the same diameters are approximately 1.0-2.1 cm and 1.0-2.3 cm [12][14][15] .

In correspondence to the fourth thoracic vertebra, the trachea branches into a pair of primary bronchi, one bronchus to each lung. The main stem bronchi are asymmetrical structures: in particular, the left bronchus has a diameter of 10–14 mm and a length of approximately 50 mm whereas the right bronchus is generally larger, but shorter (diameter ranging between 12–16 mm, and length approximately equal to 25 mm) [11]. In general, the branching angle of the left bronchus is sharper (25°- 30° circa with respect to the midline) than the right one (approximately 45° from the midline) [13]. The generation of branches of different diameter and unequal length is defined as irregular dichotomy. Because of this asymmetry, at the level of the division region it is possible to recognize a transition zone. Each stem bronchus enters the respective lung. After entering the respective lung, the main bronchus generates the lobar bronchi (superior, middle and inferior). From the lobar bronchi arise the tertiary bronchi (called also segmental bronchi) which are followed by the sub-segmental bronchi and by the terminal bronchi [16]. As far as the structure is concerned, the bronchus wall is made up of five layers: a mucosa, a muscular, a submucosa, a fibrocartilaginous layer and a peri-bronchial stratum. This wall structure is a function of the size of the bronchi. For large bronchi the structure of the wall resembles the one of the tracheal wall with the peculiarity that the cartilaginous rings are completely surround the wall [17]. On the contrary, for bronchi of medium size the walls have more irregular (sometimes helical) cartilaginous rings and, situated between the muscle and the fibrocartilaginous layer, a venous plexus can be recognized.

The Bronchioles arise from the terminal bronchi. There are three to four generations of bronchioles which eventually lead to the terminal bronchioles [11]. Each terminal bronchiole

divides to form either another terminal bronchiole or a respiratory bronchiole which are the narrowest and smallest airway aimed at the transport of air to and from the alveolar ducts. Because of the presence of some alveolar structures, gas exchange (in minimal part) already takes place in the respiratory bronchioles. The number of alveoli lining the bronchioles walls tends to increase moving closer to the alveolar ducts [10]. These ducts are completely covered by alveoli as their wall can be seen to be constituted of exclusively by entry tips of alveoli. At least five or more ramifications of alveolar ducts have been described. Those ducts terminate into the alveolar sac which is the closed end and final (distal) airway. As regard the structure, the bronchiolar wall can be subdivided in three layers: one layer of mucosa, one of muscle fibers (the thickest) and a thin outer layer made of connective tissue which is connected to the lung parenchyma and tends to disappears in small bronchioles. This entire structure is lined by an epithelium that stops at the entrance of the alveoli [11]. The alveoli are the basic structures of the lung deputed to gas exchange. The dimensions and shape of the alveoli are subject to a certain variability but they can be approximated as spherical objects sized between 150–300 μm. The alveolar space is separated from the pulmonary capillary by an extremely thin (thickness 0.2 μm) barrier. Gas exchange between oxygen (O_2) and carbon dioxide (CO_2) occurs by simple diffusion, in a process which lasts approximately 0.25 s and is extremely efficient thanks to huge number of alveoli (estimated around 300 millions) which creates an exchange surface approximately equal to 80 m^2 [11]. To conclude, the airways divide by asymmetric dichotomous branching which implies that, although the division of a segment into two daughter branches is common, it still exists a certain variability in both the size and the number of the branches [16]. As a general statement, it can be inferred that the higher the generation number, the narrower and the shorter are the respiratory conduits. It is also verified that the number of conduits increases accordingly to the generation level. TABLE 1

reports some noteworthy features of the human lower respiratory tract. Approximately 23 generations of branches are identifiable starting from the trachea down to the alveoli. These generations are generally categorized in three zones [12]:

1. Conductive Zone: beginning with the trachea corresponding to generations 1-16;

2. Transitory Zone identifiable with the respiratory bronchioles (generations 17-19);

3. Respiratory Zone: composed by alveolar ducts and sacs (generations 20-23).

TABLE 1: GEOMETRICAL FEATURES OF HUMAN LOWER RESPIRATORY TRACT

	Human
Anatomy	Right Lung: 3 lobes Left Lung: 2 lobes
Diameter of the trachea [mm]	13-27
Diameter of the main bronchus [mm]	10-16
Diameter of the bronchiole [mm]	< 1
Diameter of the terminal bronchiole [mm]	0.6
Diameter of the respiratory bronchiole [mm]	0.5
Diameter of the alveoli [mm]	0.2-0.4

1.2.2   Gross Anatomy of Lungs

The lungs are cone-like organs primarily deputed to respiration. Humans are characterized by the presence of two lungs: right lung and left lung. The structure of each lung is characterized by the presence of a spherical apex which extends into the root of the neck, a convex upward base in the

lower part, 3 borders (inferior, anterior and posterior), and 2 faces (the coastal one, pointing outward and the mediastinal one which is internal and with pericardial depression). The diaphragm lies under the base of each lung.

The right lung has three sub-sections, named lobes (lower, middle, upper). The left lung has only two (lower and upper). The separation among between lobes is determined anatomically by fissures. Pulmonary lobes are sectioned into segments, segments into lobules. The right upper lobe has three segments (posterior, anterior, apical); the right middle two (lateral, medial), the right inferior five (superior, anterior basal, lateral basal, posterior basal, medial basal). Two compartments can be identified in the left upper lobe: superior and inferior (or lingular) which consists of three segments (posterior, anterior and apical) and two segments (inferior and superior), respectively. The left lower lobe includes five segments (superior or apical, lateral and medial basal and anterior and posterior basal). TABLE 2 adapted from [11] summarizes the structure of the human lungs. Although the left lung, contrarily to the right one, is not anatomically characterized by a middle lobe, it does show a corresponding feature. Indeed, it can be observed a protuberance of the upper lobe which goes under the name of lingula. This projection on the left lobe can be considered as an anatomical counterpart to the right middle lobe. Both lungs at their root show a central recession called hilum, where both the airways and blood vessels enter and exit the lung [11]. The septa and sheaths among the pulmonary compartments (lobes, segments, lobules, and acini) and among the alveoli are interconnected thanks to the lung parenchyma. The lung parenchyma is the essential tissue of the lungs, and is generally described as a three dimensional deformable tissue network [11]. The pulmonary parenchyma is enclosed by the visceral pleura to which is also attached. Two pleurae are present in the lungs: the visceral pleura which covers the surface of each lung and dips into the cavity between the lobes and the parietal

pleura, which is the outer membrane attached to the thoracic cavity. The parietal pleura also separates the pleural cavity from the mediastinum that is the cavity located between the vertebral column, the sternum and the lungs, containing the heart and its and the related circulatory vessels, the esophagus, the thymus, the esophagus, the first two generations of the airway tree (namely trachea and main bronchi) and the vessels related to the lymphatic circulation. The two pleurae are separated from each other thanks to a thin (20–80 μm) fluid space which allows the two layers to slide without restrains one with respect to the other [11]. The pleural fluid is generated from parietal pleura itself and reabsorbed by the lymphatic system, this process results in a total volume of fluid ranging between 25-30 cm^3 [10], [11]. Several functions are associated to the pleural fluid. First, it creates a moist, slippery surface which allows the opposing membranes of the pleurae to slide across one another as the lungs move within the thorax. Second, it holds the lungs tight against the thoracic wall therefore avoiding the collapse of the whole structure [10].

1.2.3 **Respiratory Muscles and Bones**

The thorax is bounded by the bones of the spine and rib cage and their associated muscles. The joint structure of muscles and bones goes under the name of thoracic cage. The side and the top the thoracic cage are formed by the chest wall (i.e. the ribs and the spine), on the back side the thoracic vertebrae from T2 to T12 and the vertebral column are located. The musculature of the thorax includes the intercostal muscles and the diaphragm. During inspiration, the contraction of both the muscles is observed. This causes the diaphragm to move down and the ribs cage to rise. In this way, when the air is sucked into the lungs, thoracic cavity is enlarged. The increasing volume of the thoracic cavity causes a drop in the pressure around the lungs and their consequent expansion. During expiration, the relaxation of the muscles causes the reverse process. For this

reason, the quiet expiration is assumed to be passive, the inspiration is active (in other words the contraction of the muscles is involved) [18].

TABLE 2: LUNGS LOBES AND SEGMENTS

Lung	Lobe	Segments
Right	Upper	Apical
		Anterior
		Posterior
	Middle	Medial
		Lateral
	Lower	Superior Basal
		Medial Basal
		Anterior Basal
		Lateral Basal
		Posterior Basal
Left	Upper	Apical
		Anterior
		Posterior
	Lower	Superior Basal
		Medial Basal
		Anterior Basal
		Lateral Basal
		Posterior Basal

1.3   <u>Pathologies of the Airways Tree</u>

The pathologies considered in this dissertation are asthma, generalized fibrosis and pulmonary infiltrate. In the following paragraphs a brief description of the modification induced at the level of the respiratory system by those pathologies is provided. In relation to the further developments in this work, the attention is focused on the pathology-induced alterations in terms of mechanical and geometrical properties at a macroscopic level. The cellular modifications at the microscopic level, as well as the pathogenesis of the disease in terms of cellular response will be not be described.

1.3.1   <u>Asthma</u>

The clinical significance of asthma has remarkably increased over the last decades [19]. The latest estimates by the Center for Disease Control and Prevention (CDC) indicate that roughly 1 American over 13 is affected by this pathology, resulting in a total number of approximately 24.5 million of subjects. This impressive number corresponds to 7.4 and 8.6 percent of adults and children population of the United States of America, respectively. For this reason, asthma is nowadays considered one of most diffused and costly disease in the US.

Despite its relevance, the pathogenesis of asthma still is not fully understood [19]. In a very generic and simplified description, asthma can be referred as an inflammatory pathology affecting the small airways (i.e. airways with a diameter smaller than 2 mm). Indeed, *ex vivo* examination of airways of patient who died of asthma has shown an airway lumen severely occluded by mucus plugs made up of glycoproteins generated from epithelial cells and plasma proteins exuded from airway vasculature. The mechanism of generation of the inflammatory process will not be

discussed in this dissertation. The three most common and characteristic features of asthma are the following [19]:

1. airways inflammation;

2. mucous hypersecretion;

3. airways hyper-responsiveness.

The result of the combination of these factors is bronchoconstriction and airflow obstruction. An average value of reduction of the airway diameter in asthma can be approximated around the 50/60 % [20], although the duration and severity of the pathology can deeply affect wall thickening [21]. Although the three conditions mentioned above are theoretically reversible in their initial stages, if the pathology is not stopped in its progression those changes tend to become more permanent leading to the process of airway remodeling which is a term used to refer to the alterations in composition, quantity and organization of the constituting elements of the airway wall. Consequently, even if most attention has been focused on the acute inflammatory phase of this disease, it is important to remark asthma is a chronic disease. The general features recognizable in patients with airway remodeling are an increment of tissue under the epithelium of the airway wall, a thickening of the wall itself and hypertrophy of the smooth muscle.

The clinical most significant consequence of asthma is, as already mentioned, the obstruction of the airway lumen. This constriction causes the resistance of the airway to increase and consequently, per Heigen-Poiseuille Law, a reduction of the airway flow to the lungs.
In this situation, in order to restore the flow some compensatory mechanisms take place [19]:

1. increment of the tension generated by the inspiratory muscles;

2. hyperventilation.

Although temporarily effective, over a long period the mechanisms mentioned above cause an

increased work of breathing associated to the inspiratory phase, complicated also by dynamic hyperinflation of the lungs (it is important to remember that at high volumes the respiratory muscles can generate less power determining the so-called length-tension inappropriateness).

The reduction the airway flow can also affect the oxygenation of the lungs. In general, the human body, can compensate for this effect by redirect the blood flow from the constricted areas to the healthy ones. This phenomenon goes under the name of hypoxic vasoconstriction and it can only happen because asthma is a heterogeneous disease process, which can severely affect some areas of the lungs, while leaving other areas relatively normal. Hyperventilation and hypoxic vasoconstriction generally prevent the oxygen level to become critically low, nonetheless when the bronchoconstriction is severe those two mechanisms cannot be sufficient to guarantee a correct oxygen distribution causes symptoms of dyspnea in patients. Some of the most common symptoms of asthma are here listed below:

- Shortness of Breath;

- Cough;

- Chest Tightness;

- Dyspnea;

- Mucus Production;

- Wheezing.

1.3.2 **Fibrosis**

In its general meaning, the term fibrosis refers to the growth of fibrous connective tissue as a restorative response to trauma or damage. This tissue deposition can occur as a part of the physiological healing process meant to the reestablish the normal structure and function of the

damaged tissue or, when excessive and uncontrolled, can be associated to different pathological processes. In its pathological form, fibrosis is determined by an abnormal accumulation of extracellular matrix (ECM) proteins results in scarring and stiffening of the affected tissue, which end up interfering with the normal functioning of the tissue.

Airways fibrosis is associated with a variety of pathologies among which asthma, chronic obstructive pulmonary disease and cystic fibrosis can be mentioned [22]. From what stated above it is clear that airways fibrosis needs to be analyzed considering the complexity of the clinical picture of the mentioned pathologies. However, it is also verified that by itself fibrosis of the airways causes a remarkable stiffening of the airways wall which results in the modification of the physiology of the whole respiratory system [23].

1.3.3   Pulmonary Infiltrates

The term "pulmonary infiltrate" was born in the radiological clinical practice to generically describe any sort of blockage in the air space of the lungs that is recognizable on a radiology scan. The causes the blockages can generally include any substance foreign to the lung that progressively accumulates and eventually occludes an air space. They can also be ascribed to naturally-occurring substances in the lung that accumulate in a quantity greater than the physiological condition. Pulmonary infiltrates lead to increased soft tissue density of the lung, that is easily observable on a scan and to a reduction of the respiratory capacity of the subject. Although the causes of the infiltrations can be both infectious and non-infectious, pulmonary infiltrates are most commonly associated with the condition of pneumonia [24]. Other possible causes can be acknowledged such as acute respiratory distress syndrome, atelectasis, tuberculosis and the prolongated exposure to radiotherapy as a consequence of breast or lung cancer [23], [25]. Recently also sickle cell disease

has been demonstrated to be a likely cause of this pathological condition [26]. The pulmonary infiltrates are generally localized in one lobe, even though they can also affect more lobes at the same time. The lobe(s) involved can be either be either localized on the same lung (unilateral infiltrate) or on different lungs (bilateral infiltrate). The position and the dimension of the infiltrate can vary significantly according to the severity of the pathology. In general, the alveoli and the terminal branches are the locations that are more likely to be affected. However, in case of severe pathologies the increase resistance of the last generations, can affect also medium sized airways and eventually prevent the air from sufficiently propagates in an entire lobe.

1.4   Abnormal Breath Sounds and Pathologies

In accordance to their acoustic properties, respiratory sounds are categorized into normal and abnormal (or adventitious). Normal respiratory sounds are the ones generated in healthy airways and lungs by physiological unforced breathing. Normal respiratory sounds are generally subdivided in tracheobronchial and vesicular, the former are heard at the level of the trachea, the latter over the thorax [27]. The deficiency of the normal breath sounds or the manifestation of adventitious (i.e. superimposed to normal sounds) breath sounds can be symptom of a pulmonary disease. For this reason, the ability to discriminate between normal respiratory sounds and adventitious ones is fundamental for an accurate medical diagnosis. The analysis of the respiratory sounds allows to obtain invaluable information regarding the physiopathology of lungs and airways [28]. As shown in Figure 1, thanks to clinical practice it is nowadays possible to associate the presence of a given breath sound to one or more pathologies. The integration of these information with the analysis of the overall medical case, results in an effective way to diagnose pathologies.
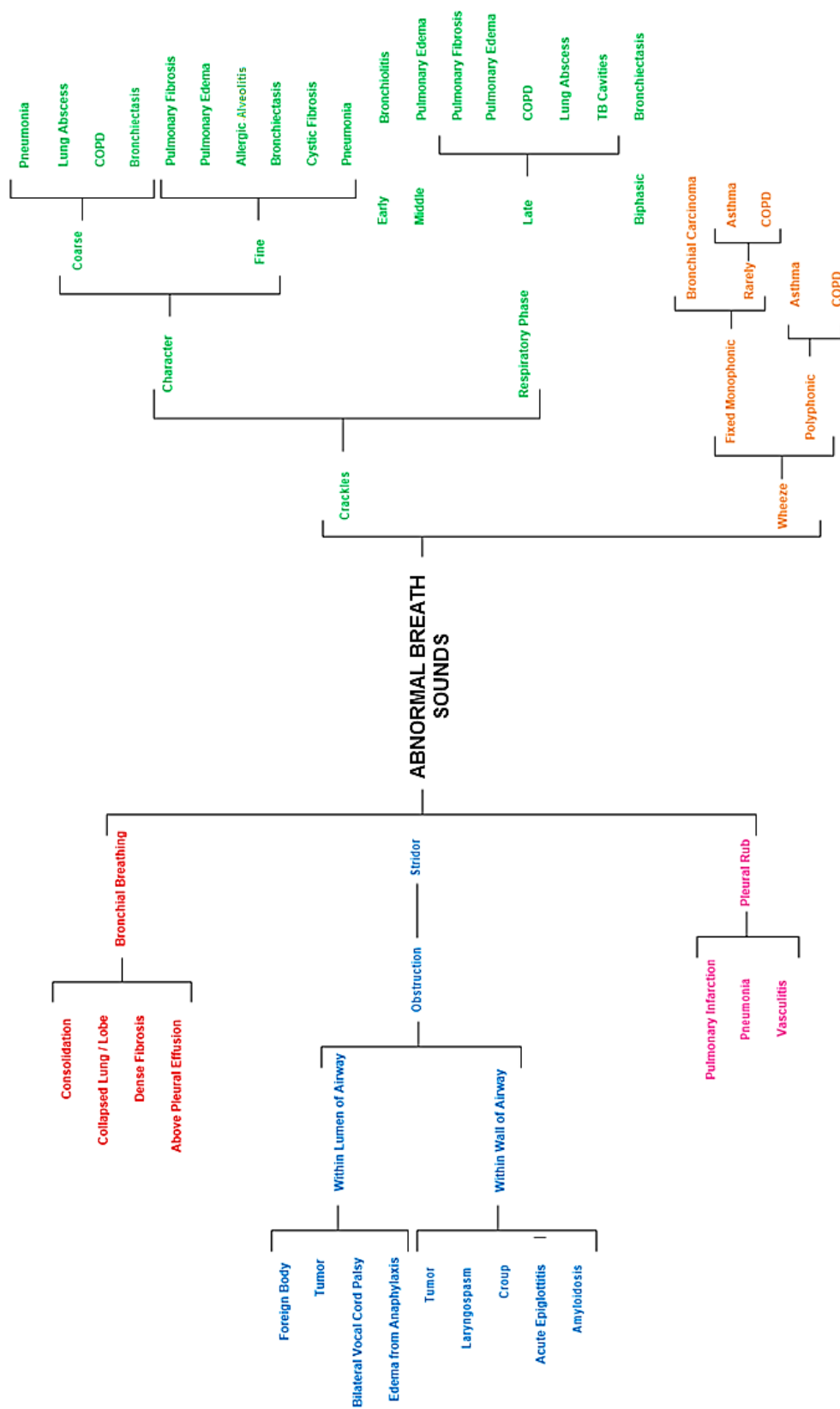
Figure 1: Schematics of the abnormal breath sounds and associated pathologies

1.4.1 **Crackles**

Crackles (also known as crepitations) correspond to short, discontinuous and non-stationary sounds [28]. They are generated when airways that were abnormally closed (due to accumulation of secretions or to airway collapse) open in the inspiration phase. The sudden opening of an obstructed airway causes an immediate re-equilibration of the pressures on both sides determining peculiar vibrations in the airway walls. They can be heard also during expiration, though this is far less common to happen [29]. Fredberg et Al. [30] suggested that the cross-section of the airways which are subjected to the sudden closing and opening is one of the possible factors affecting the character of crackling sounds . Crackles are generally distinguished in [29]:

- Fine Crackles which are characterized by a shorter duration (around 5 ms) and a higher pitch. Often they are also repetitive. Typical frequency is around 650 Hz. From the clinical point of view, they usually start in the basal part of the lung. They are altered by body position change, but not by coughing and they are not transmitted to mouth.

- Coarse Crackles which are characterized by a longer duration (15 ms) and a lower pitch. Typical frequency is around 350 Hz. From the clinical point of view there is no a specific location where the sound starts, however it can be altered by coughing (but not body position changes) and it can be transmitted to mouth.

- Biphasic Crackles which are a combination of coarse and fine crackles.

Although some reference values of the characteristic frequency have been mentioned, it is important to observe that, in general, the frequency range of crackles is extremely broad and ranges between 300 Hz and 1000 Hz. It is also verified that fine crackles have a higher frequency content with respect to coarse crackles, extending up to 2000 Hz [29]–[31].

From a clinical perspective, the classification of the American Thoracic Society (ATS) is adopted: fine and coarse crackles are categorized considering two time domain parameters 2CD (two Cycle Duration) and IDW (Initial Deflection Width) [29]. 2CD is the duration of a crackle from the beginning of the initial deflection to the end of two cycle whereas IDW is the length of time of the first deflection in a crackle waveform. Those parameters as well as other more qualitative information are reported in TABLE 3.

TABLE 3: CLASSIFICATION AND FEATURES OF CRACKLES

	Intensity	Pitch	2CD duration	IDW duration
Coarse crackles	Loud	Low	About 10 ms	About 1.5 ms
Fine crackles	Less loud	Higher	<5 ms	About 0.7 ms

Crackles are associated to a variety of pathologies like bronchiectasis, chronic obstructive pulmonary disease (COPD), edema and fibrosis [28], [29], [32], [33].

1.4.2 <u>Wheezes</u>

Wheezes are adventitious and continuous sounds which are heard at end of the inspiratory phase or in the early expiratory phase. They can be considered the result of the gradual reopening (during inspiration) or closure (during expiration) of a collapsed airway lumen. The reduction of the cross-section of the airway lumen causes the air flow velocity to increase, generating a harmonic

vibration of the airway wall. It is suggested that their generation is more likely to happen between generations 2-7 of the tracheobronchial tree [32]. Their duration is between 100 ms and 250 ms and they are generally represented as sinusoidal oscillations. The average frequency content is located between 100-1000 Hz and with some harmonics that can occasionally go far beyond 1000 Hz [31]. The application of theoretical models of flutter in a flow-limited collapsible conduit shows that the frequency of wheezing could be affected by parameters like the airway wall bending elasticity, thickness and the tension in the longitudinal direction [34].

Wheezes are divided in high pitched wheezes and low pitched wheezes. In clinical practice, it is common the association of high and low pitch wheezes with diseases of the small and large airways, respectively. However, there are few experimental evidences to confirm this association. A second distinction can be made between monophonic and polyphonic wheezes: the former has a single pitch and tone localized in a specific area, the latter show multiple pitches and tonal qualities distribute over a certain area of the lung.

Wheezes can be generally detected in subjects affected by obstructive diseases, in particular asthma and COPD [32]–[35].

1.4.3   Stridor

Stridor are intense continuous monophonic sounds which can be best heard over extra-thoracic airways. Stridor tends to be more recognizable during inspiration due to the collapse of extra-thoracic airways because of the lower internal lumen pressure. The use of the stethoscope helps to identify the areas where the intensity in maximum, although in general stridor can be heard without any specific instrument. Clinical evidences show that the maximum intensity can be recognized at the level of the larynx or at the thoracic inlet. For this reasons, stridor is usually

considered as an indicator of upper airway obstruction. Signal analysis reveals that stridor have a sinusoidal waveform with fundamental frequency generally higher 500 Hz [28], [32].

1.4.4 <u>Bronchial Breath Sounds</u>

Bronchial breath sounds are blasting sounds and are audible throughout inspiration and expiration. They occur due to the lack of air in the lung tissue between the chest wall and the large airways. This is likely to happen in the consolidated lung of pneumonia or pulmonary fibrosis. They are commonly heard in the anterior part over the manubrium of the sternum and in the posterior part between the vertebrae C7 and T3. Generally, they show as a main feature a higher frequency content with respect to normal ones: this is because in consolidation phenomena causes a reduction of the low-pass filtering role of the alveolar region. In normal auscultation, they are very similar to normal tracheal breathing and therefore particularly difficult to recognize. For this reason, their clinical relevance is relatively low [32].

1.4.5 <u>Pleural Rub</u>

Pleural Rub is described as a creaking, coarse, grating or leathery sound. It is often localized over the lung bases (posteriorly). Pleural rub tends to recur at the same moment in each respiratory cycle, often in both inspiration and expiration: ordinarily, the expiratory component is specular to the inspiratory component. It is caused by friction between inflamed visceral and parietal surfaces of the pleura during breathing [32]. The duration of the signal is in the order of 200 ms and the typical frequency content is in the range 200-2000 Hz. Clinically speaking the sound is very similar to repetitive crackles and it almost impossible to distinguish between the two especially if the rub

is limited to the inspiration phase, nonetheless pleural rub can be an indicator of pleural inflammation or pleural tumors [32].

1.4.6 <u>Ronchi</u>

Ronchi are defined as musical low-pitched sounds. They are characterized by rapidly damping periodic waveforms. The duration is generally higher than 100 ms and frequency content lower than 300 Hz. They are generally associated with abnormal airway collapsibility and the creation of breach of fluid films. As they generally clear with coughing, clinical practice suggests that secretions in larger airways play an important role in generating these sounds. For the reasons mentioned above, ronchi can be considered as indicators of airway lumen constriction associated with the thickening of the mucosa, edema or bronchospasm (e.g. bronchitis and COPD) [32].

1.4.7 <u>Squawks</u>

Squawks are defined as mixed sound since they are characterized by a crackle followed by short musical component (which resembles a wheeze). They are likely to occur in fibrotic pulmonary disorders. Acoustically, their waveform is similar to that that of short wheezes, but they are often preceded by a crackle [9]. Squawks mean duration is approximately of 90–320 ms. Forgacs [36] suggested that squawks are produced when an obstructed airway abruptly opens in inspiration, while, for a short amount of time, the airway walls remain coupled one to the other in a mechanism very similar to the one responsible for the production of wheezes [9],[32].

1.5   Objectives and Structure of the Thesis

The objective of this project is to provide a first insight of the sound propagation in the tracheobronchial tree in normal and pathological condition. To achieve this goal an analytical model in MATLAB by Brian Henry is validated via numerical simulations in COMSOL Multiphysics® in the physiological conditions. Two inspiratory phases are considered: the beginning of the inspiratory phase and the beginning of the expiratory phase. After the validation of the model, the morphometry of the trees and the mechanical properties of the airways are modified to simulate some pathology-induced alterations of the architecture of the airways and the sound propagation is analyzed under those circumstances. The effect of the pathology of asthma and the conditions of a generalized fibrosis and pulmonary infiltrate are presented.

The introductory (Chapter 1) section briefly describes the anatomy of the respiratory system as well as the main features of the pathological conditions taken into consideration in this work. In Chapter 2, the theoretical model underlying the code used for the analysis is presented. The analytical model section (Chapter 3) presents the process of generation of the geometries and the settings of the analytical simulations: it is also explained how the model was modified to account for pathology-induced alterations. Chapter 4 deals with the numerical simulations used for the validation of the analytical model. The results both in terms of validation of the model and simulations of the pathological conditions are reported in Chapter 5. Finally, the discussion of the results is developed in Chapter 6.

CHAPTER 2

THEORY

2.1 <u>Acoustic Impedance</u>

The general concept of impedance implies the ratio of a driving force to the correspondent velocity respond. The acoustic impedance Z is defined as the acoustic pressure P divided by the acoustic volumetric flow U. In the most general case, the acoustic impedance is a frequency-dependent value.

$$Z = \frac{P}{U} \qquad (2.1)$$

For a chosen frequency, it indicates the amount of sound pressure which a given air vibration can generate. The SI unit of measurement for acoustic impedance is $Pa \cdot s/m^3$, also known as acoustic ohm. Another common notation is the one of specific acoustic impedance. In this definition, the normalization of the volume flow with respect to the cross-sectional area is included, thus obtaining:

$$z = \frac{P}{u} \qquad (2.2)$$

Where u is the particle velocity.

The specific impedance, as well the volumetric one, is complex value and can expressed as:

$$z = r + jx \tag{2.3}$$

Where r and x denotes the specific acoustic resistance and the specific acoustic reactance, respectively.

2.2 <u>Impedance of a Sound Wave Propagating in Cylinder</u>

The general case of a harmonic planar sound wave propagating in a cylinder will be now considered. This is a simplified base model which will be useful in further analysis. The hypothesis of rigid walls is introduced. It is also assumed that at a certain point $x = 0$ along the cylinder the acoustic impedance changes from Z_0 to Z_T as reported in Figure 2.
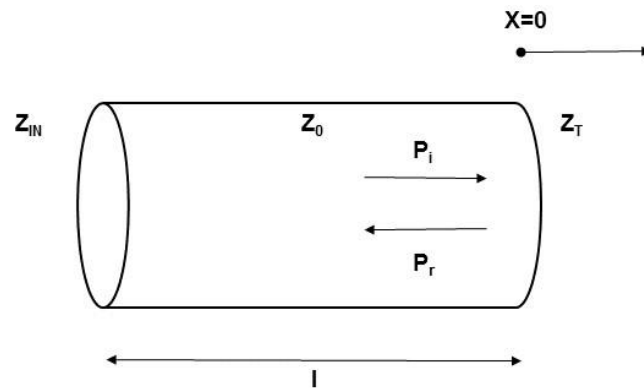
Figure 2: Exemplification of a Sound Wave Propaganting in a Cylinder

Considering a wave travelling in the positive x direction represented by:

$$P_i = Ae^{j(\omega t - kx)} \tag{2.4}$$

That reaches the above-mentioned point, it is known that a reflected wave propagating in the negative x direction will be generated. This wave will be described by the following equation.

$$P_r = Be^{j(\omega t + kx)} \tag{2.5}$$

In $x = 0$ the continuity of pressure and the continuity of the normal velocity must be satisfied. This implies:

$$P_i + P_r = P \tag{2.6}$$

and (given that the incident wave and the reflected wave generate two flows which have opposite directions):

$$U_i - U_r = U \tag{2.7}$$

By dividing (2.6) and (2.7) accordingly to the definition of impedance it holds:

$$Z = \frac{P}{U} = \frac{P_i + P_r}{U_i - U_r} \tag{2.8}$$

Recalling and inverting the definition of acoustic impedance, it is possible to write

$$U_i = \frac{P_i}{Z_0} = Y_0 P_i = Y_0 A e^{j(\omega t - kx)} \tag{2.9}$$

$$U_r = \frac{P_r}{Z_0} = Y_0 P_r = Y_0 B e^{j(\omega t + kx)} \tag{2.10}$$

The substitution of (2.4), (2.5), (2.9), (2.10) in (2.8) and the simplification of the term $e^{-j\omega t}$, lead to:

$$Z = \frac{P}{U} = \frac{Ae^{-jkx} + Be^{jkx}}{Ae^{-jkx} - Be^{jkx}} \tag{2.11}$$

The definition of the reflection coefficient R as the ratio between the pressure of the incident wave and the pressure of the reflected wave as expressed below,

$$R = \frac{P_i}{P_r} = \frac{Ae^{j(\omega t - kx)}}{Be^{j(\omega t + kx)}} \tag{2.12}$$

and the evaluation in $x = 0$, allow to write:

$$Z_T = \frac{A + RA}{\dfrac{A - RA}{Z_0}} = Z_0 \frac{1 + R}{1 - R} \tag{2.13}$$

Solving (2.13) for R:

$$R = \frac{Z_T - Z_0}{Z_0 + Z_T} \tag{2.14}$$

The generic impedance Z is dependent on the position on the tube and of chosen frequency can consequently be written as:

$$Z = \frac{P}{U} = \frac{Ae^{-jkx} + Be^{jkx}}{Ae^{-jkx} - Be^{jkx}} = Z_0 \frac{Ae^{-jkx} + RAe^{jkx}}{Ae^{-jkx} - RAe^{jkx}} =$$

$$= Z_0 \frac{Ae^{-jkx} + \dfrac{Z_T - Z_0}{Z_0 + Z_T} Ae^{jkx}}{Ae^{-jkx} - \dfrac{Z_T - Z_0}{Z_0 + Z_T} Ae^{jkx}} =$$

$$= Z_0 \frac{(Z_0 + Z_T)Ae^{-jkx} + (Z_T - Z_0)Ae^{jkx}}{(Z_0 + Z_T)Ae^{-jkx} - (Z_T - Z_0)Ae^{jkx}} \tag{2.15}$$

By substituting in (2.15)

$$e^{-jkx} = cos(-kx) + jsin(-kx) = cos(kx) - sin(kx) \tag{2.16}$$

$$e^{jkx} = cos(kx) + jsin(kx) \tag{2.17}$$

It is possible to obtain

$$Z = \frac{P}{U} = Z_0 \frac{Z_T \, cos(kx) - Z_0 jsin(kx)}{Z_0 \, cos(kx) - Z_T jsin(kx)} \tag{2.18}$$

Rearranging (2.18) and computing the impedance at the input of the cylinder (i.e. for $x = -l$)

$$Z_{IN} = Z_0 \frac{Z_T + Z_0 jtan(kl)}{Z_0 + Z_T jtan(kl)} \tag{2.19}$$

Recalling that the following equality holds:

$$jtan(kl) = tanh(jkl) \tag{2.20}$$

Equation (2.20) can be written as:

$$Z_{IN} = Z_0 \frac{Z_T + Z_0 tanh(jkl)}{Z_0 + Z_T tanh(jkl)} \tag{2.21}$$

Finally, by introducing the following relations:

$$\gamma^2 = -k^2 \tag{2.22}$$

$$\gamma = \alpha + j\beta \tag{2.23}$$

$$k = \beta - j\alpha \tag{2.24}$$

The input impedance in (2.21) can be expressed as:

$$Z_{IN} = Z_0 \frac{Z_T + Z_0 tanh(\gamma l)}{Z_0 + Z_T tanh(\gamma l)} \tag{2.25}$$

Or, equivalently,

$$Z_{IN} = \frac{Z_T + Z_0 tanh(\gamma l)}{1 + \frac{Z_T}{Z_0} tanh(\gamma l)} \tag{2.26}$$

For the discussion that will be done in this chapter it is useful to compute the acoustic pressure inside the cylinder, in particular it is possible to take advantage of the analogy with the transmission line in order to compute the ratio between the pressure at the input and the pressure at the output of the tube as done in Jackson et Al [3].

This leads to the following result:

$$\frac{P_T}{P_{IN}} = \frac{1}{cosh(\gamma l) + \frac{Z_0}{Z_T} sinh(\gamma l)} = Z_T \frac{1}{Z_T cosh(\gamma l) + Z_0 sinh(\gamma l)} \tag{2.27}$$

For the analysis that will be performed later in this discussion, it is worth expressing equation (2.27) as:

$$Z_T \frac{P_{in}}{P_T} = Z_T cosh(\gamma l) + sinh(\gamma l) Z_0 \qquad (2.28)$$

2.3   Mathematical and Acoustical Description of the Lower Respiratory Tract

To deal with the model of sound transmission in the region below the glottis, it necessary to consider two fundamental parts:

1. the description, in terms of mathematical formulation, of the acoustical properties of the single airway segment;

2. the complexity of the airway tree which, for a human subject, approximately involves 10^7 terminal branches.

As far as the first part is concerned, the discussion in 2.2 can be easily extended to accomplish this objective. The second task is a more challenging one as it implies the introduction of a mathematical and geometrical model. The model proposed in this dissertation will be the Horsfield model.

2.3.1   The Horsfield Model

The Horsfield model is a geometrical representation if the bronchial tree able to properly take into account its natural asymmetric dichotomy and based on the assumption of self-consistency [8]. It was proposed by Horsfield and Al. in the 1982 and, although some approximations are reasonably introduced, it can be considered a comprehensive morphometric model of the airways [4]. For a

human subject, 35 segments of different sizes and characteristics are identified. Number n=35 is assigned to the trachea (the largest) and n=1 is assigned to terminal bronchiole which is supposed to branch directly into two alveoli (no respiratory bronchioles are here considered). For each segment the model specifies the length, the diameter, wall thickness and area fraction of cartilage. The so-called recursion index (Δ^n) allows to account for the asymmetry of the system at each airway bifurcation. That is to say, a nth ordered airway generates two segments of order n-1 and n-1-Δ^n, respectively. The recursion index (Δ^n) is considered as a structural parameter and is not constant all over the bronchial tree. Although Horsfield et Al. proposed a table containing some reference values for the parameters mentioned above, in this dissertation the one in Habib et Al. [5] will be considered as it allows to account for the non-rigidity of the airway wall and the presence of the terminal respiratory tissues. The Habib table readapted from [5] is reported in TABLE 4.

As a final, but relevant remark on these data, it is important to notice that they are based on casts of the lung airways, consisting of tube-shaped segments that bifurcate progressively into smaller components which all can be regarded as mono-dimensional as far as the acoustical point of view is concerned. This consideration further legitimates the use of equations in 2.2 to describe the acoustic impedances and the acoustic pressures, provided that the non-rigidity of the walls is already taken into account in the definition of the structural properties themselves as already specified. The self-consistency of the model is given by the fact that for a chosen airway order n, the daughter segments are of same two orders, independently on the position in the lung.

TABLE 4: MORPHOLOGICAL PARAMETERS OF HUMAN AIRWAY MODEL; n IS THE HORSFIELD ORDER, l AND d ARE THE LENGTH AND DIAMETER, h IS THE WALL THICKNESS AND C THE FRACTION OF CARTILAGE.

n	$l^{(n)}$ [cm]	$d^{(n)}$ [cm]	$h^{(n)}$ [cm]	$C^{(n)}$	$\Delta^{(n)}$
1	0.0480	0.0800	0.00520	0.0000	0
2	0.0480	0.0800	0.00520	0.0000	0
3	0.0480	0.0800	0.00520	0.0000	0
4	0.0480	0.0800	0.00520	0.0000	0
5	0.0480	0.0800	0.00520	0.0000	0
6	0.0590	0.0800	0.00520	0.0000	0
7	0.0750	0.0430	0.00290	0.0000	0
8	0.1050	0.0480	0.00320	0.0000	0
9	0.1310	0.0530	0.00360	0.0000	0
10	0.1100	0.0630	0.00420	0.0000	0
11	0.2500	0.0760	0.00500	0.0000	1
12	0.3100	0.0950	0.00600	0.0000	2
13	0.3600	0.1100	0.00670	0.0000	2
14	0.4200	0.1400	0.00490	0.0000	3
15	0.4800	0.1600	0.00850	0.0000	3
16	0.5170	0.1800	0.00910	0.0000	3
17	0.6300	0.2000	0.00960	0.0224	3
18	0.6400	0.2180	0.0100	0.0262	3
19	0.7700	0.2400	0.0105	0.0309	3
20	0.8100	0.2500	0.0107	0.0329	3
21	0.8200	0.2700	0.0111	0.0370	3
22	0.9200	0.2800	0.0112	0.0390	3
23	0.8000	0.2900	0.0114	0.0410	3
24	0.9900	0.3100	0.0118	0.0450	3
25	0.9500	0.3500	0.0126	0.0526	3
26	0.8600	0.3500	0.0126	0.0526	3
27	1.0800	0.4300	0.0149	0.0671	3
28	0.9700	0.5400	0.0205	0.0851	3
29	1.13000	0.5900	0.0244	0.0926	3
30	1.13000	0.5900	0.0244	0.2000	3
31	1.05000	0.7300	0.0409	0.2500	3
32	1.1000	0.8000	0.0528	0.3300	3
33	2.2000	1.4000	0.1348	0.5000	3
34	5.0000	1.2000	0.1735	0.5000	2
35	10.0000	1.6000	0.3724	0.6700	1

From an acoustical point of view, it is significant the possibility to compute the acoustic impedance at the input of the trachea as well as the acoustic pressure distribution in the airways. Indeed, both these parameters will be dependent on the airway geometry and the changes it can possibly experience. Thanks to the self-consistency of the model the computation of the acoustic impedance can be performed in a "relatively" simple way. The first step is the computation of this impedance at the level of the terminal bronchiole (n=1) and then reiterate the procedure for n=2, 3, …, 35 (where n=35 is the trachea). Taking as a reference Figure 3:
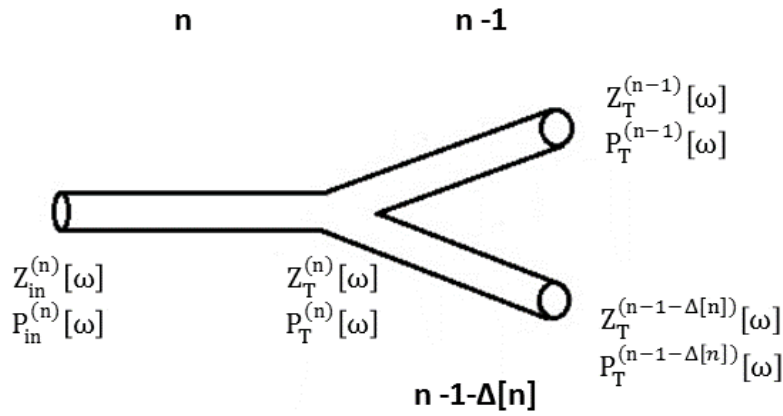
Figure 3: The acoustic model of a single bifurcating airway segment

By a simple extension of the formula (2.18), the input (i.e. considered at the end adjacent to the trachea) acoustic impedance Z_{in} can be defined as:

$$Z_{in}^{(n)}[\omega] = \frac{Z_T^{(n)}[\omega] \cosh(\gamma_0^{(n)}[\omega]l^{(n)}) + Z_0^{(n)}[\omega]\sinh(\gamma_0^{(n)}[\omega]l^{(n)})}{\cosh(\gamma_0^{(n)}[\omega]l^{(n)}) + \left(Z_T^{(n)}[\omega]/Z_0^{(n)}[\omega]\right)\sinh(\gamma_0^{(n)}[\omega]l^{(n)})} \qquad (2.29)$$

Or, by the definition of $\tanh(x) = \frac{\sinh(x)}{\cosh(x)}$, as:

$$Z_{in}^{(n)}[\omega] = \frac{Z_T^{(n)}[\omega] + Z_0^{(n)}[\omega]tanh(\gamma_0^{(n)}[\omega]l^{(n)})}{1 + \left(Z_T^{(n)}[\omega]/Z_0^{(n)}[\omega]\right)tanh(\gamma_0^{(n)}[\omega]l^{(n)})} \tag{2.30}$$

Where $Z_0^n[\omega]$ is the characteristic impedance and $\gamma_0^n[\omega]$ is characteristic propagation coefficient

of the nth airway segment [4]. The values of these two parameters can be computed thanks to the

following equations [5], [37], [38]:

$$Z_0^{(n)}[\omega] = \sqrt{Z^{(n)}[\omega]/Y^{(n)}[\omega]} \tag{2.31}$$

$$\gamma_0^{(n)}[\omega] = \sqrt{Z^{(n)}[\omega]Y^{(n)}[\omega]} \tag{2.32}$$

$$Z^{(n)}[\omega] = \frac{j\omega\rho_g}{A^{(n)}\left(1 - F_v^{(n)}[\omega]\right)} \tag{2.33}$$

$$Y^{(n)}[\omega] = \frac{j\omega A^{(n)}}{\rho_g c_g^2}\left(1 + 0.402F_t^{(n)}[\omega]\right) + \frac{1}{Z_w^{(n)}[\omega]l^{(n)}} \tag{2.34}$$

$$F_v^{(n)}[\omega] = \frac{2}{a^{(n)}\sqrt{(-j\omega\rho_g/\eta_g)}}\frac{J_1[a^{(n)}\sqrt{(-j\omega\rho_g/\eta_g)}]}{J_0[a^{(n)}\sqrt{(-j\omega\rho_g/\eta_g)}]} \tag{2.35}$$

$$F_t^{(n)}[\omega] = \frac{2}{a^{(n)}\sqrt{(-j\omega C_g/\kappa_g)}}\frac{J_1[a^{(n)}\sqrt{(-j\omega C_g/\kappa_g)}]}{J_0[a^{(n)}\sqrt{(-j\omega C_g/\kappa_g)}]} \tag{2.36}$$

$$Z_w^{(n)}[\omega]^{-1} = \frac{c^{(n)}}{Z_{w,c}^{(n)}[\omega]} + \frac{1 - c^{(n)}}{Z_{w,s}^{(n)}[\omega]} \tag{2.37}$$

In the equations described above $Y^{(n)}[\omega]$ represents the admittance. The subscript "g" denotes the

properties related to the gas (i.e. air) component:

- ρ_g is the density;

- c_g is the wave speed in the given gas;

- η_g is the viscosity;

- C_g is the specific heat at constant pressure;

- κ_g is the coefficient of heat conduction;

- A(n) and a(n) are respectively the cross section and the radius of the n order segment.

- J_1 is the Bessel function of order 1;

- J_0 is the Bessel function of order 0;

- $F_t^{(n)}[\omega]$ is a term related to the storage of kinetic energy and its dissipation at the walls due to viscous losses;

- $F_v^{(n)}[\omega]$ is a term associated to the thermal dissipation occurring at the walls due to the failure of adiabaticity condition;

The term $Z_w^{(n)}[\omega]$ denotes the effective volumetric impedance of the wall of the nth-order airway segment. Since the wall can be constituted of two different materials, namely cartilage and soft tissue, their relation in terms of fractional content are exemplified by $c^{(n)}$ and $1 - c^{(n)}$, respectively. As it can be observed from TABLE 4 the presence of cartilage rings is characterized by a decreasing proportion moving downward from the trachea to the terminal segments. In particular, for a human subject the cartilage content is maximum at the trachea $c^{(35)} = 0.67$, gets gradually reduced up to the seventieth order $c^{(n)} = 0.0224$ and is completely absent form airways order $n = 1, \dots, 16$ where, consequently, exclusively soft tissue is considered [6].

The use of a series compliance (C_w), inertance (I_w) and resistance (R_w), and exemplification of each wall section allow the computation of the impedance of the cartilage component $Z_{w,c}^{(n)}[\omega]$ and the soft tissue component $Z_{w,s}^{(n)}[\omega]$. The following relations hold:

$$Z_{w,c\ or\ s}^{(n)}[\omega] = R_w^{(n)} + j\left(\omega I_w^{(n)} - \frac{1}{\omega C_w^{(n)}}\right) \tag{2.38}$$

where

$$R_{w,c\ or\ s}^{(n)} = \frac{4h^{(n)}\eta_{c\ or\ s}}{\pi(d^{(n)})^3 l^{(n)}} \tag{2.39}$$

$$I_{w,c\ or\ s}^{(n)} = \frac{h^{(n)}\rho_{c\ or\ s}}{\pi d^{(n)} l^{(n)}} \tag{2.40}$$

and

$$C_{w,c\ or\ s}^{(n)} = \frac{\pi\left(d^{(n)}\right)^3 l^{(n)}}{4h^{(n)}E_{c\ or\ s}} \tag{2.41}$$

In the equations presented above $\eta_{c\ or\ s}$ denotes the viscosity, $\rho_{c\ or\ s}$ the density $E_{c\ or\ s}$ the elastic Young's modulusof the cartilage or soft tissue respectively.

Nominal material property values are reported in [6]:

- $\eta_c = 18000$ Pa·s

- $\eta_s = 160$ Pa·s

- $\rho_c = 1140$ Kg/m^3

- $\rho_s = 1060$ Kg/m^3

- $E_c = 4.40\times10^6$ Pa

- $E_s = 3.92\times 10^4$ Pa

Finally, the term Z_T express the acoustic impedance at the terminal end of each segment and is provided by:

$$Z_T^{(n)}[\omega] = \begin{cases} \dfrac{N_T}{j\omega c_g + 1/[R_t + j(\omega I_t - 1/[\omega C_t])]}, & n = 1 \\[4mm] \dfrac{1}{1/Z_T^{(n-1)}[\omega] + 1/Z_T^{(n-1-\Delta[n])}[\omega]}, & n = 2, \dots, 35 \end{cases} \qquad (2.42)$$

Where N_T is the total number of extremity (n=1) bronchiole branches in parallel to the culmination of the lung parenchyma into the soft tissue.

For the model here analyzed, this total number can be computed thanks to the recursive formulation reported below, considering $N_T^{(1)} = 1$ and $N_T = N_T^{(35)}$:

$$N_T^{(n)} = N_T^{(n-1)} + N_T^{(n-1-\Delta[n])} \qquad (2.43)$$

The term C_g represents the alveolar gas compliance under compression as expressed by the Dubois six elements terminal airway model [39]. R_t, I_t, C_t denotes properties of the terminal tissue, more specifically resistance, inertia and compliance.

The computation of the acoustic pressure as a function of an input acoustic pressure is extremely complex. This is because (unlike the acoustic impedance case) the hypothesis of self-consistency does not hold for the acoustic pressure since it is not the same among airways of the same order n as it is dependent on the length of the path to the trachea. In other words, it is possible to have segments with the same n, but which are not connected to the trachea by an equal number of segments. Although the levels of acoustic pressure levels are not alike among segments with the

same order, it can be demonstrated that given a certain order n the ratio $P_{rat}^{(n)}[\omega]$ between the acoustic pressure at the far end $P_T^{(n)}[\omega]$ and that at the near end (adjacent to the trachea) $P_{in}^{(n)}[\omega]$ is equal for every airway segment of that order and can be obtained by [6]:

$$P_{rat}^{(n)}[\omega] = \frac{P_T^{(n)}[\omega]}{P_{in}^{(n)}[\omega]} = Z_T^{(n)}[\omega] \left\{ \frac{cosh\left(\gamma_0^{(n)}[\omega]l^{(n)} \right)}{Z_{in}^{(n)}[\omega]} - \frac{sinh\left(\gamma_0^{(n)}[\omega]l^{(n)} \right)}{Z_0^{(n)}[\omega]} \right\} \quad (2.44)$$

Equation (2.41) above can be alternatively expressed as [8]:

$$P_{rat}^{(n)}[\omega] = \frac{Z_T^{(n)}[\omega]Z_0^{(n)}[\omega]}{Z_{in}^{(n)}[\omega] \left(Z_T^{(n)}[\omega]sinh\left(\gamma_0^{(n)}[\omega]l^{(n)} \right) + Z_0^{(n)}[\omega] cosh\left(\gamma_0^{(n)}[\omega]l^{(n)} \right) \right)} \quad (2.45)$$

Either one formulation or the other is extremely useful because it states the dependence of this $P_{rat}^{(n)}[\omega]$ on the impedances $Z_{in}^{(n)}[\omega]$, $Z_T^{(n)}[\omega]$, and $Z_0^{(n)}[\omega]$ which, as explained before, are easier to compute. Furthermore, if the input pressure at the top of the trachea is known and the ratio can be computed, the acoustic pressure at the lower extremity of the trachea can be derived. The pressure at the distal part of the trachea corresponds to the input the pressure at the proximal end of the two main stem bronchi, by knowing the impendence at this new order the corresponding ratio can be computed and finally the pressure at the end of both the main bronchi can be obtained. This procedure can be iteratively performed for the pressure at base or top of any airway order. It can be demonstrated that, by properly rearranging equation (2.45) and substituting the definition of input impedance as expressed in equation (2.30) the very same result of Jackson et Al. reported in equation (2.27) can be found (see Appendix for details). Finally, the pressure in function of the coordinate x along a certain segment can be computed applying the following formula [40]:

$$P^{(n)}[x,\omega] = \frac{Z_0^{(n)}[\omega]}{\sinh\left(\gamma_0^{(n)}[\omega]l\right)}\left(\frac{P_{in}^{(n)}[\omega]}{Z_{in}^{(n)}[\omega]}\cosh\left(\gamma_0^{(n)}[\omega](x-l)\right) - \frac{P_T^{(n)}[\omega]}{Z_T^{(n)}[\omega]}\cosh\left(\gamma_0^{(n)}[\omega]x\right)\right) \qquad (2.46)$$

Where x varies between 0 (end of the segment closest to the trachea) and l (end of the segment distant from the trachea).

As far as the validity of this model is concerned, it reported that this approach is to be considered valid for frequency lower than 5000 Hz [6]. For higher frequencies, pressure variations can occur across the cross-section of the larger airways: this phenomenon cannot be properly predicted by the current description and therefore a more complex three-dimensional acoustic model should be introduced.

CHAPTER 3

ANALYTICAL MODELS

The first computational step performed in this work was the simulation via analytical model in MATLAB of the acoustic pressure propagation and wall radial velocity in a human tracheobronchial tree for a frequency range of 200-800 Hz. The choice of a multifrequency analysis is justified by the frequency dependency of the mechanical and acoustic properties of the tissues. The range of frequency tested was decided taking into consideration that clear majority of the frequency content of physiological and pathological breath sounds is located below 800 Hz. The lower limit was arbitrary chosen at 200 Hz, nonetheless the model could be easily extended to lower frequencies.

3.1   Generation of the Models

The human data used for the analytical acoustical analysis were obtained from de-identified Computed Tomography (CT) images provided by Dr. Ching-Long (IIHR – Hydro-science and Engineering and the Department of Mechanical and Industrial Engineering, University of Iowa) and generated via the procedure described in [41]. For the given tracheobronchial tree, two different phases of the respiratory cycle were considered: the beginning of expiratory phase and the beginning of inspiratory phase. Images have been acquired at normal respiratory volume. To generate the geometry and to collect the information related to morphology, the length and the diameter of the constituent segments a Graphic User Interface (GUI) in MATLAB was used. The extrapolation of geometrical and morphological features was performed on the voxelized CT images of the given airways; the whole process was aimed at the generation of a one-dimensional

airways tree to be input and analyzed in MATLAB. For each segment the central proximal and distal points were identified and the tree build as the centerline of the 3D segment. A visual example of the procedure for the extraction of the information mentioned above is shown in Figure 4 for the expiratory tracheobronchial tree (the same task was accomplished also for the inspiratory one).
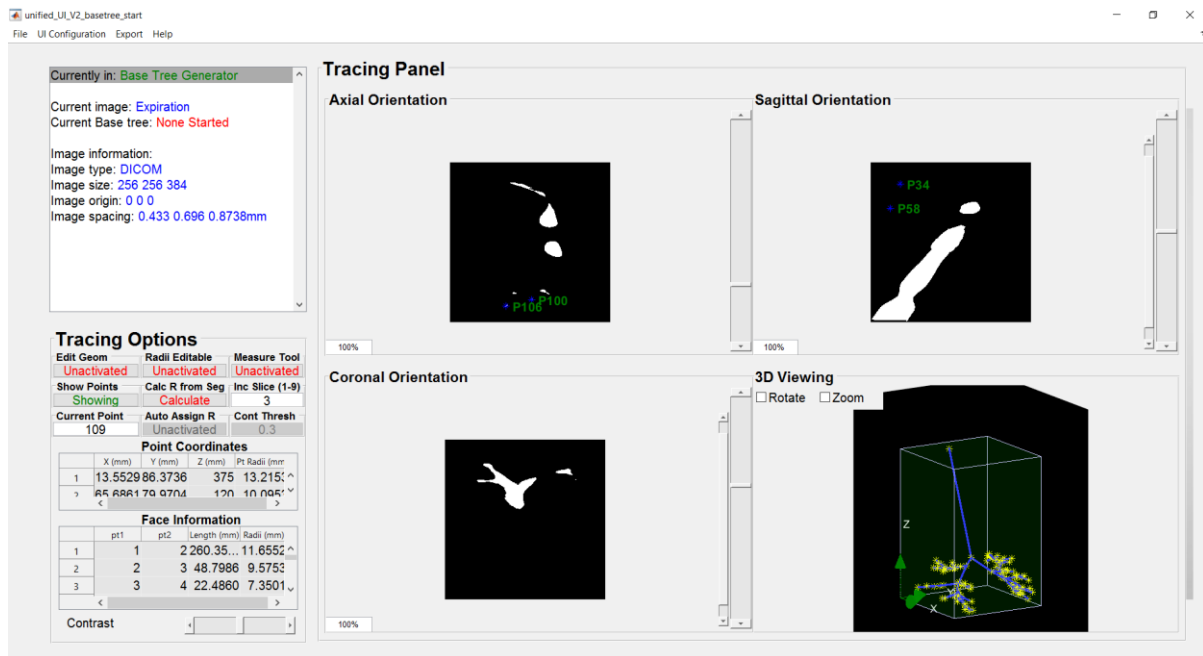
Figure 4: Visual layout of the process of identification and generation of the morpho-geometrical features of the airway tree (case of expiration is reported)

The thickness was manually assigned by evaluating the diameter and fitting it to the closest order of the Habib table (see TABLE 4). In order simplify the successive numerical analysis, the lowest value of thickness accepted for the terminal segments was assumed to be 500 micrometers: if the thickness of any segment was lower than that value, it was approximated to be as exactly equal to

it. The two generated tracheobronchial trees for the beginning of the of inspiratory and the beginning of the expiratory phase are shown in Figure 5 and Figure 6, respectively.
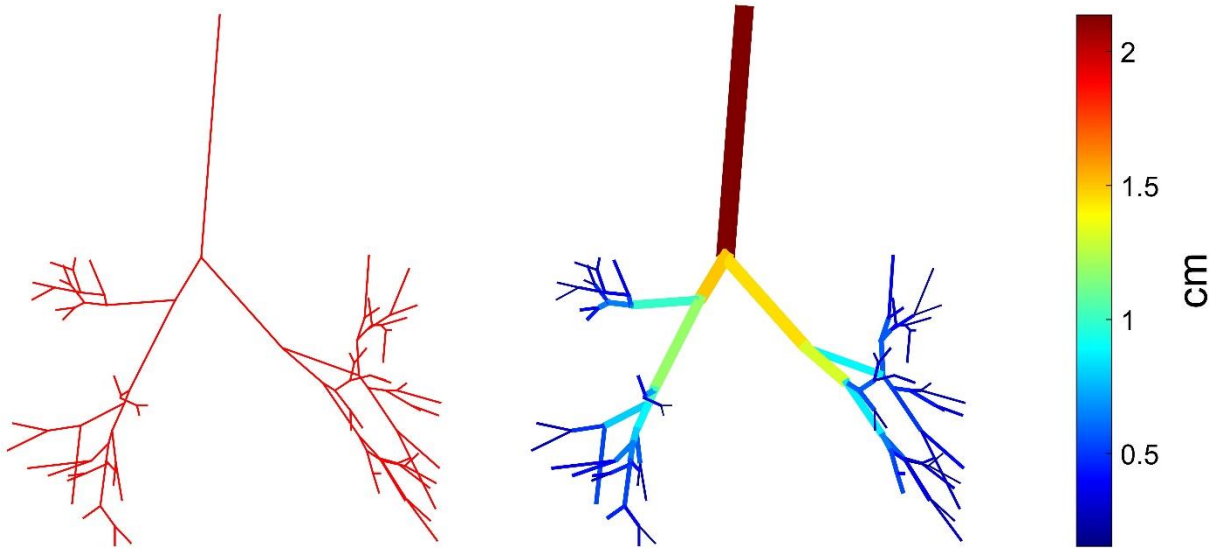
Figure 5: Geometry (left) and diameter distribution (right) at the beginning of the inspiratory phase
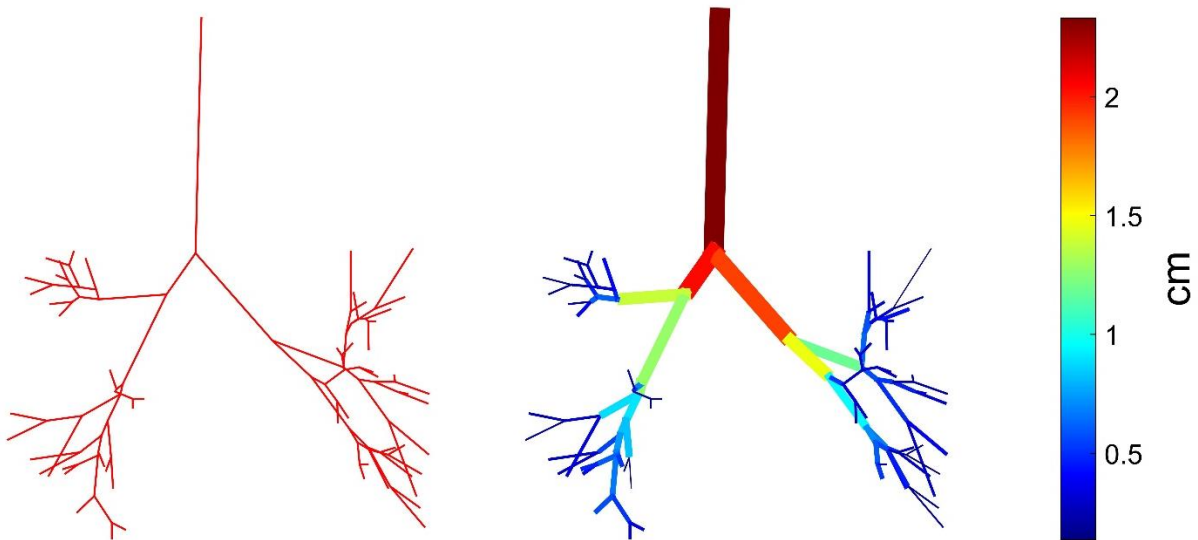
Figure 6: Geometry (left) and diameter distribution (right) at the beginning of the expiratory phase

3.2   <u>**Acoustical Analysis**</u>

The acoustic analysis was analytically performed in MATLAB (r2016a, The MathWorks Inc., Natick, MA, 2016). The code models 1D quasi-planar wave propagation in a branching system. This approach reasonably approximates most of the dynamic behavior up to several kHz [8]. At extremely high frequencies the assumptions underlying the model namely the hypotheses of the one dimensionality and quasi planarity of the propagation, begin to lose validity in the larger airways. This is because, in general, the hypothesis of planarity and the approximation of the system by a 1-D wave equation are proven to be valid only if the wavelength corresponding to the highest frequency is sufficiently wider than the cross-section of the largest segment of the tubular structure to be modeled [42]. The pressure can be input either at the inlet of the trachea or in a chosen location: for all the acoustical analysis reported in this dissertation, a pressure with an amplitude of 1 Pa input at the level of the trachea was considered. As mentioned above, the frequency of the input pressure wave was varied between 200 and 800 Hz. The algorithm allows the computation of the acoustic impedance and acoustic pressure according to the formulas reported in paragraph 2.3.1 above. In addition to those information, the radial velocity of the wall of each airway segment was obtained thanks to the following formula:

$$u_{radial} = P/Z_{w,radial}/i \qquad\qquad (3.1)$$

Where the term $Z_{w,radial}$ is defined as the volumetric impedance Z_w over the lateral area of the cylinder considered. In this way, the results regarding the wall radial were obtained in the conventional SI unit of m/s.

As for the Horsfield model, in the analytical code each segment was modeled as cylinder of known radius, length and thickness, but the calculations are not limited to an always-bifurcating network. The fractional content of cartilage and soft tissue for each segment are defined taking as a reference Habib and Al [5]. The fractional content $c(n)$ of cartilage is assigned for each generation whereas the soft tissue fraction is simply computed as unity minus the cartilage fraction. i. e. $1 - c(n)$.

The material properties of the constituent elements included in the model are assigned in a specific function in accordance to (2.39) - (2.41). The mechanical properties of the cartilage were approximated to be the same of the soft tissue. Thus, in terms of acoustic analysis, the airways walls were assumed to be composed of soft tissue only. The soft tissue behavior was approximated with a Voigt model with Young's Modulus Y_s and the viscosity η_s. The complex elastic modulus of the chosen rheological model is reported in equation:

$$E = Y_s + i\omega\eta_s \tag{3.2}$$

The mechanical parameters characterizing the airways wall soft tissue (density, elastic modulus and viscosity) are reported in TABLE 5.

TABLE 5: MECHANICAL PROPERTIES OF THE SOFT TISSUE

Property	Symbol	Value
Density of Soft Tissue $[Kg/m^3]$	ρ_s	1060
Elastic Modulus of Soft Tissue $[Pa]$	Y_s	3.92×10^5
Viscosity of Soft Tissue $[Pa \cdot s]$	η_s	101.90

Parameters characterizing the air, namely density (ρ_g), wave speed (c_g), viscosity (η_g); specific heat at constant pressure (C_g) and coefficient of heat conduction (κ_g), were set at body temperarature and are reported in TABLE 6.

TABLE 6: MECHANICAL PROPERTIES OF AIR

Property	Symbol	Value
Density [Kg/m^3]	ρ_g	1.14
Wave Speed [m/s]	c_g	343
Viscosity [$Pa \cdot s$]	η_g	1.86×10^{-5}
Poisson coefficient [-]	ν_g	0.4995
Specific Heat at Constant Pressure [$J/Kg \cdot °C$]	C_g	1004.2
Coefficient of Heat Conduction [$J/Kg \cdot °C$]	k_g	0.0268

To recursively perform all the calculations, the terminal impedances of the last generations were assigned. This was done because none of the input tree reaches the terminal bronchioles ($n = 1$ of the Horsfield model) and therefore equation (2.42) for the case $n = 1$, although fully defined from an analytical point of view, could not be used. The chosen version of the code assigned a constant value of impedance to all the terminal segments, instead of it being variable. In this process either the order of the terminal branches was given as an input for the given tracheobronchial tree or it was matched with the closest order of the Habib table by evaluating the

measure of the diameter. The numerical values of the terminal impedance, were previously obtained for all the orders of the Habib table over a much wider frequency range.

Once the impedance of the terminal segments was known, equation (2.42) allowed to compute the terminal impedance for each upstream generation. The characteristic impedance and the impedance of the airways walls were obtained thanks to the relations (2.31)-(2.37). The acoustic pressure of each segment was calculated by evaluating formula (2.46) in nine different points along the segment itself. These results were eventually interpolated to obtain the final solution. The wall radial velocity was also interpolated over the same points.

3.2.1   Simulation of the Asthma Pathology

The pathology of asthma was simulated taking as a reference Ionescu et Al [43].

It was decided to evaluate the morphologic changes induced by the pathology in terms of radii and thickness of the constituent segments. The inflammation and thickening (due to the infiltration of mucus) of the airways was modeled by increasing the thickness (h) of each segment of 1.5 times. The increased thickness was related to the alteration of the radii through the following equation:

$$R_{asthma} = R_{healthy} - 0.5 \times h \qquad (3.3)$$

3.2.2   Simulation of the Airways Fibrosis Condition

The stiffening of the airways wall determined by the abnormal connective tissue growth characterizing the pathological fibrosis was modeled by increasing the elastic modulus of the airways wall. It was decided to multiply the physiological value by a factor 5.

3.2.3   <u>Simulation of Pulmonary Infiltrate Condition</u>

A unilateral pulmonary infiltrate was simulated. The occlusion was supposed to be localized on the lower lobe of the left lung. The consequent increased resistance of the tree was modelled by multiplying the impedance of the left lower lobe (LLL) terminal branches by a factor 10^5.

CHAPTER 4

NUMERICAL MODELS

Numerical simulations were performed in COMSOL Multiphysics® using the dedicated Acoustic - Solid Interaction Frequency Domain Modulus.

4.1   Generation of the Meshes

The meshes for the Finite Element Analysis (FEA) were generated in ANSYS ICEM CFD (ANSYS® Academic Research, Release 16.2). The geometries were exported from MATLAB generating 4 TCL (Tool Command Language) files: two for the inner part and two for the outer points. Each couple of files was meshed separately and then merged together. Some relevant features of the final merged meshes for the human model are reported in TABLE 7.

TABLE 7: FEATURES OF THE FINAL MERGED MESHES IN THE TWO RESPIRATORY PHASES CONSIDERED

Parameter	Inspiration	Expiration
Mesh Type	Tetrahedral/Mixed	Tetrahedral/Mixed
Number of Elements	1723666	1924363
Max Element Size	111.81x176.51x217.20	110.09x178.26x219.57
Min Element Size	24.37x0.63x2.87	23.15x1.15x1.89

Figure 7 and Figure 8 show the two generated meshes in ANSYS®.
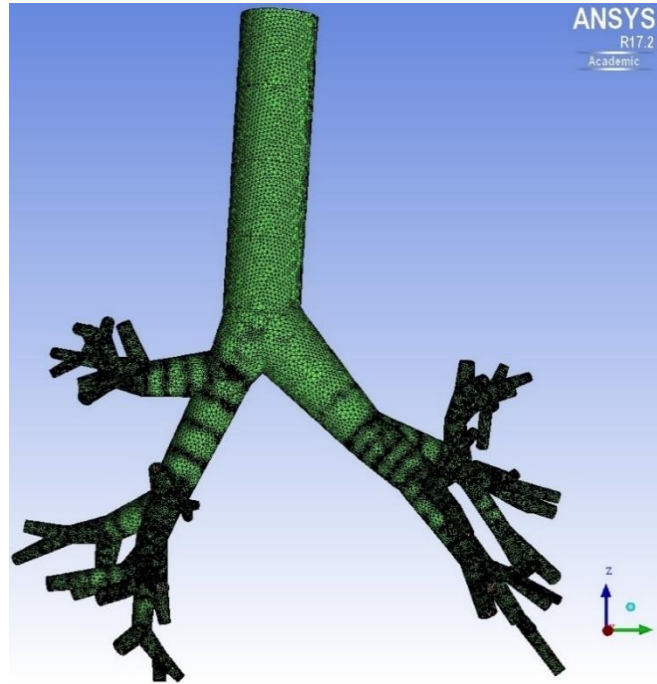
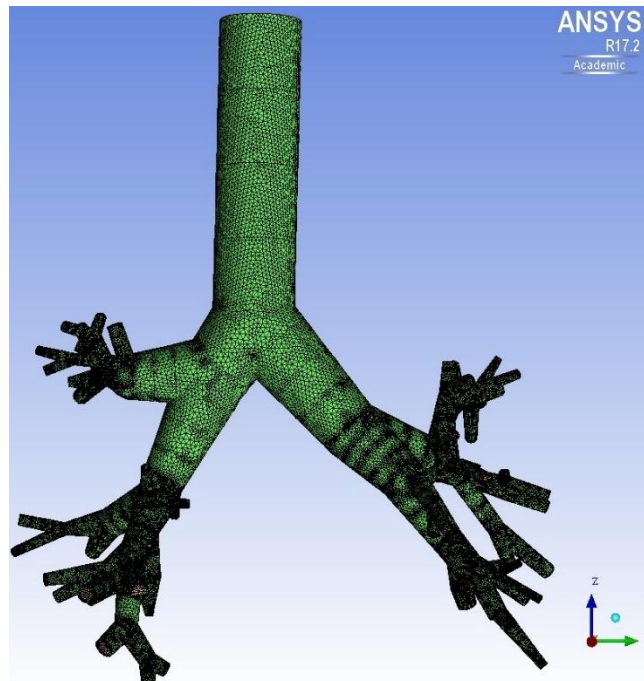Figure 7: Generated mesh in ANSYS® for the beginning of the inspiratory phase

Figure 8: Generated mesh in ANSYS® for the beginning of the expiratory phase.

4.2 <u>Acoustical Simulations</u>

The mesh was imported in COMSOL Multiphysics® as a data file. The computation of the geometry was automatically accomplished by the software. The analysis was performed in the frequency domain using the Acoustic - Solid Interaction Frequency Domain Modulus. The range of frequencies considered was 200-800 Hz, in accordance to the analytical model. The amplitude of the input pressure was assumed to be equal to 1 Pa in accordance with the analytical model. The pressure was input at the level of the trachea. Three boundaries were defined: two for the inlet and the outlets and one for the annulus of the trachea. Furthermore, for both air and thickness two domains were introduced. The airways wall was assumed to be composed by soft tissue only. The acoustic properties of the model were set in the acoustic modulus. The acoustic impedance of the terminal branches was assumed to be constant over a chosen frequency. The frequency dependent values were obtained by curve fitting the trend of those terminal impedances in MATLAB for both the real and imaginary part. The complex-valued impedance was then multiplied by the average cross-sectional area of the terminal branches themselves. The results of the fitting were the same for both the expiratory and inspiratory phase and are reported in Figure 9.
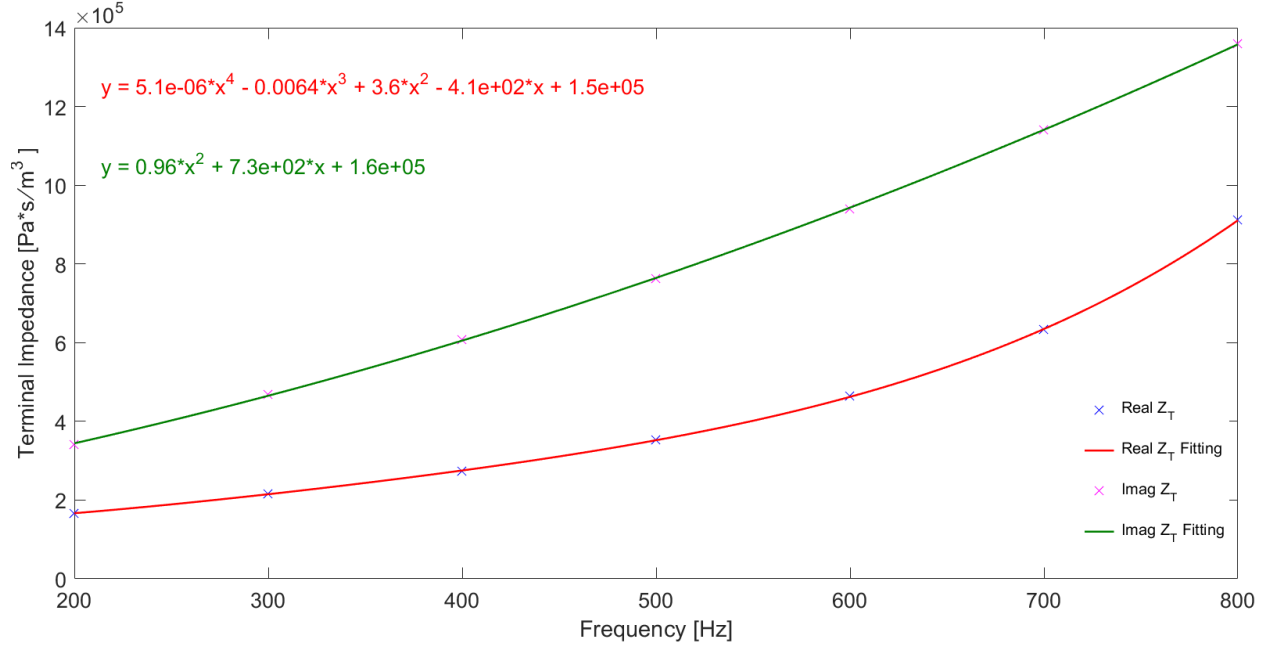
Figure 9: Terminal impedance (Z_T) curve fitting. Results were proven to be valid for both the inspiratory and expiratory phase

It can be observed that the real part of the terminal impedance was fit with a 4th order polynomial whereas the imaginary part was well approximated by a quadratic form.

The mechanical properties of the constituent materials were defined in accordance to the analytical model. Both the properties of the biological tissue and the air were introduced and are reported in TABLE 8 and TABLE 9, respectively.

TABLE 8: SOFT TISSUE MECHANICAL PROPERTIES FOR THE NUMERICAL SIMULATIONS

Property	Symbol	Value
Density of Soft Tissue [Kg/m^3]	ρ_s	1060
Elastic Modulus of Soft Tissue [Pa]	Y_s	3.92×10^5

TABLE 9: AIR MECHANICAL PROPERTIES FOR THE NUMERICAL SIMULATIONS

Property	Symbol	Value
Density of Air [Kg/m^3]	ρ_a	1.14
Speed of Sound [m/s]	c_a	343
Poisson Ratio	ν_a	0.4995

In the solid-mechanics module, the hold bar boundary at the level of the annulus of the trachea was defined as a fixed constrain (no displacement).

CHAPTER 5

RESULTS

In this section the results of the study are reported. In first place, it is demonstrated the validity of the analytical model by comparing the results of the analytical MATLAB simulations with the numerical COMSOL Multiphysics® simulations for the healthy case of both the inspiratory and expiratory phase. For sake of simplicity and effectiveness of the visualization, the results will be shown only for the following frequencies: 200 Hz, 400Hz, 600Hz and 800 Hz.

5.1   <u>Validation of the Analytical Model</u>

The results for the inspiratory and expiratory phases from both analytical and numerical model are reported for the four frequencies of interest. The results for the beginning of the inspiratory phase are introduced first. Figure 10 and Figure 11 report a plot of the magnitude of the acoustic pressure normalized in logarithmic scale whereas the results in terms of real part of the acoustic pressure are shown in Figure 12 and Figure 13.

As regards the results for the beginning of the expiratory phase at the frequencies of interest. Figure 14-Figure 15 and Figure 16-Figure 17 show the trend of the magnitude (expressed in logarithmic scale) and of the real part of the acoustic pressure, respectively.

Analytical Result at 200 Hz

Numerical Result at 200 Hz

Analytical Result at 400 Hz

Numerical Result at 400 Hz

Figure 10: Magnitude of acoustic pressure in logarithmic scale [dB]. Comparison between the analytical (left) and numerical (right) results for 200 Hz (top) and 400 Hz (bottom) at the beginning of the inspiratory phase

Analytical Result at 600 Hz

Numerical Result at 600 Hz

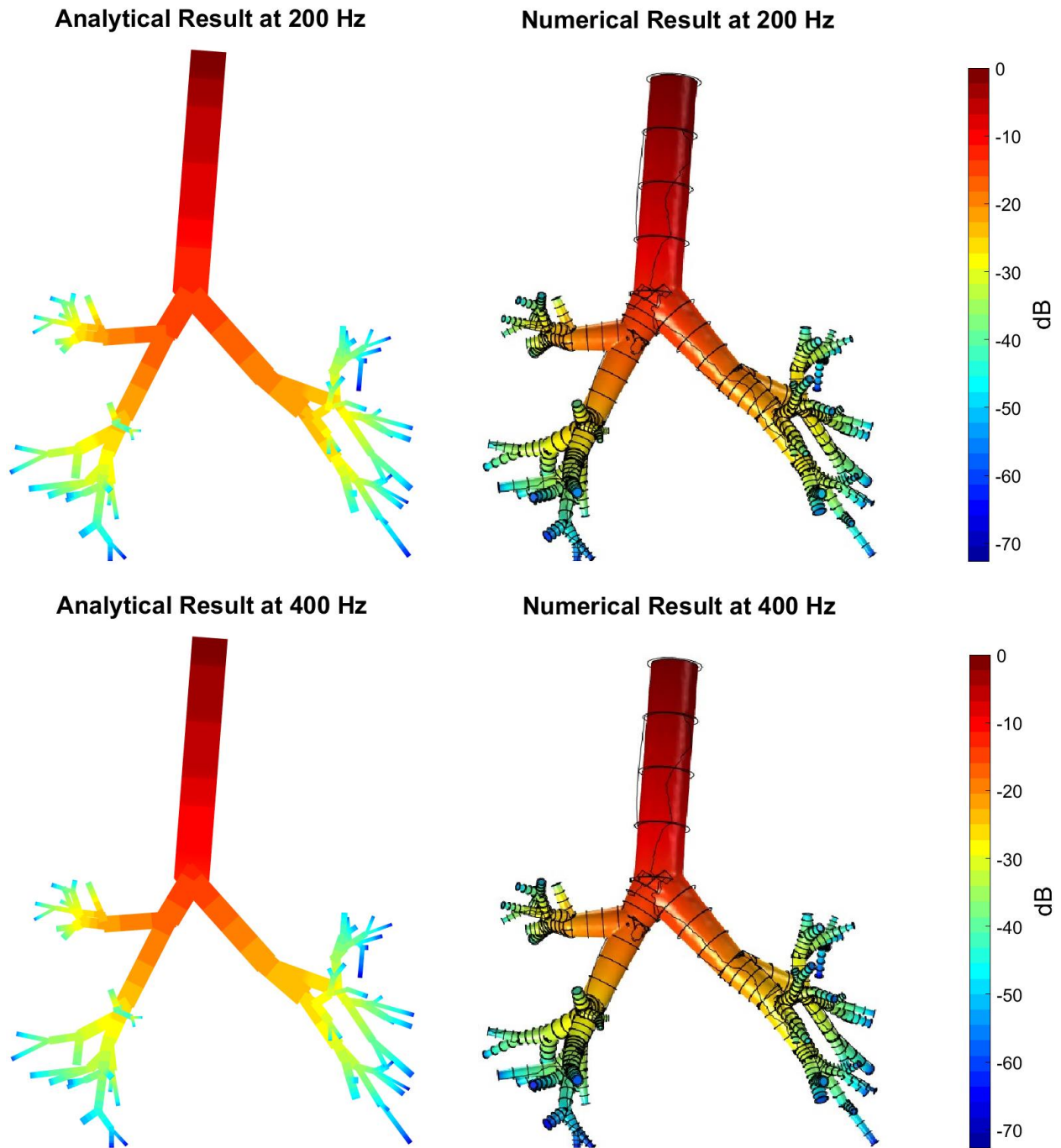**Analytical Result at 800 Hz**

Numerical Result at 800 Hz

Figure 11: Magnitude of acoustic pressure in logarithmic scale [dB]. Comparison between the analytical (left) and numerical (right) results for 600 Hz (top) and 800 Hz (bottom) at the beginning of the inspiratory phase

Analytical Result at 200 Hz

Numerical Result at 200 Hz

Analytical Result at 400 Hz

Numerical Result at 400 Hz

Figure 12: Real part of acoustic pressure. Comparison between the analytical (left) and numerical (right) results for 200 Hz (top) and 400 Hz (bottom) at the beginning of the inspiratory phase

Figure 13: Real part of acoustic pressure. Comparison between the analytical (left) and numerical (right) results for 600 Hz (top) and 800 Hz (bottom) at the beginning of the inspiratory phase

Analytical Result at 200 Hz

Numerical Result at 200 Hz

Analytical Result at 400 Hz
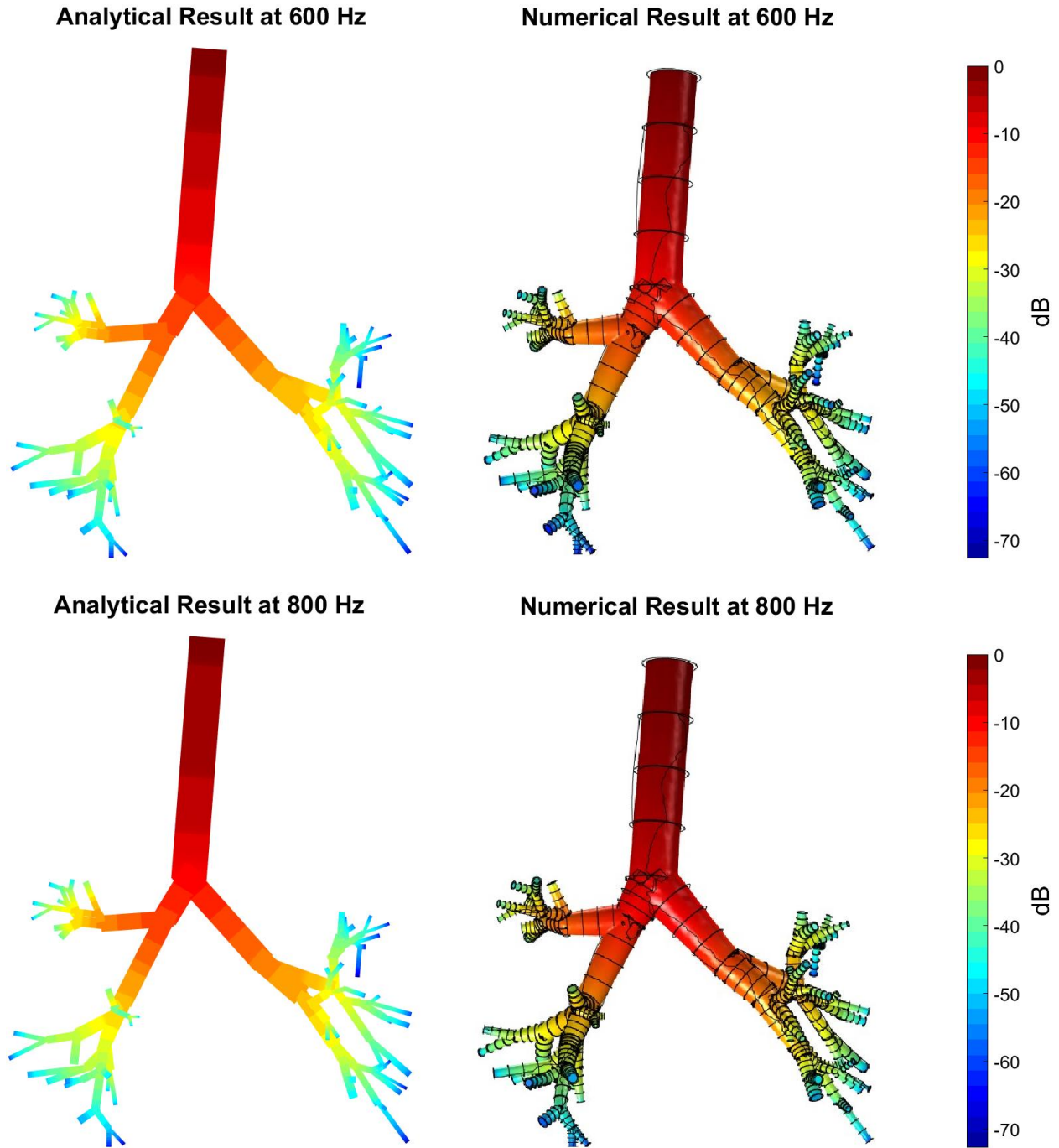
Numerical Result at 400 Hz

Figure 14: Magnitude of acoustic pressure in logarithmic scale [dB]. Comparison between the analytical (left) and numerical (right) results for 200 Hz (top) and 400 Hz (bottom) at the beginning of the expiratory phase
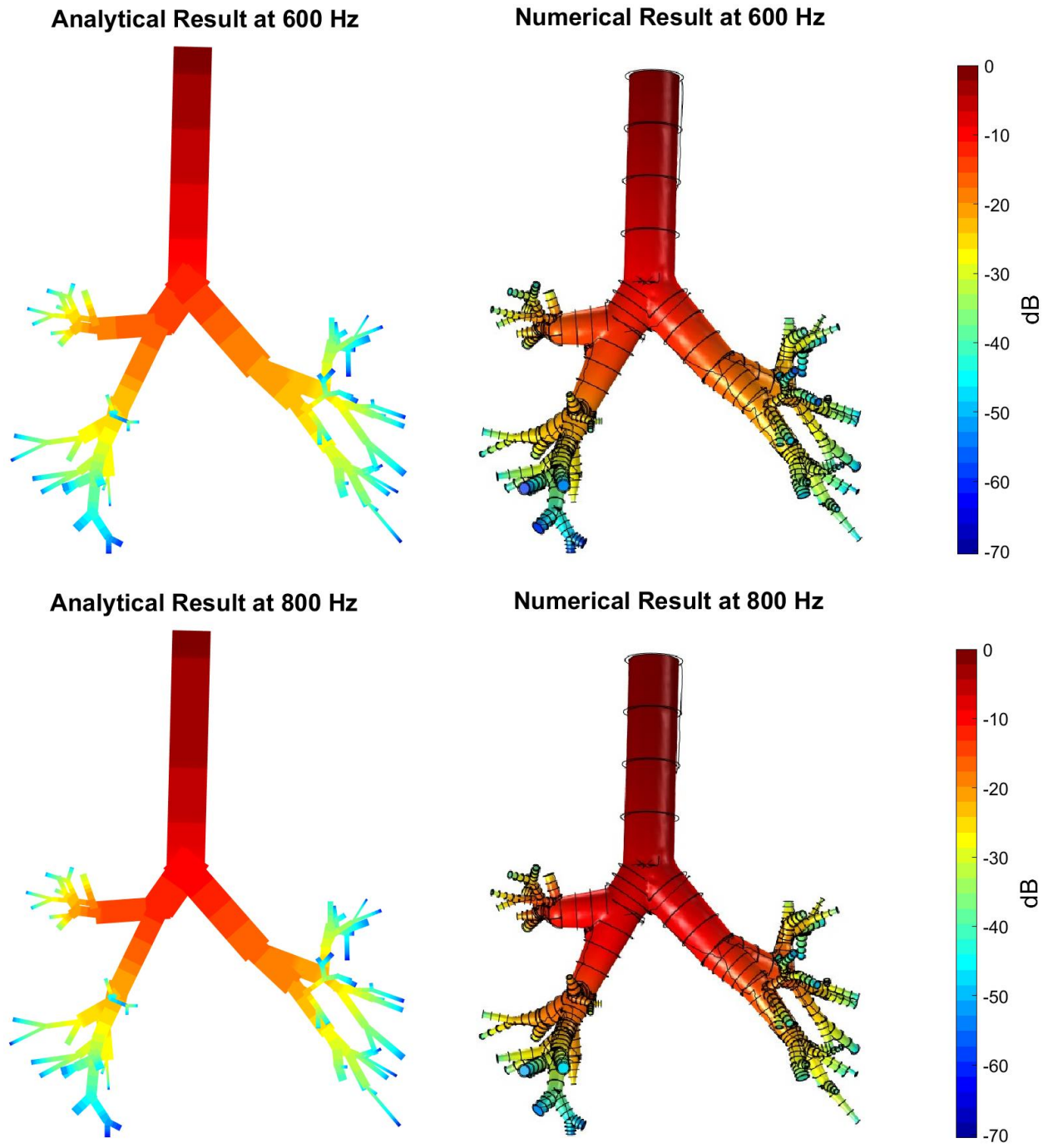
Figure 15: Magnitude of acoustic pressure in logarithmic scale [dB]. Comparison between the analytical (left) and numerical (right) results for 600 Hz (top) and 800 Hz (bottom) at the beginning of the expiratory phase

Analytical Result at 200 Hz **Numerical Result at 200 Hz**

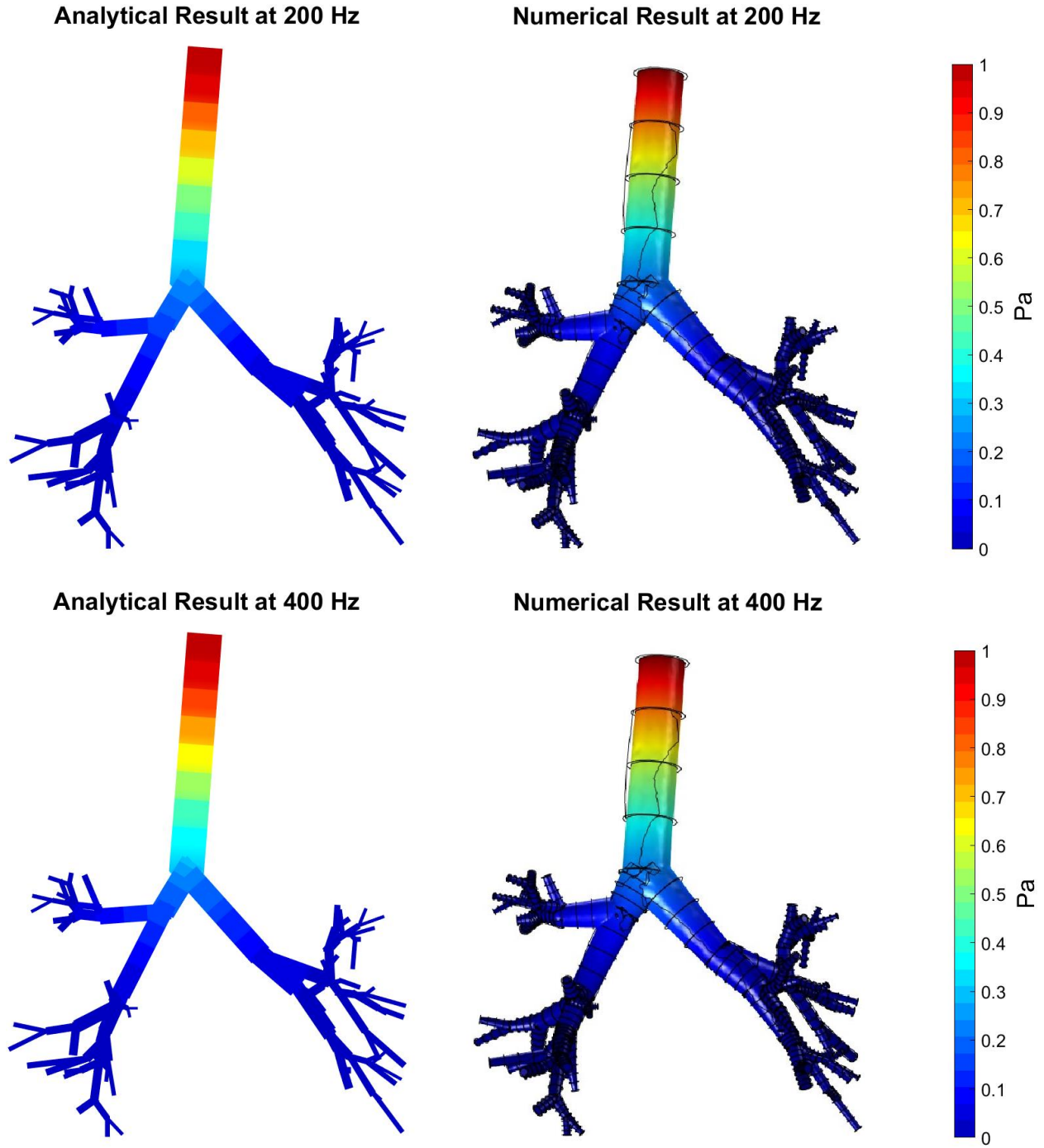**Analytical Result at 400 Hz** **Numerical Result at 400 Hz**

Figure 16: Real part of acoustic pressure. Comparison between the analytical (left) and numerical (right) results for 200 Hz (top) and 400 Hz (bottom) at the beginning of the expiratory phase
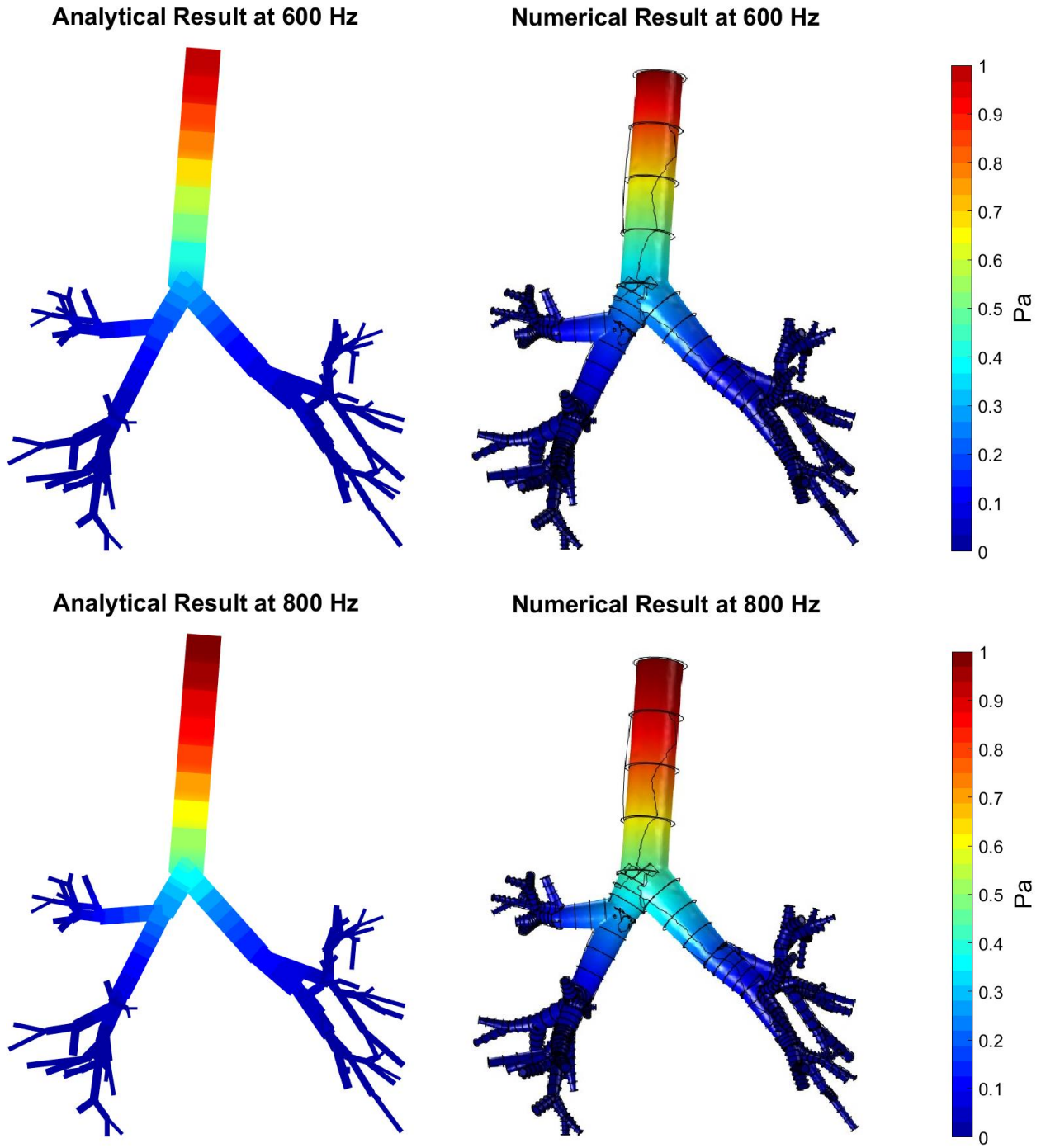
Figure 17: Real part of acoustic pressure. Comparison between the analytical (left) and numerical (right) results for 600 Hz (top) and 800 Hz (bottom) at the beginning of the expiratory phase
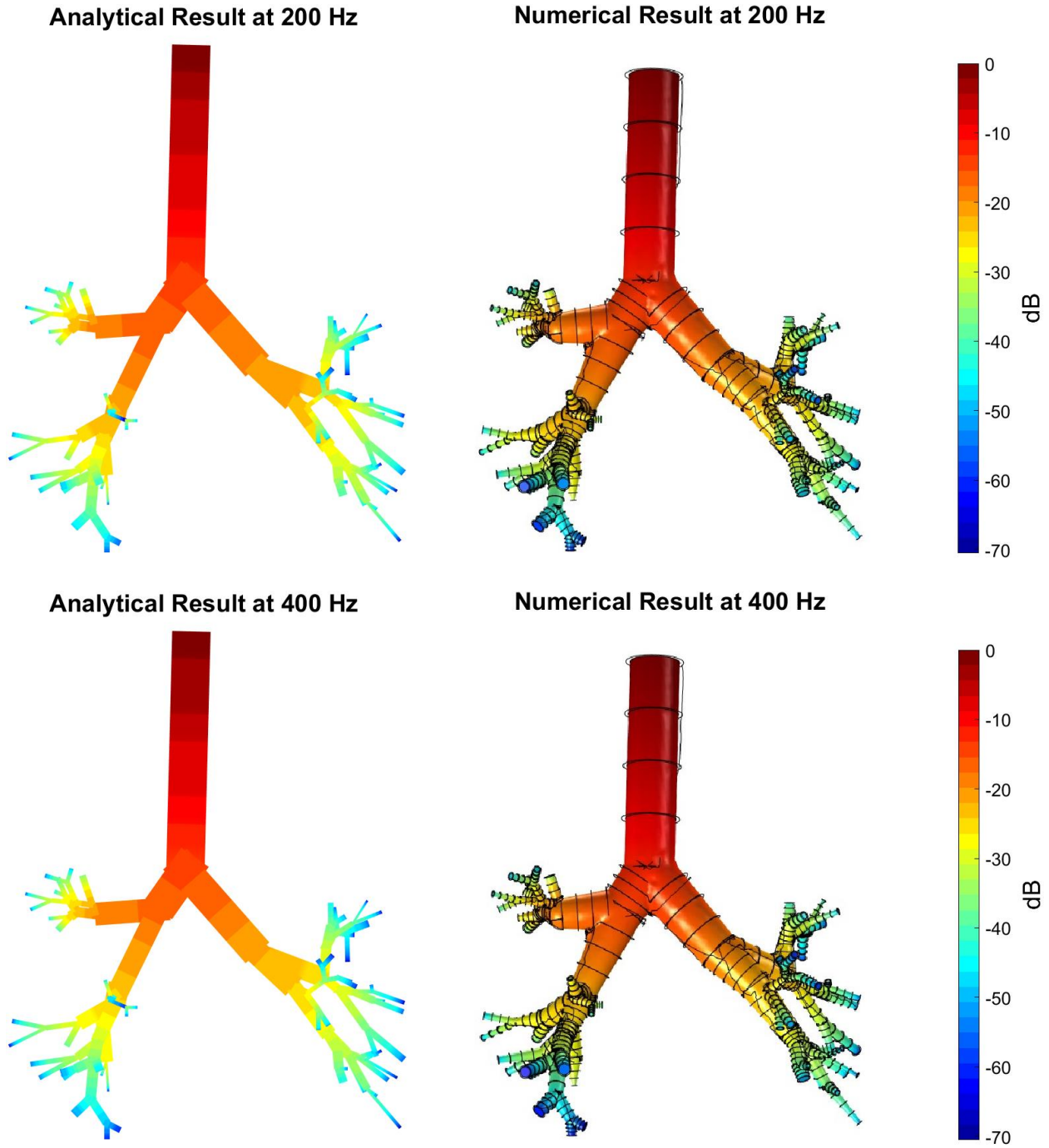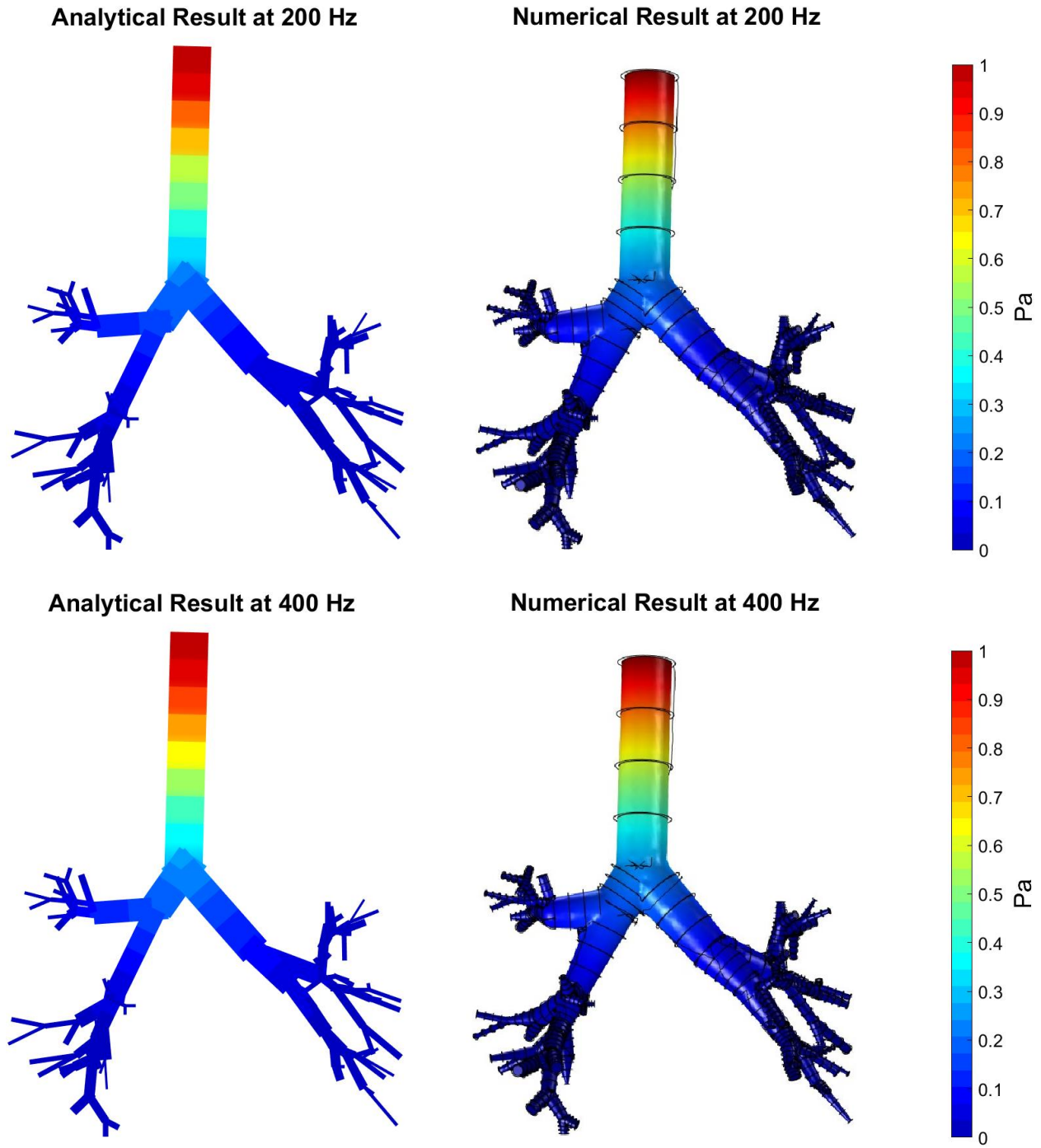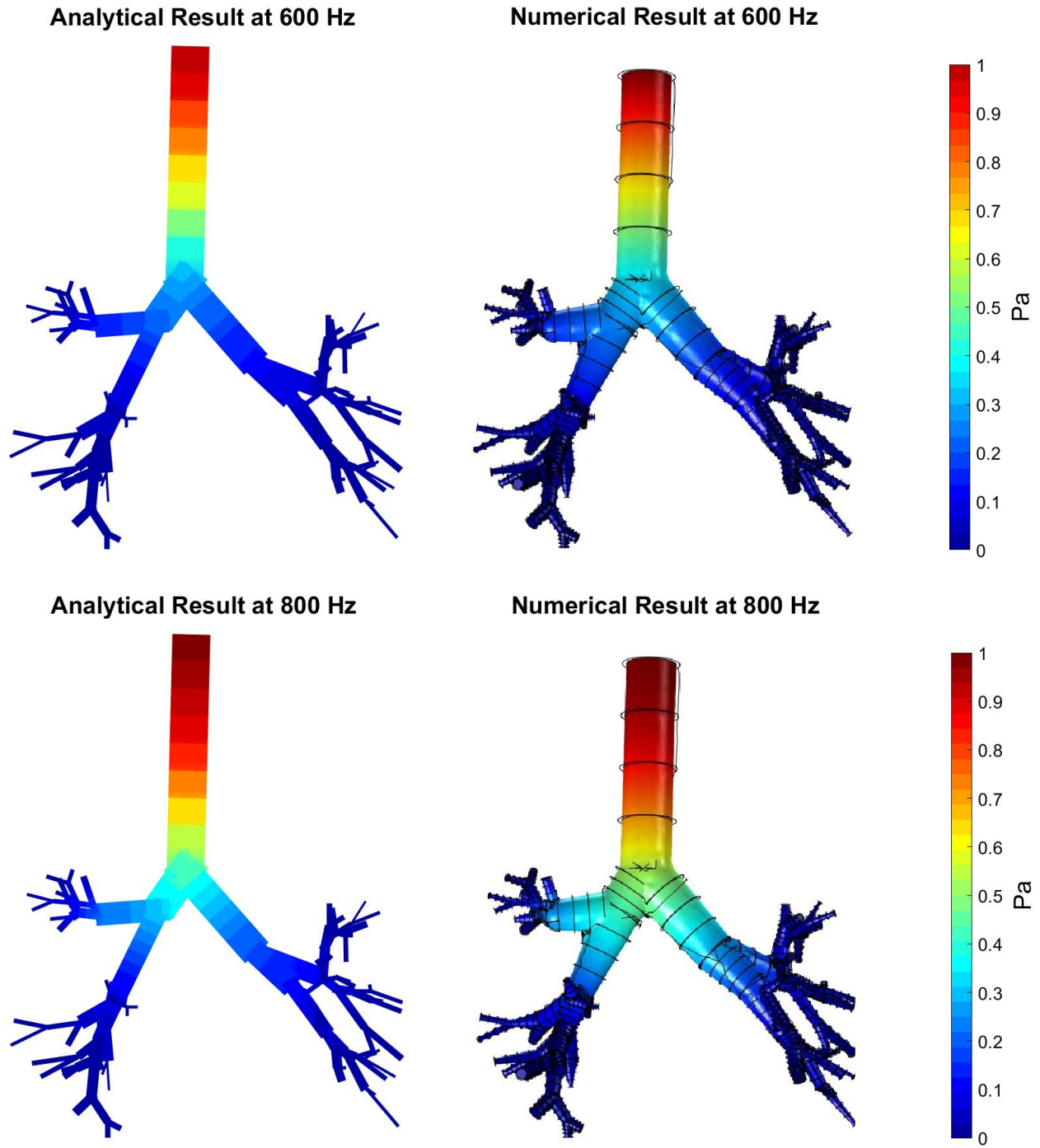
To obtain a quantitative evaluation of the degree of precision of the analytical model an error analysis was performed in MATLAB. The parameter assessed in this analysis was the magnitude of the acoustic pressure expressed in logarithmic scale. For each branch, the numerical data were exported from COMSOL Multiphysics® in correspondence to the 9 interpolating points used in MATLAB to maximize the level of accuracy of the analysis. Figure 18 shows the procedure of identification of the interpolating points in the COMSOL Multiphysics® interface for the inspiratory model, the very same procedure was performed on the expiratory one.

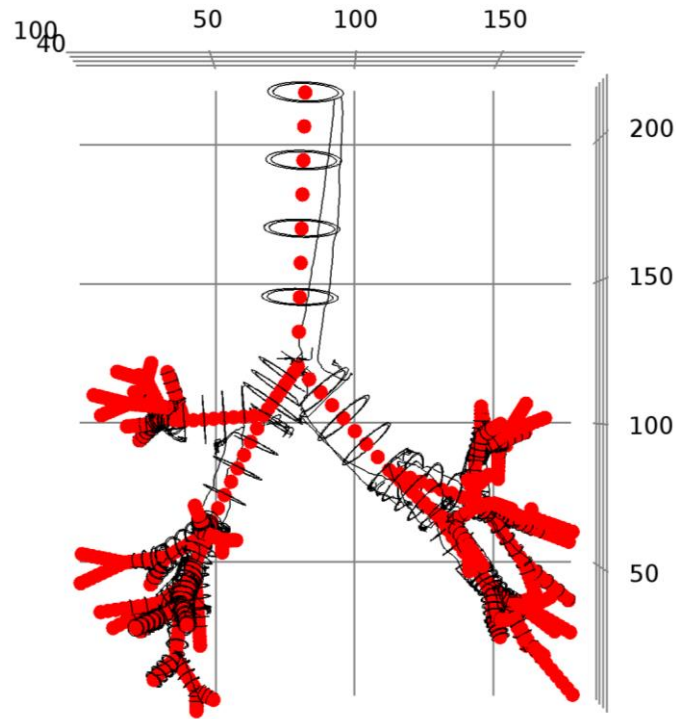Figure 18: Identification of the interpolating points in COMSOL Multiphysics®.

Starting from the model of the beginning of inspiration the results of the analysis of the error in terms of visual representation and distribution are reported in the Figure 19 and Figure 20.
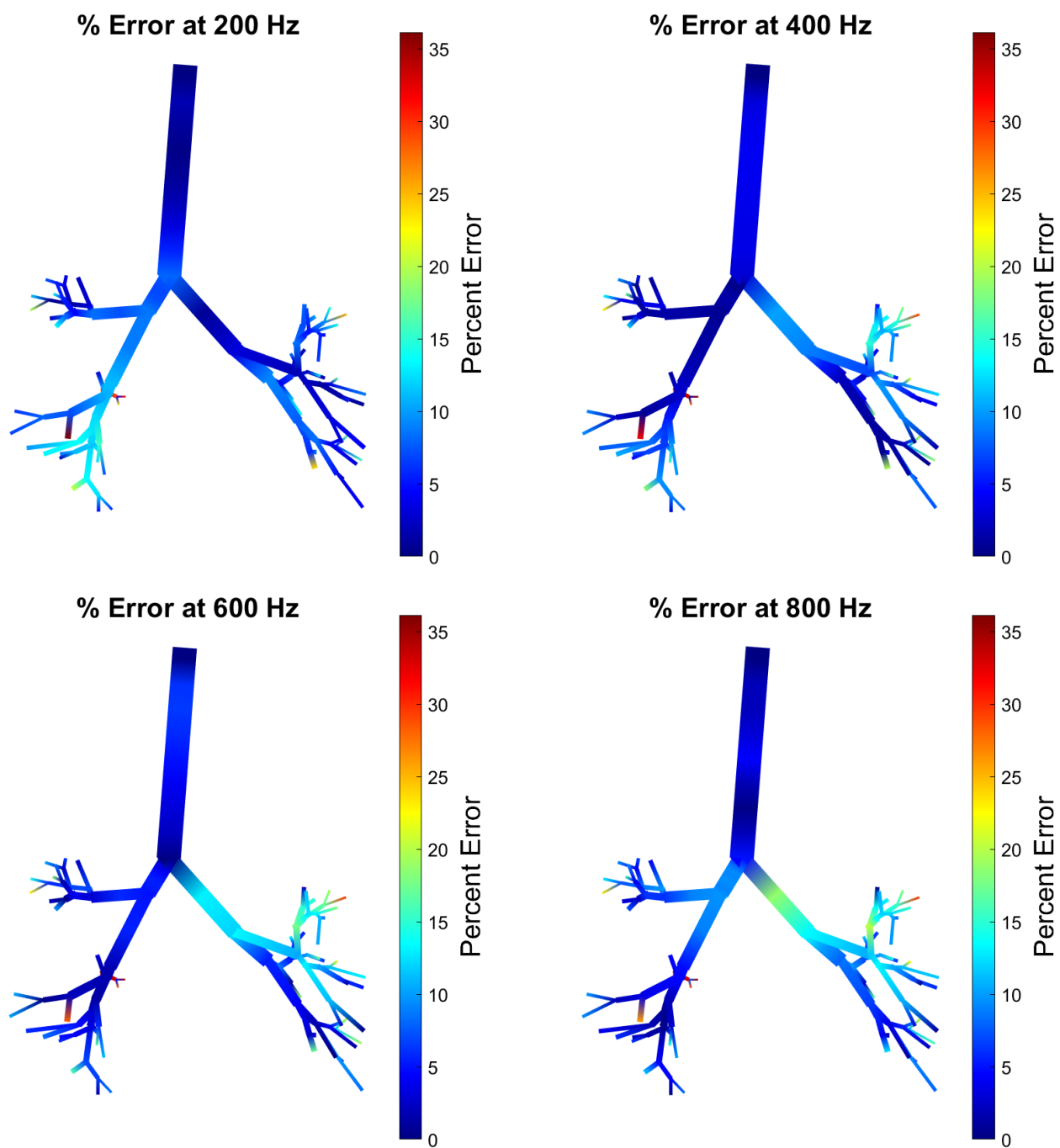
Figure 19: Error representation for the beginning of the inspiratory phase at 200 Hz (top-left), 400 Hz (top-right), 600 Hz (bottom-left) and 800Hz (bottom-right)

Figure 20: Beginning of the inspiratory phase - distribution of the error for the four frequencies of interest

The median and the maximum value of the error in the case of the inspiratory phase and for the frequencies of interest are reported in TABLE 10.

TABLE 10: ANALYSIS OF THE ERROR FOR THE BEGINNING OF INSPIRATORY PHASE – MEDIAN AND MAXIMUM VALUE FOR THE FOUR FREQUENCIES OF INTEREST

Frequency [Hz]	200	400	600	800
Median Error [%]	5.43	4.60	5.86	7.87
Max Error [%]	34.96	31.14	32.75	36.14

The results of the analysis concerning the beginning of expiration are shown in Figure 21 and Figure 22.
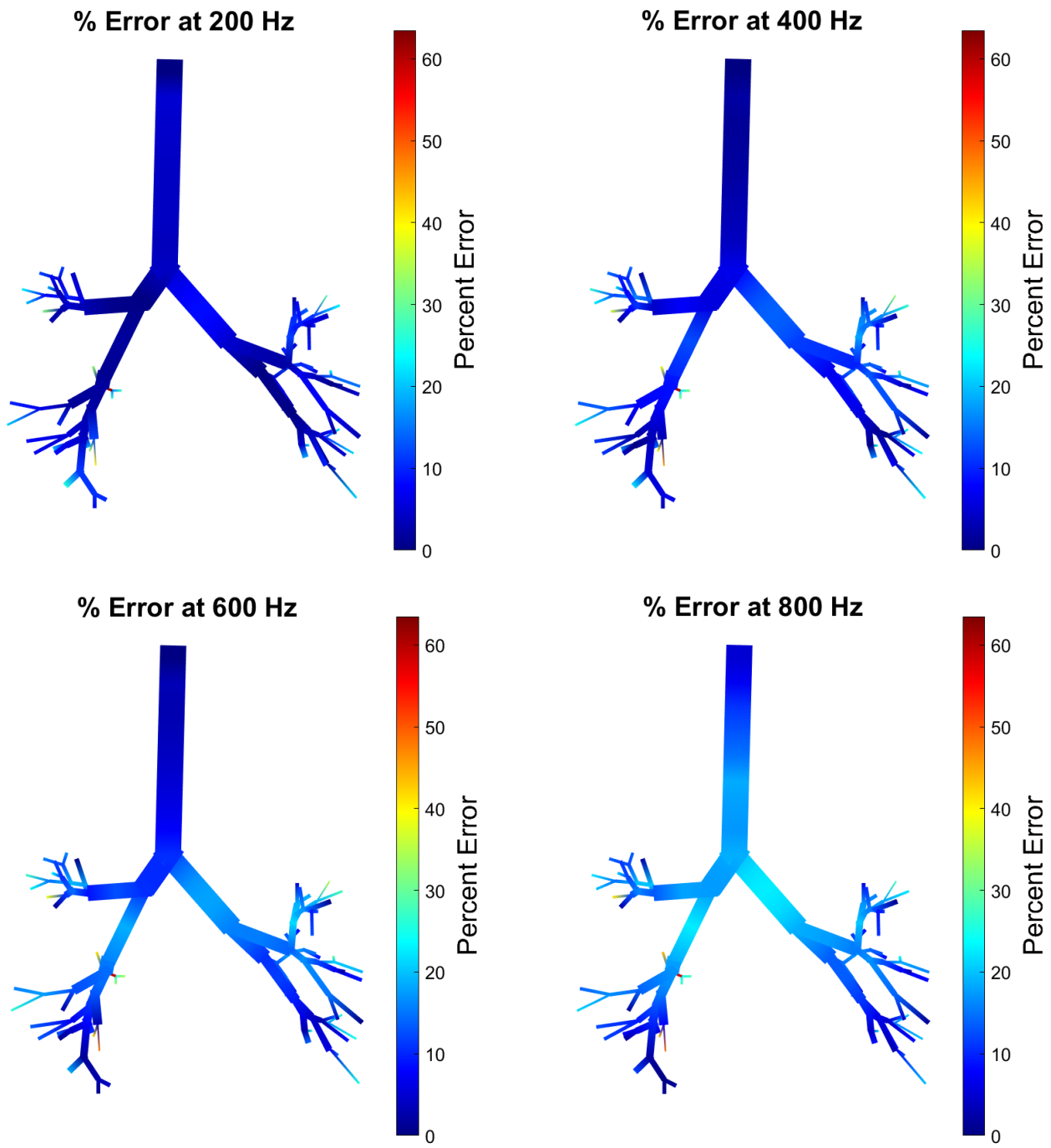
Figure 21: Error representation for the beginning of the expiratory phase at 200 Hz (top-left), 400 Hz (top-right), 600 Hz (bottom-left) and 800Hz (bottom-right)
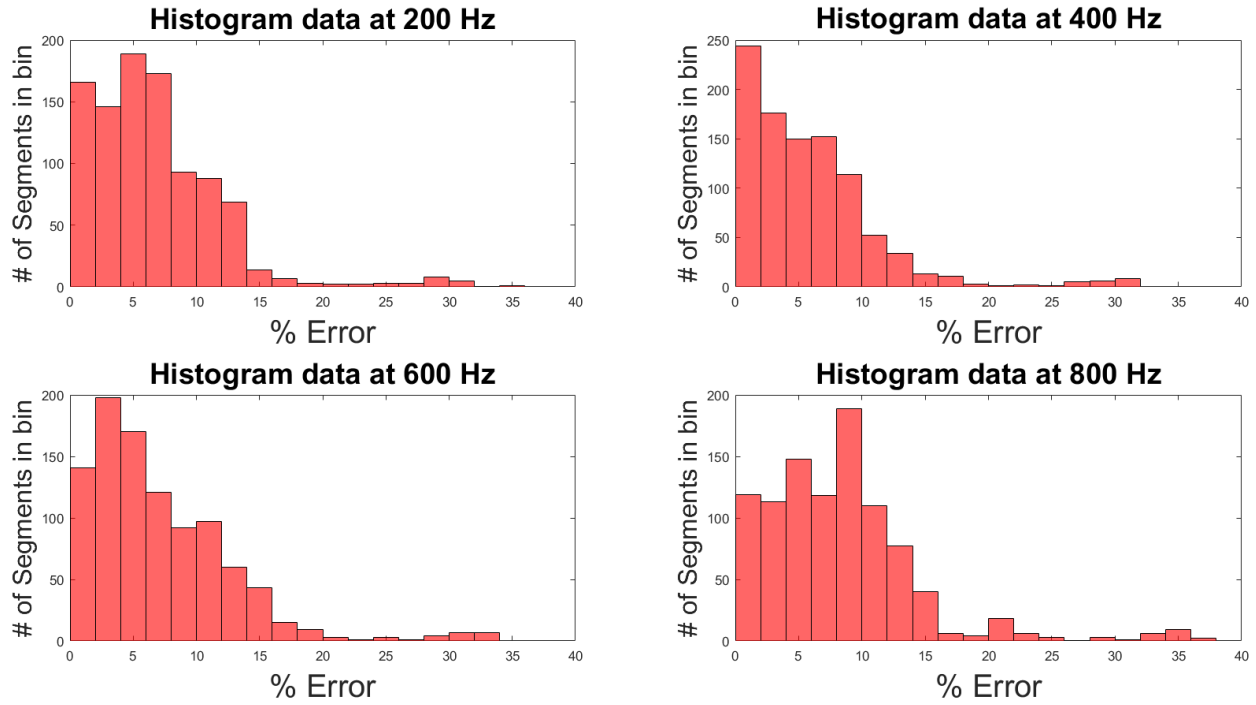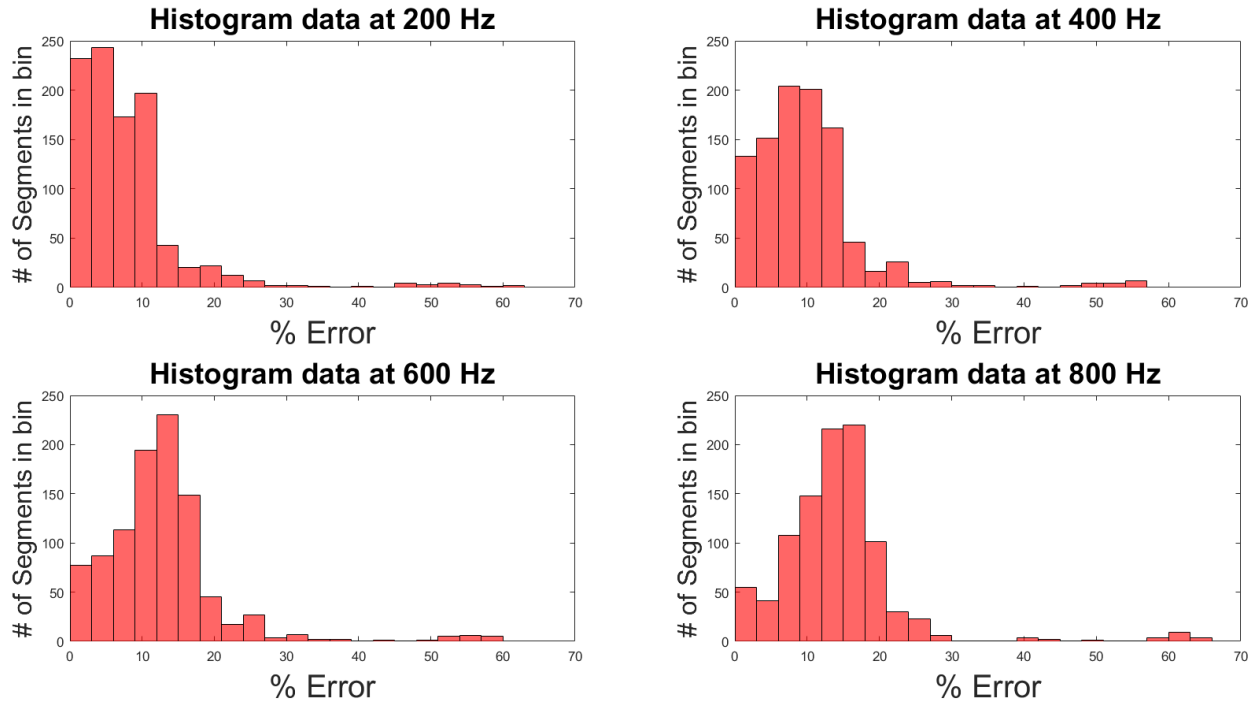
Figure 22: Beginning of the expiratory phase - distribution of the error for the four frequencies

The median and the maximum value of the error in the case of the expiratory phase and for the frequencies of interest are reported in TABLE 11.

TABLE 11: ANALYSIS OF THE ERROR FOR THE BEGINNING OF EXPIRATORY PHASE – MEDIANF AND MAXIMUM VALUE FOR THE FOUR FREQUENCIES OF INTEREST

Frequency [Hz]	200	400	600	800
Median Error [%]	6.37	9.01	12.40	13.91
Max Error [%]	62.74	56.55	57.64	63.48

Given the results presented in this section and the as it will be further discussed in 6.1, the model results to be validated.

5.2   <u>**Comparison Between the Beginning of Inspiratory and Expiratory Phases**</u>

The response to the inlet pressure of both the beginning of the inspiratory phase and the beginning of the expiratory phases are reported. The comparison is reported only for two frequencies: the lowest and the highest one, namely 200 Hz and 800 Hz. Three parameters are presented: the magnitude (in logarithmic scale) and the real part of the acoustic pressure and the magnitude of the airways wall radial velocity (in logarithmic scale). For the parameters related to pressure, it was also analyzed the trend in the trachea and the main two bronchi. As regard, the magnitude of the wall radial velocity for sake of effectiveness of the visualization and of the comparison, it was chosen to assume the velocity to be constant over the segment and equal to the value computed at the distal interpolating point of the segment. For this parameter, the distal value of the trachea and the two main bronchi will be evaluated.

Figure 23: Magnitude of the acoustic pressure in logarithmic scale at 200 Hz. Comparison between the beginning of the inspiratory phase (left) and the beginning of expiratory phase (right)

Figure 24: Trend of the magnitude of the acoustic pressure in logarithmic scale at 200 Hz in the trachea (left), left main Bronchus (middle) and right main bronchus (right) for the inspiratory (blue) and expiratory (orange) phases.

**Magnitude of Pressure at 800 Hz
Beginning of Inspiratory Phase**

**Magnitude of Pressure at 800 Hz
Beginning of Expiratory Phase**

Figure 25: Magnitude of the acoustic pressure in logarithmic scale at 800 Hz. Comparison between the beginning of the inspiratory phase (left) and the beginning of expiratory phase (right).

Figure 26: Trend of the magnitude of the acoustic pressure in logarithmic scale at 200 Hz in the trachea (left), left main Bronchus (middle) and right main bronchus (right) for the inspiratory (blue) and expiratory (orange) phases.
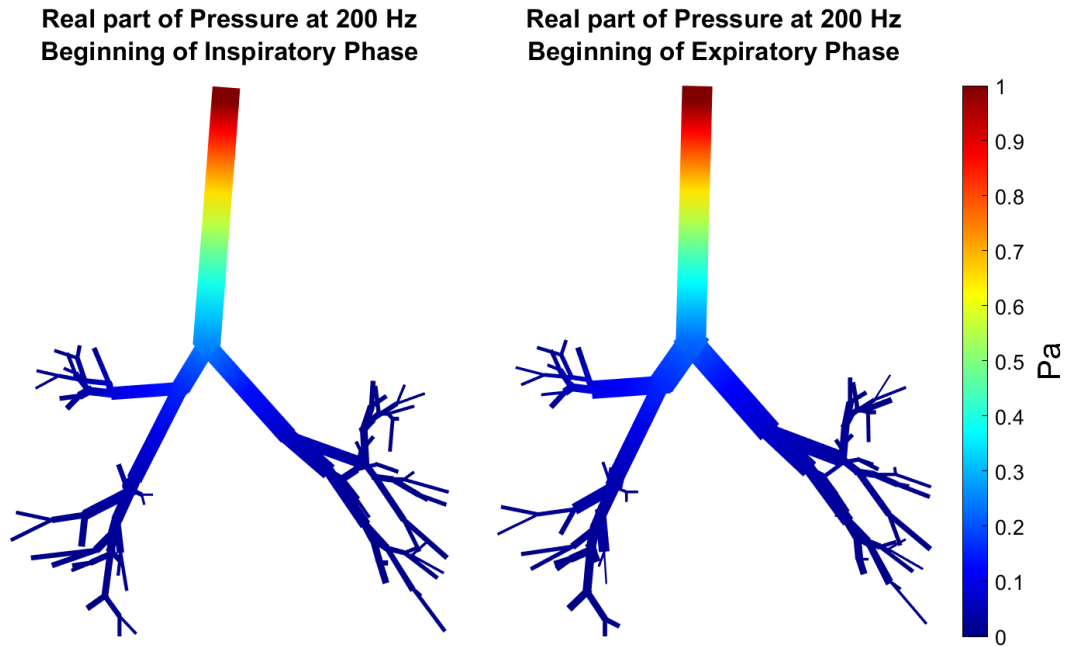
Figure 27: Real part of the acoustic pressure in logarithmic scale at 200 Hz. Comparison between the beginning of the inspiratory phase (left) and the beginning of expiratory phase (right).

Figure 28: Trend of the real part of the acoustic pressure in logarithmic scale at 200 Hz in the trachea (left), left main Bronchus (middle) and right main bronchus (right) for the inspiratory (blue) and expiratory (orange) phases.
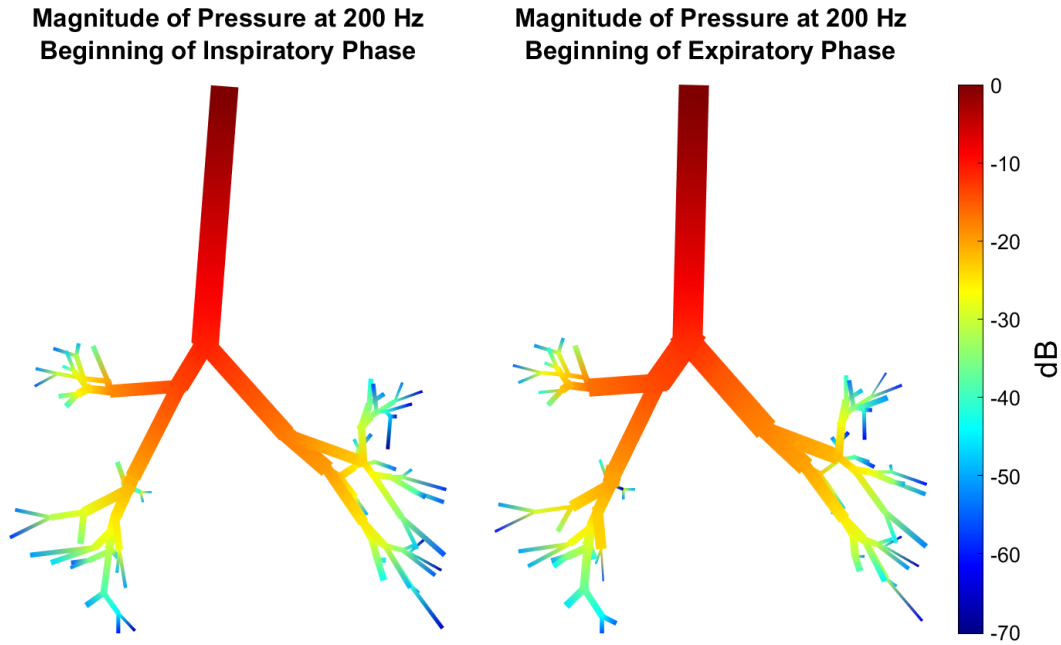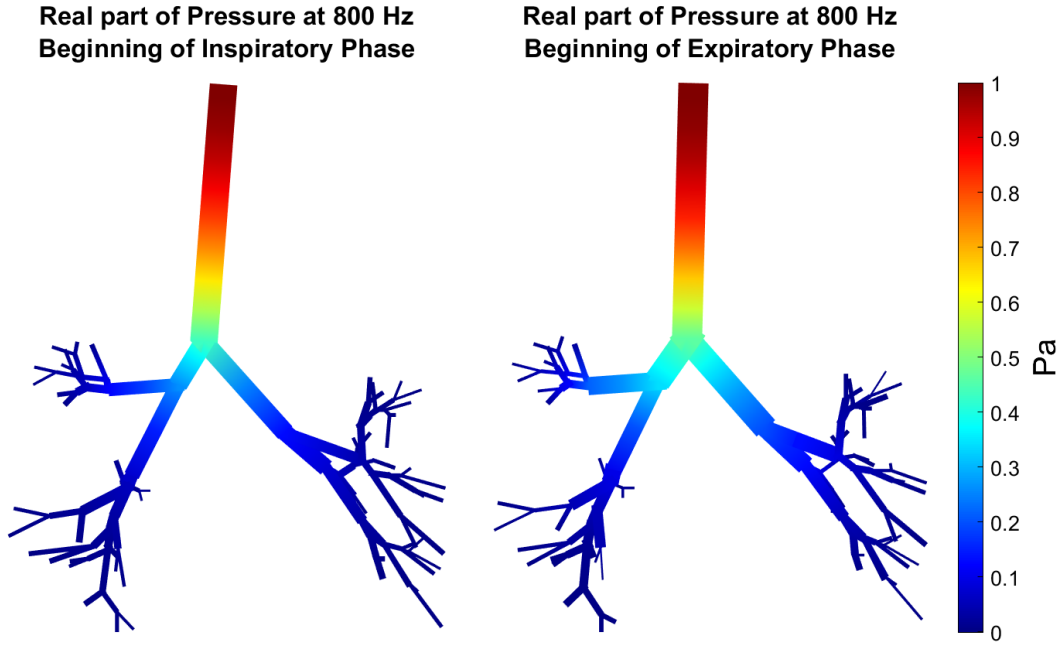
Figure 29: Real part of the acoustic pressure in logarithmic scale at 800 Hz. Comparison between the beginning of the inspiratory phase (left) and the beginning of expiratory phase (right).
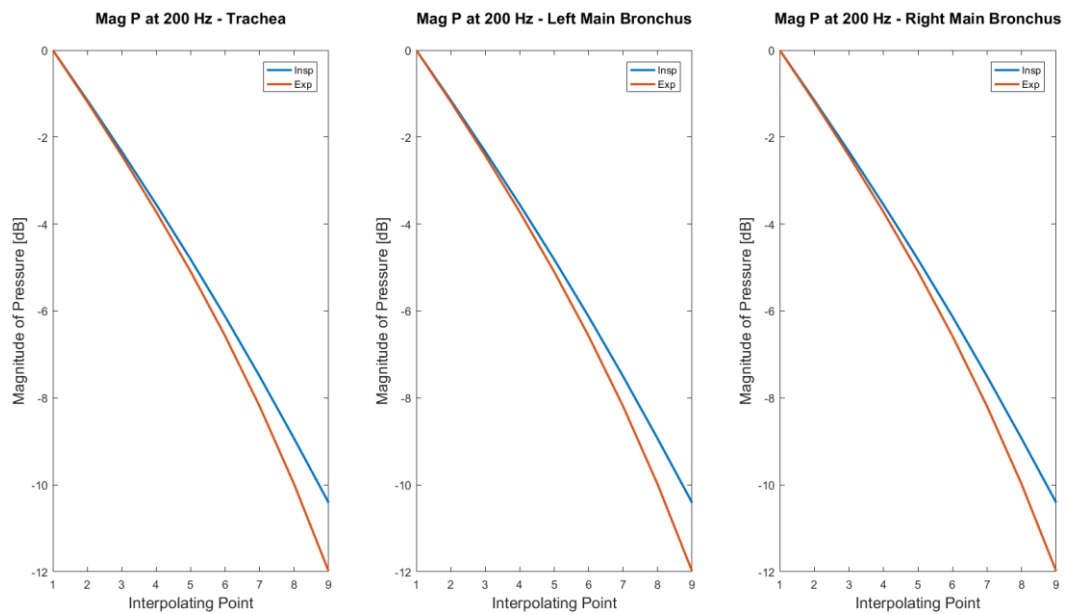

Figure 30: Trend of the real part of the acoustic pressure in logarithmic scale at 800 Hz in the trachea (left), left main Bronchus (middle) and right main bronchus (right) for the inspiratory (blue) and expiratory (orange) phases.
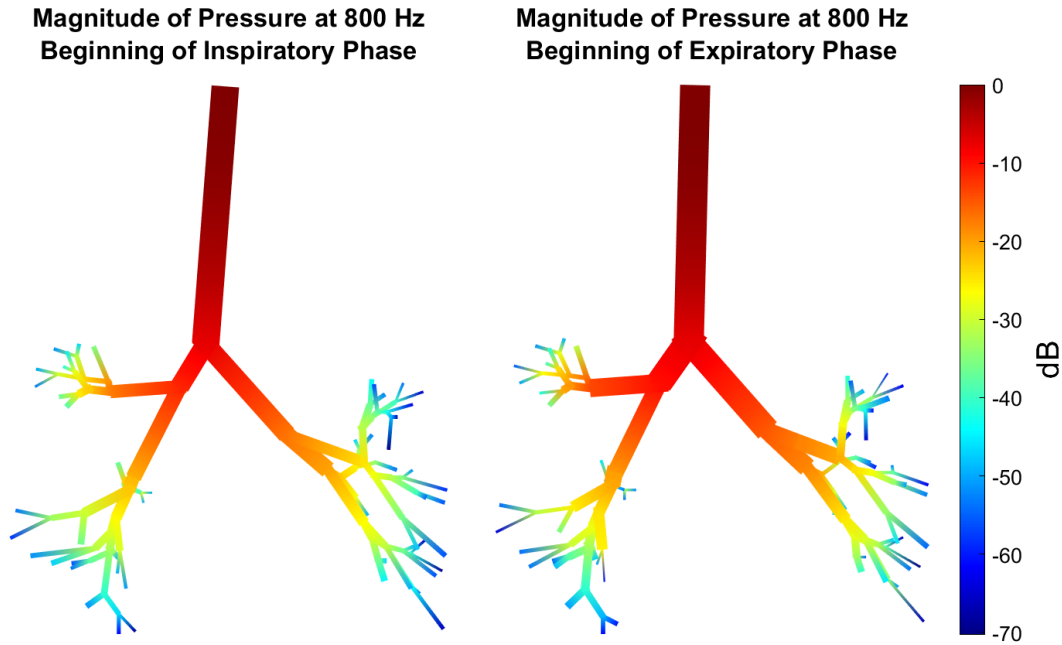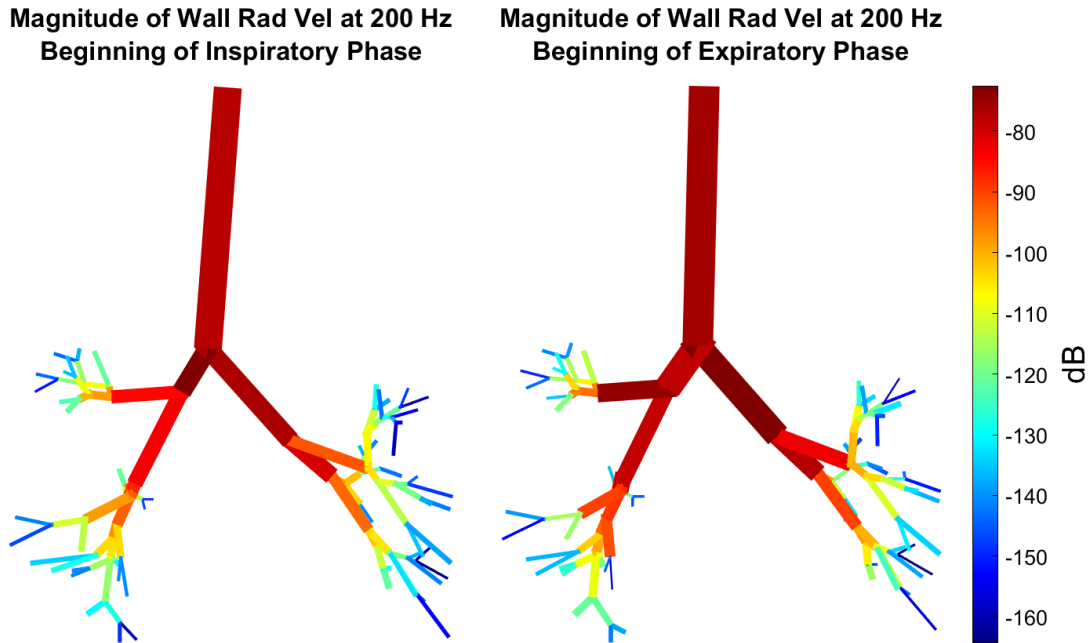
Figure 31: Magnitude of the wall radial velocity in logarithmic scale at 200 Hz. Comparison between the beginning of the inspiratory phase (left) and the beginning of expiratory phase (right).
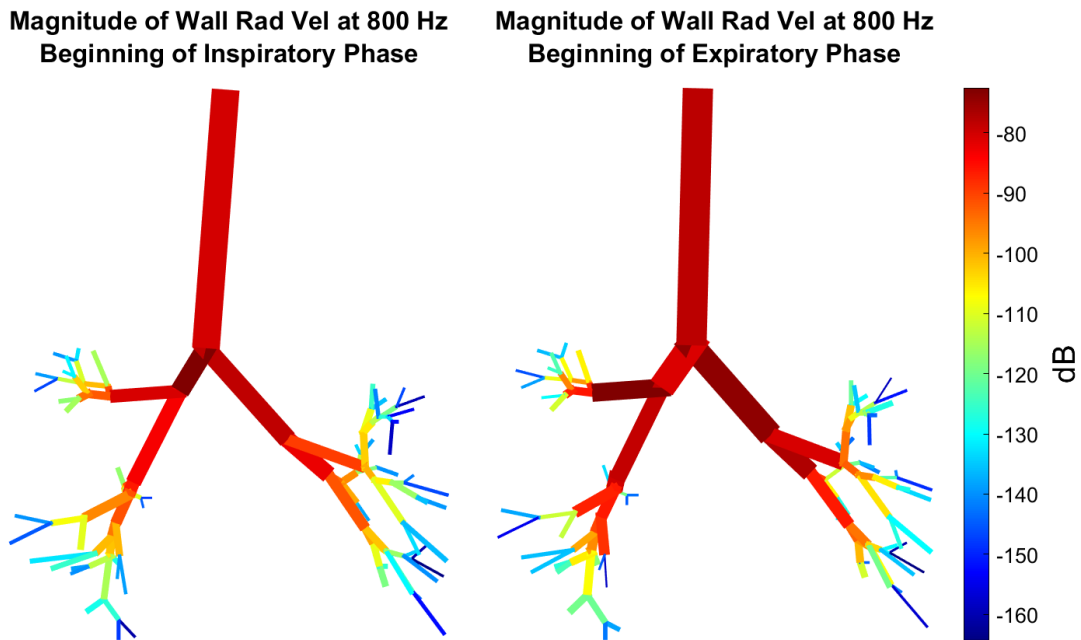
Figure 32: Magnitude of the wall radial velocity in logarithmic scale at 800 Hz. Comparison between the beginning of the inspiratory phase (left) and the beginning of expiratory phase (right).

5.3   **<u>Simulation of Pathological Conditions</u>**

The results concerning the simulations of the pathological conditions analyzed in this dissertation are reported in the following paragraphs. Given the similarity in terms of results of the two respiratory phases considered (see Section 5.2) and the associated discussion in Chapter 6, the results concerning the modification induced by the pathological conditions are here reported for the inspiratory phase only. Exclusively the results concerning the response the response of the system for the 200 Hz and 800 Hz frequencies will be presented. Three parameters will be evaluated: the magnitude (in logarithmic scale) and the real part of the acoustic pressure and the magnitude of the airways wall radial velocity.

5.3.1   **<u>Simulation of the Asthma Pathology</u>**

The results regarding the simulation of the asthma pathology are reported in the following paragraph. For each parameter, the qualitative distribution over the entire tree and the trend in the trachea and the main bronchi are presented.

Figure 33: Magnitude of the acoustic pressure in logarithmic scale at 200 Hz. Comparison between healthy (left) and asthma (right)
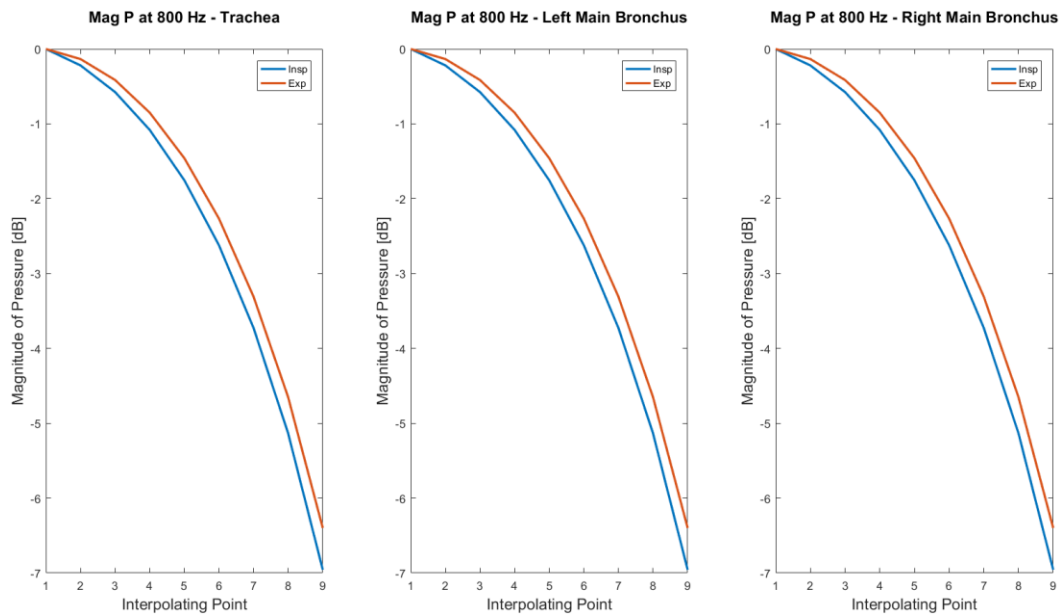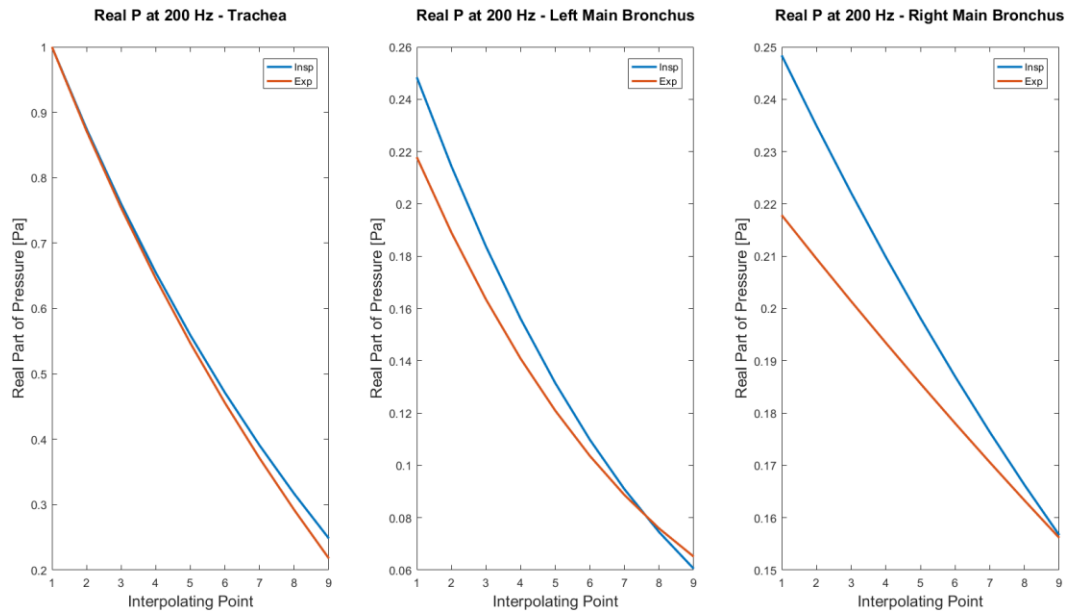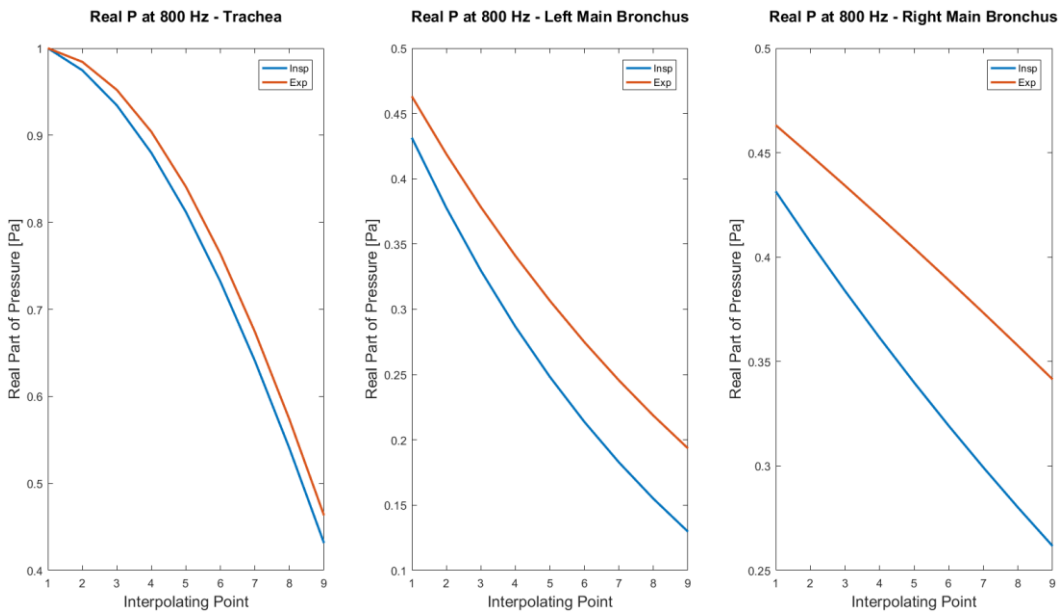

Figure 34: Trend of the magnitude of the acoustic pressure in logarithmic scale at 200 Hz in the trachea (left), left main Bronchus (middle) and right main bronchus (right) for the healthy case (green) and asthma case (red).

Figure 35: Magnitude of the acoustic pressure in logarithmic scale at 800 Hz. Comparison between healthy (left) and asthma (right)

Figure 36: Trend of the magnitude of the acoustic pressure in logarithmic scale at 800 Hz in the trachea (left), left main Bronchus (middle) and right main bronchus (right) for the healthy case (green) and asthma case (red).

Figure 37: Real part of the acoustic pressure in logarithmic scale at 200 Hz. Comparison between healthy (left) and asthma (right)

Figure 38: Trend of the real part of the acoustic pressure in logarithmic scale at 200 Hz in the trachea (left), left main Bronchus (middle) and right main bronchus (right) for the healthy case (green) and asthma case (red).

Figure 39: Real part of the acoustic pressure in logarithmic scale at 800 Hz. Comparison between healthy (left) and asthma (right)
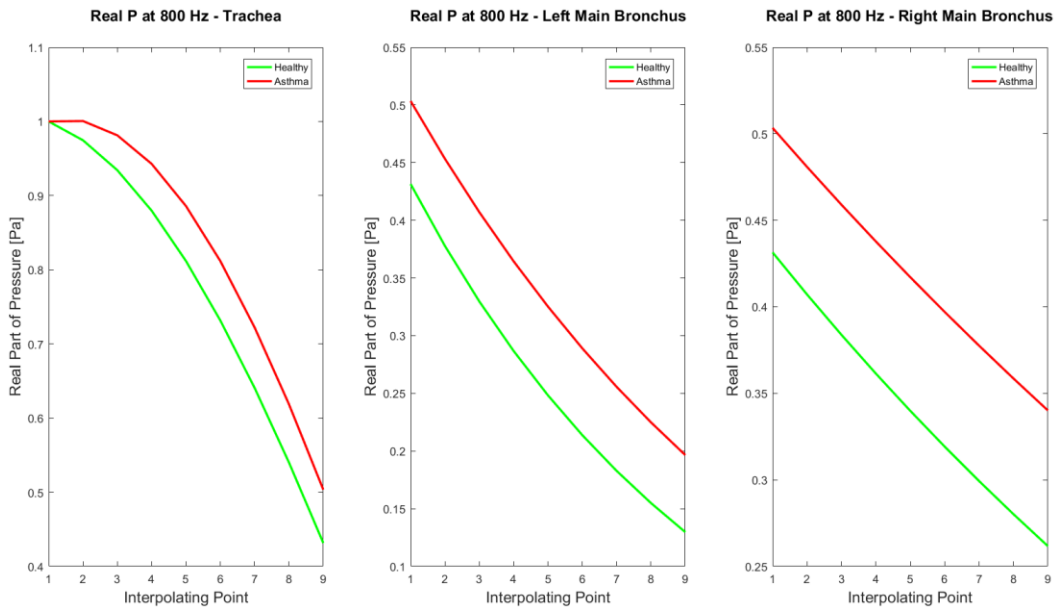
Figure 40: Trend of the real part of the acoustic pressure in logarithmic scale at 800 Hz in the trachea (left), left main Bronchus (middle) and right main bronchus (right) for the healthy case (green) and asthma case (red).

Figure 41: Magnitude of the wall radial velocity in logarithmic scale at 200 Hz. Comparison between healthy (left) and asthma (right)

Figure 42: Magnitude of the wall radial velocity in logarithmic scale at 800 Hz. Comparison between healthy (left) and asthma (right)

5.3.2   <u>Simulation of the Fibrosis Condition</u>

The results regarding the simulation of the fibrosis condition are reported in the following paragraph. For the pressure-related parameters, the qualitative distribution over the entire tree and the trend in the trachea and in the main bronchi is presented. As far as the magnitude of the acoustic pressure is concerned, the analysis will be performed by the comparison of the overall distribution only.
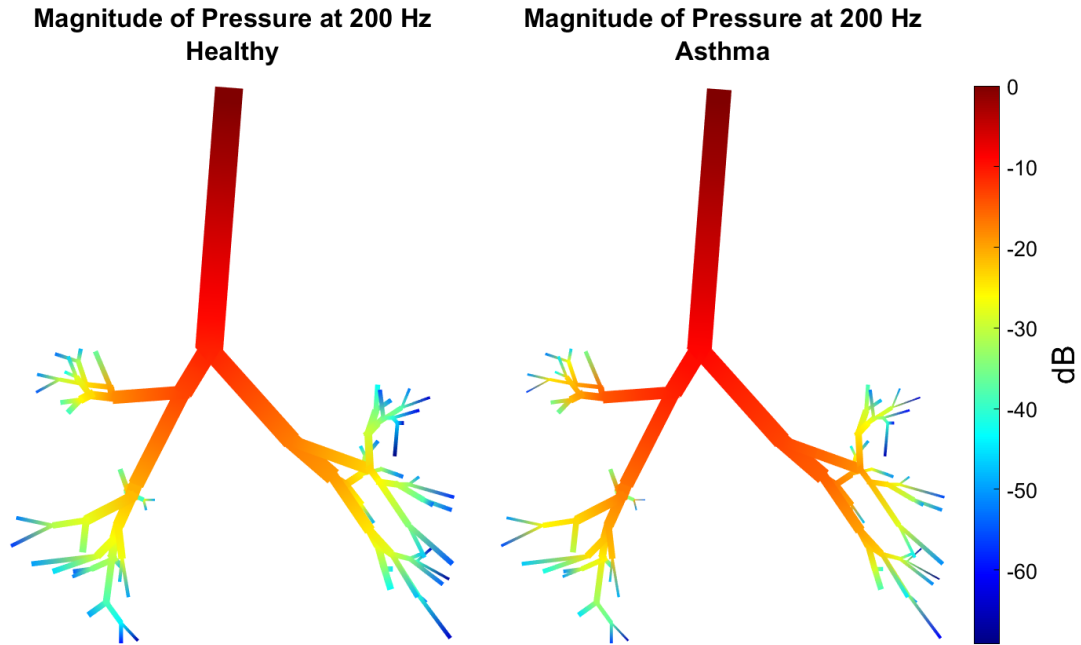
Figure 43: Magnitude of the acoustic pressure in logarithmic scale at 200 Hz. Comparison between healthy (left) and Fibrosis (right)
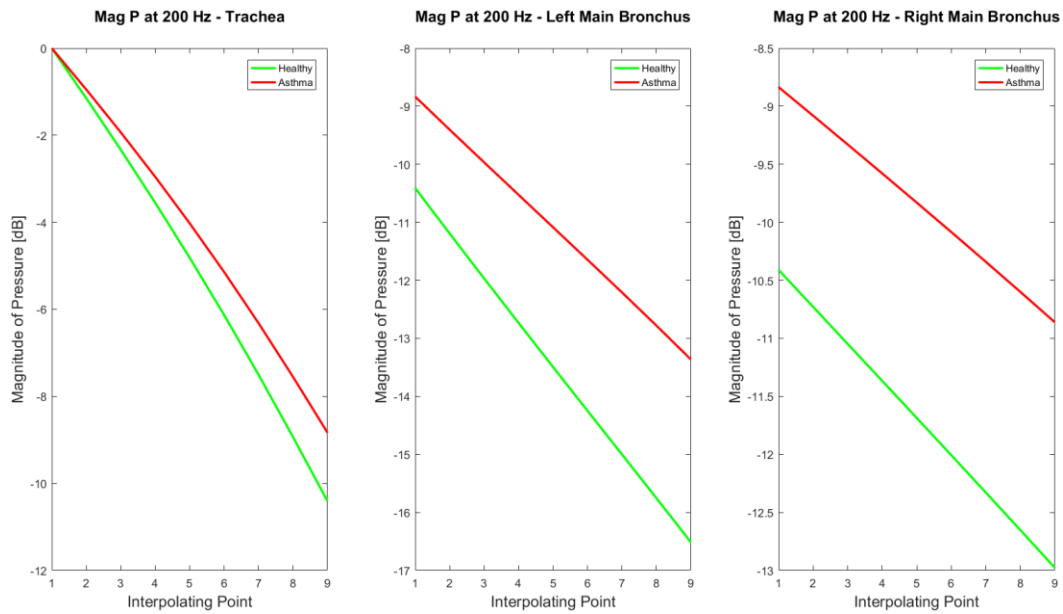

Figure 44: Trend of the magnitude of the acoustic pressure in logarithmic scale at 200 Hz in the trachea (left), left main Bronchus (middle) and right main bronchus (right) for the healthy case (green) and fibrosis case (red).

Magnitude of Pressure at 800 Hz Healthy

Magnitude of Pressure at 800 Hz Fibrosis
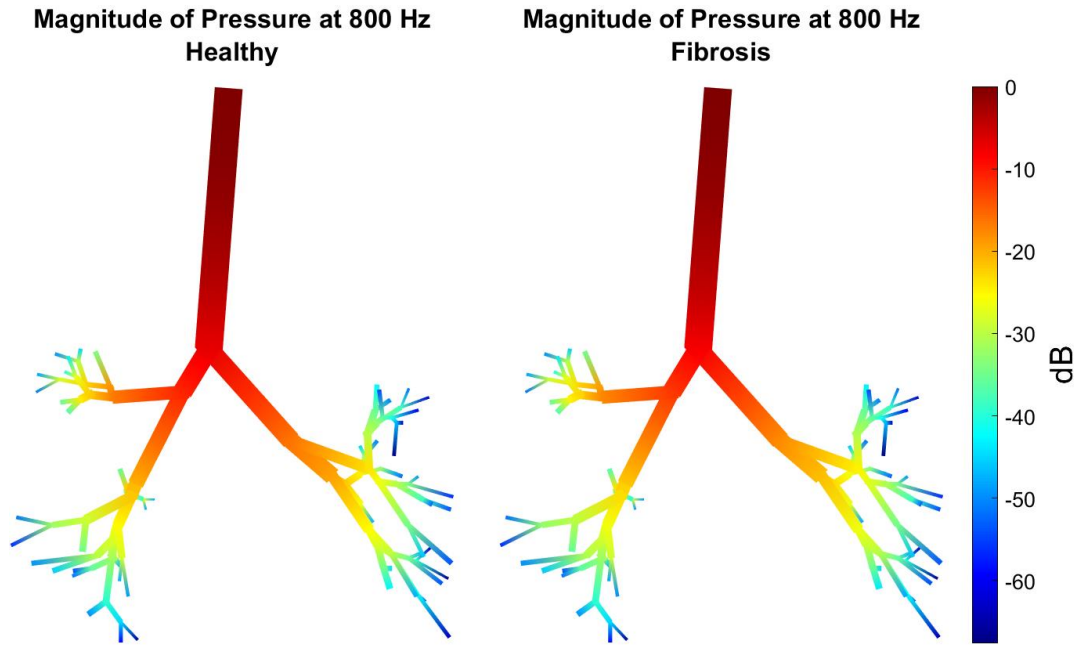
Figure 45: Magnitude of the acoustic pressure in logarithmic scale at 800 Hz. Comparison between healthy (left) and Fibrosis (right)
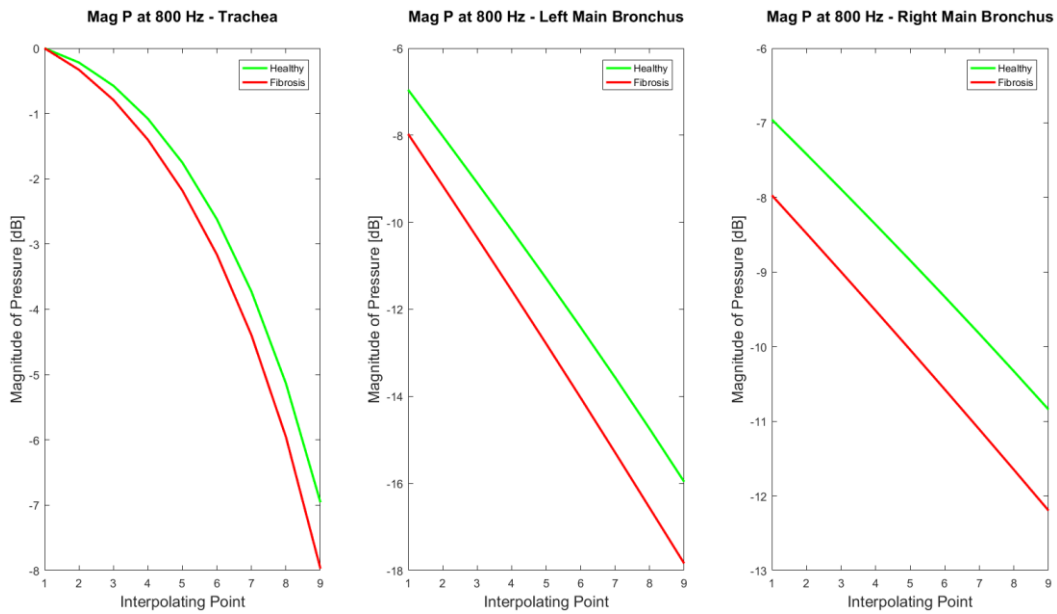
Figure 46: Trend of the magnitude of the acoustic pressure in logarithmic scale at 800 Hz in the trachea (left), left main Bronchus (middle) and right main bronchus (right) for the healthy case (green) and fibrosis case (red).
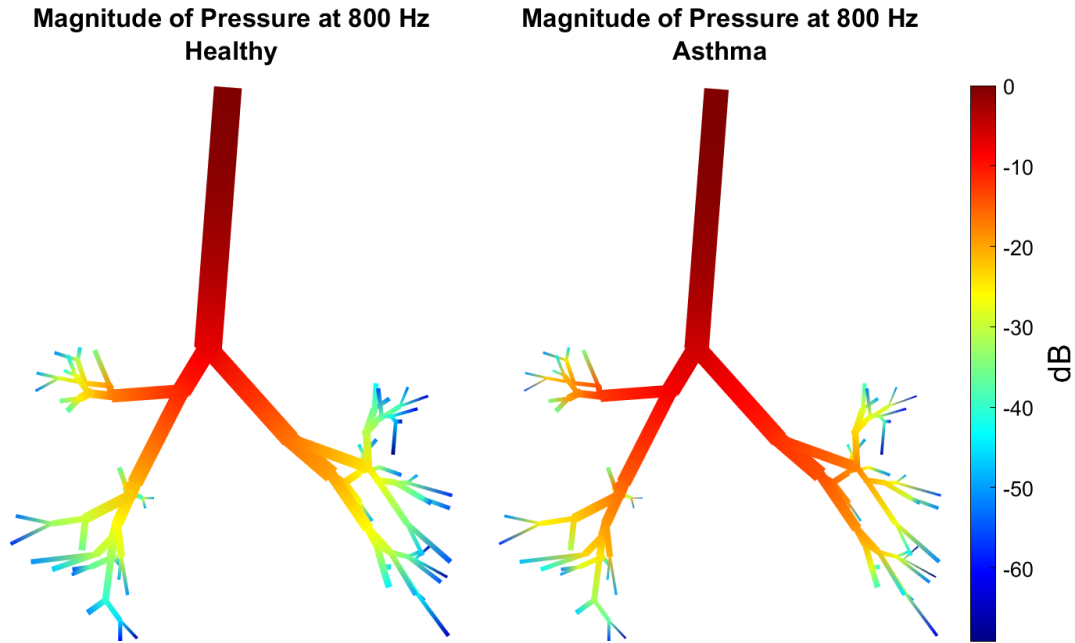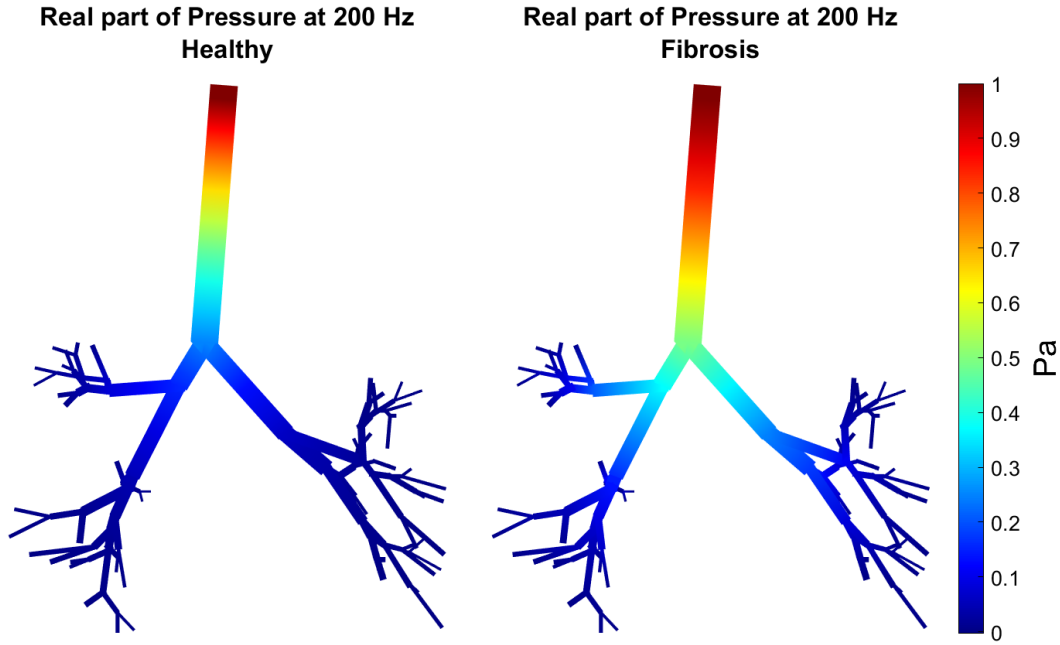
Figure 47: Real part of the acoustic pressure in logarithmic scale at 200 Hz. Comparison between healthy (left) and Fibrosis (right)
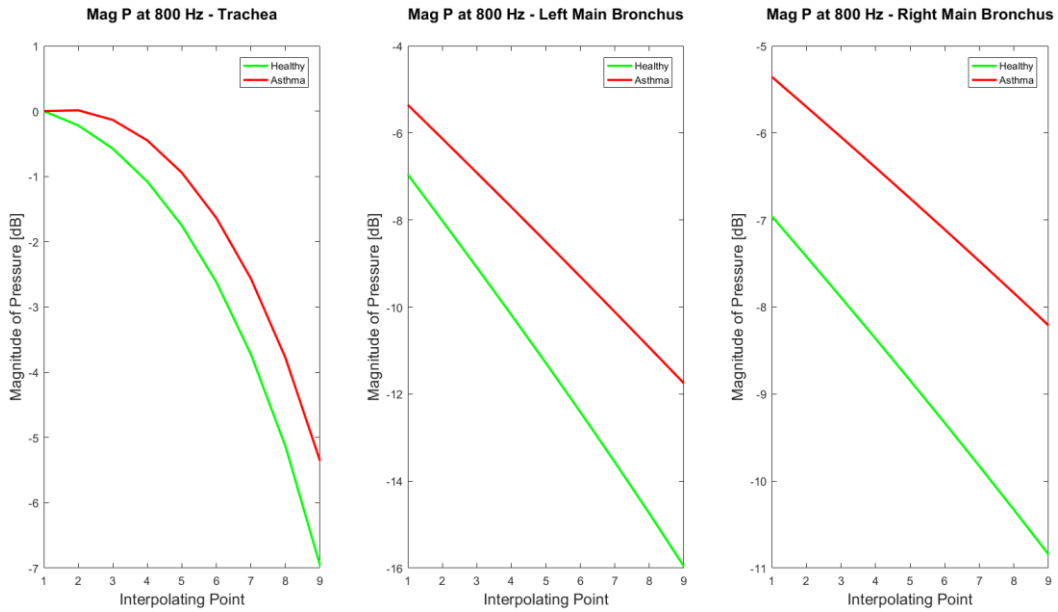

Figure 48: Trend of the magnitude of the acoustic pressure in logarithmic scale at 200 Hz in the trachea (left), left main Bronchus (middle) and right main bronchus (right) for the healthy case (green) and fibrosis case (red).
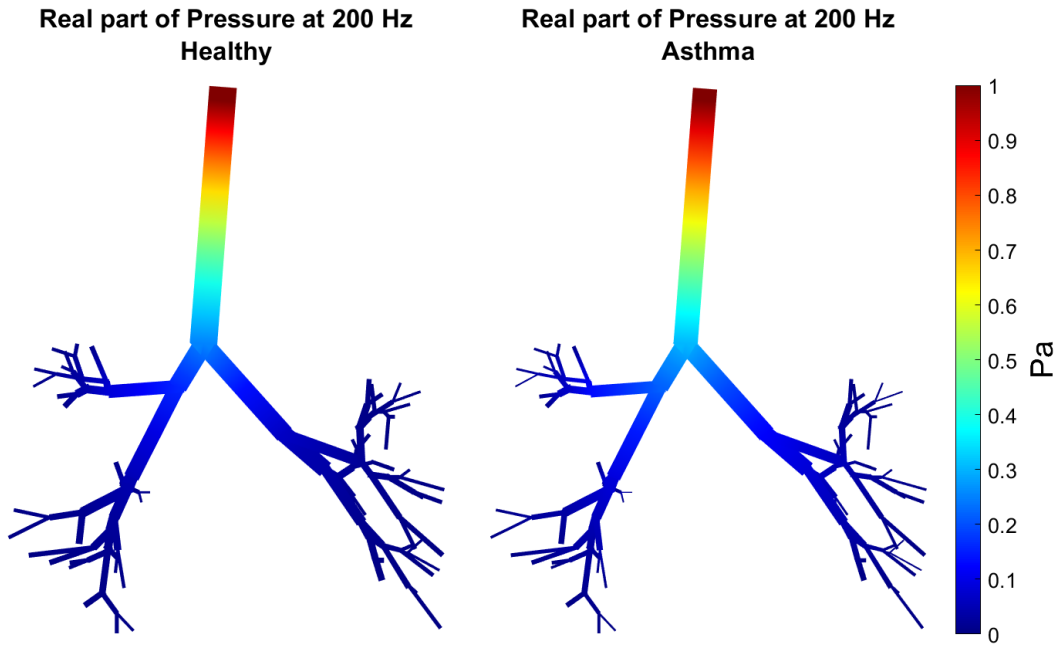
Figure 49: Real part of the acoustic pressure in logarithmic scale at 800 Hz. Comparison between healthy (left) and Fibrosis (right)
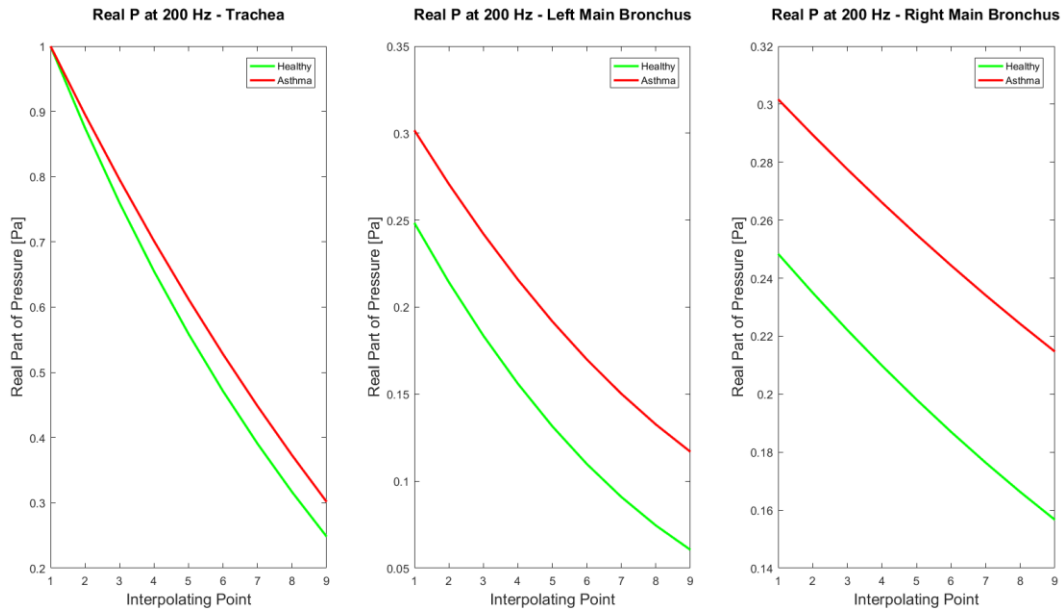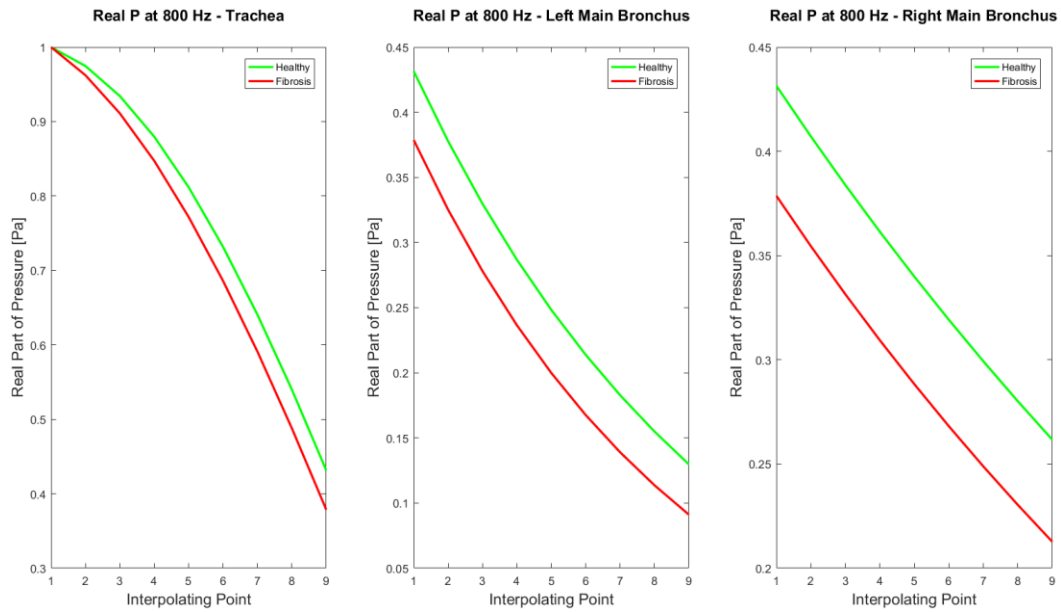

Figure 50: Trend of the magnitude of the acoustic pressure in logarithmic scale at 800 Hz in the trachea (left), left main Bronchus (middle) and right main bronchus (right) for the healthy case (green) and fibrosis case (red).
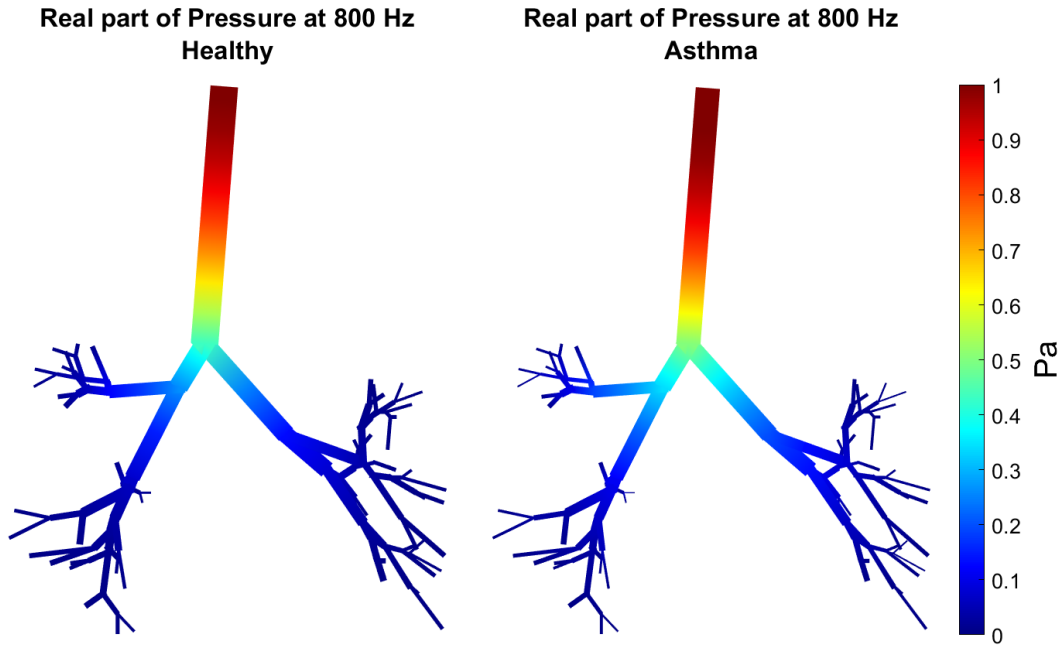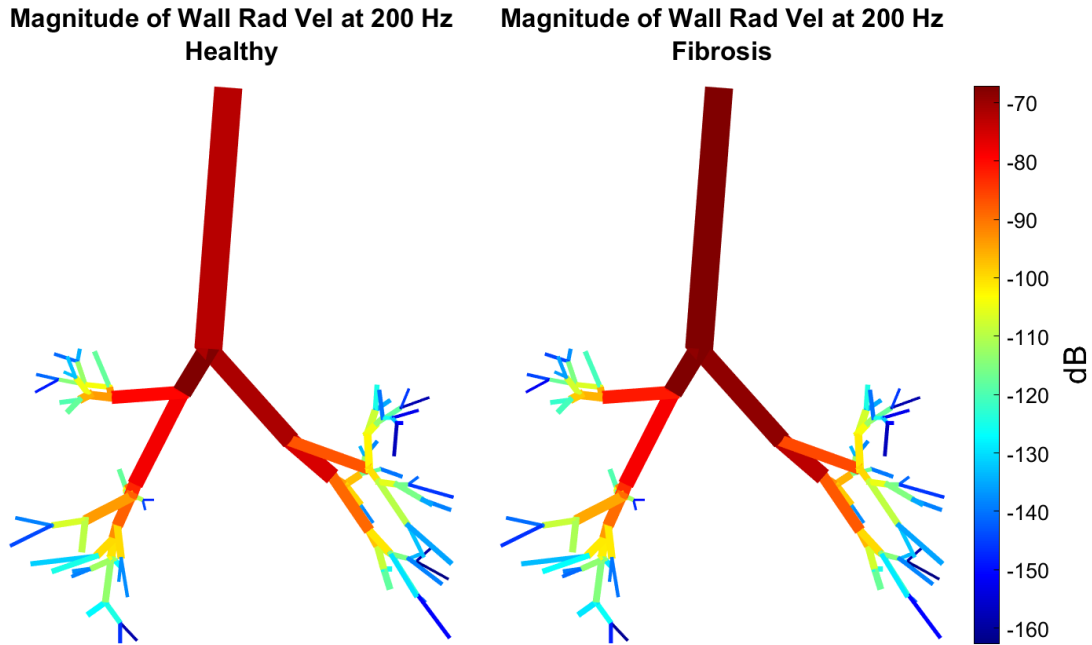
Figure 51: Magnitude of the wall radial velocity in logarithmic scale at 200 Hz. Comparison between healthy (left) and Fibrosis (right)
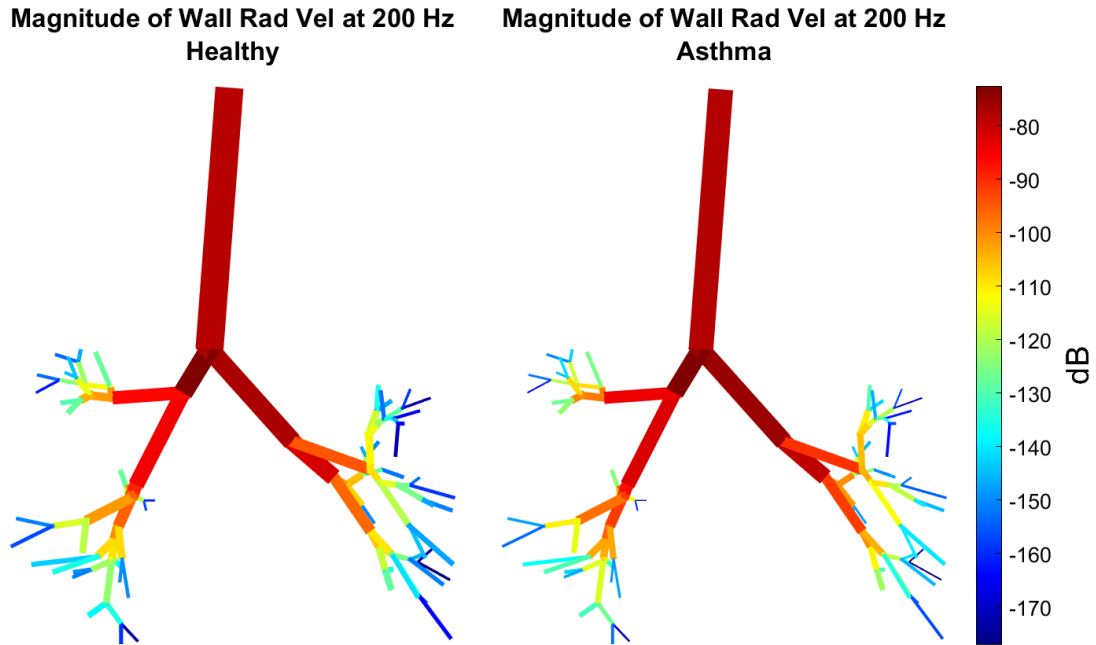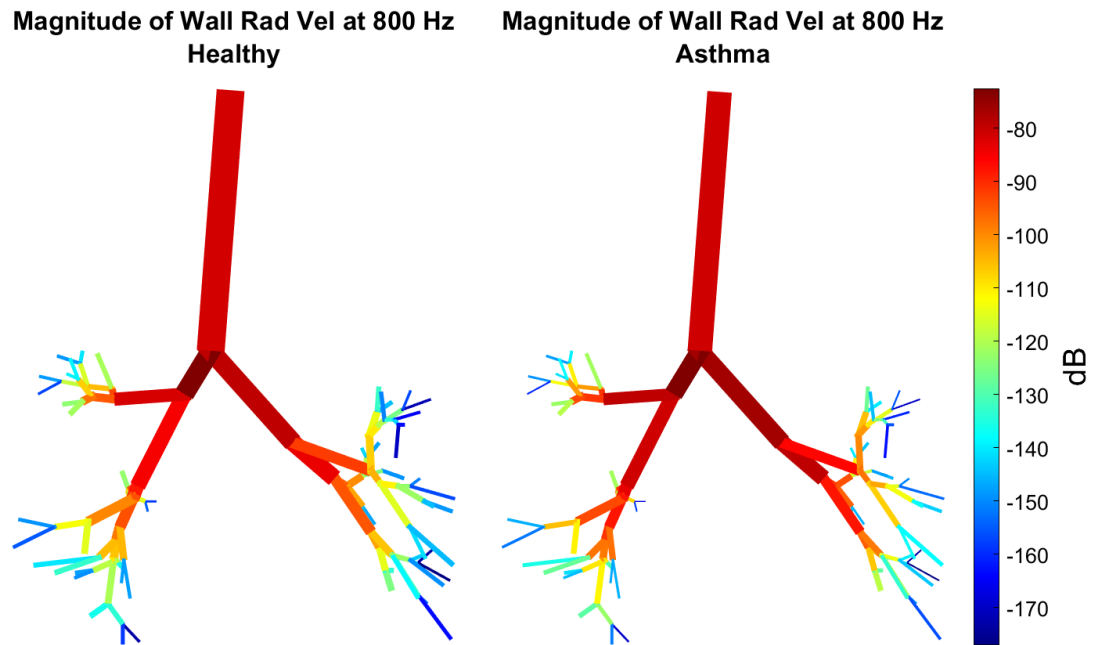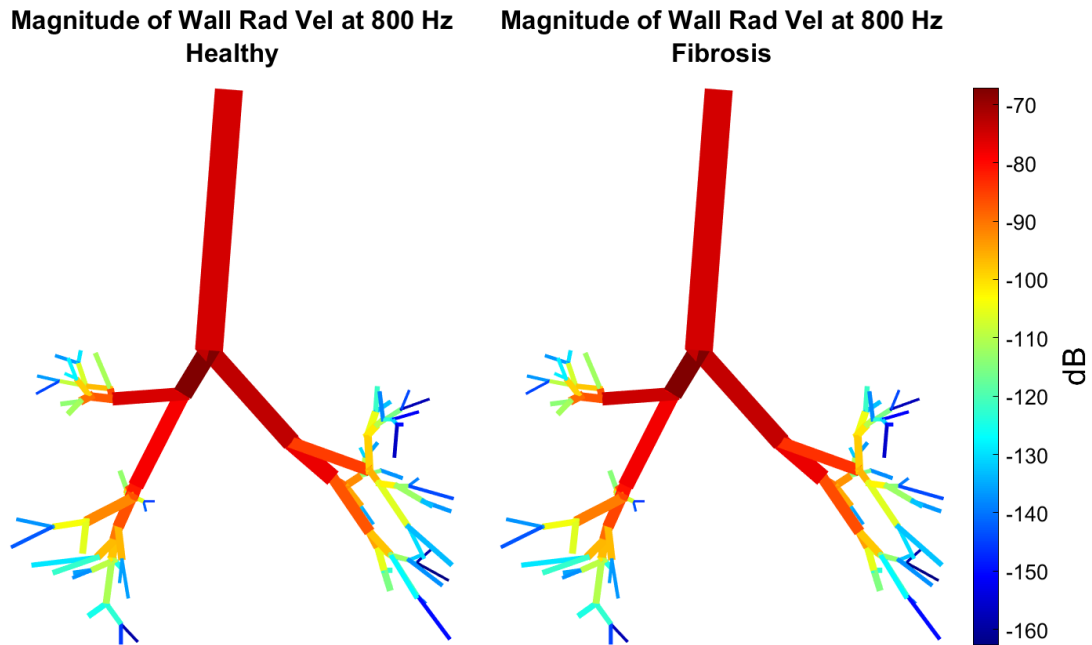

Figure 52: Magnitude of the wall radial velocity in logarithmic scale at 800 Hz. Comparison between healthy (left) and Fibrosis (right)

5.3.3 Simulation of the Pulmonary Infiltrate Condition

The results concerning the simulation of a pulmonary infiltrate in the lower left lobe (LLL) are here reported. For this specific pathology, it was chosen to visualize the distribution of the parameters (magnitude and real part of acoustic pressure and wall radial velocity) on the tracheobronchial tree at the frequencies of 200 Hz and 800 Hz together with the trend of the acoustic pressure (both magnitude and real part) in the inferior lobar bronchus, namely segment leading to the lower left lobe immediately after the bifurcation between upper and lower lobe. The segment was chosen as it is the first and largest segment moving downward the tree which is expected to face a significant variation with respect to the physiological case. For sake of clarity the position of the segment is reported in red in Figure 53.
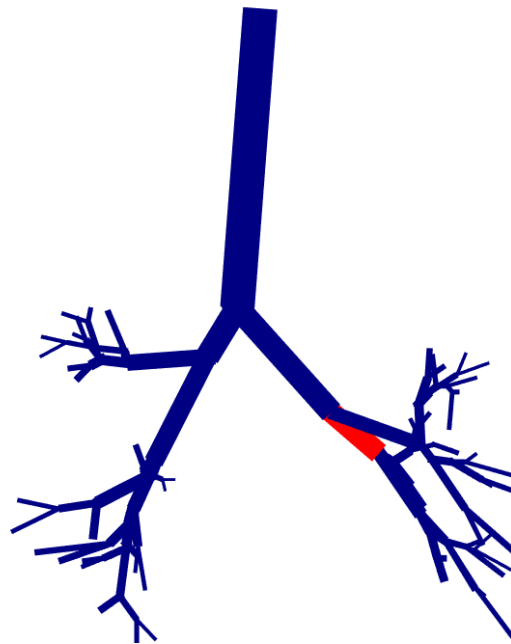
Figure 53: Position of the inferior lobar bronchus analyzed in the case of the LLL Pulmonary infiltrate

**Magnitude of Pressure at 200 Hz
Healthy**

**Magnitude of Pressure at 200 Hz
LLL - Pulmonary Infiltrate**
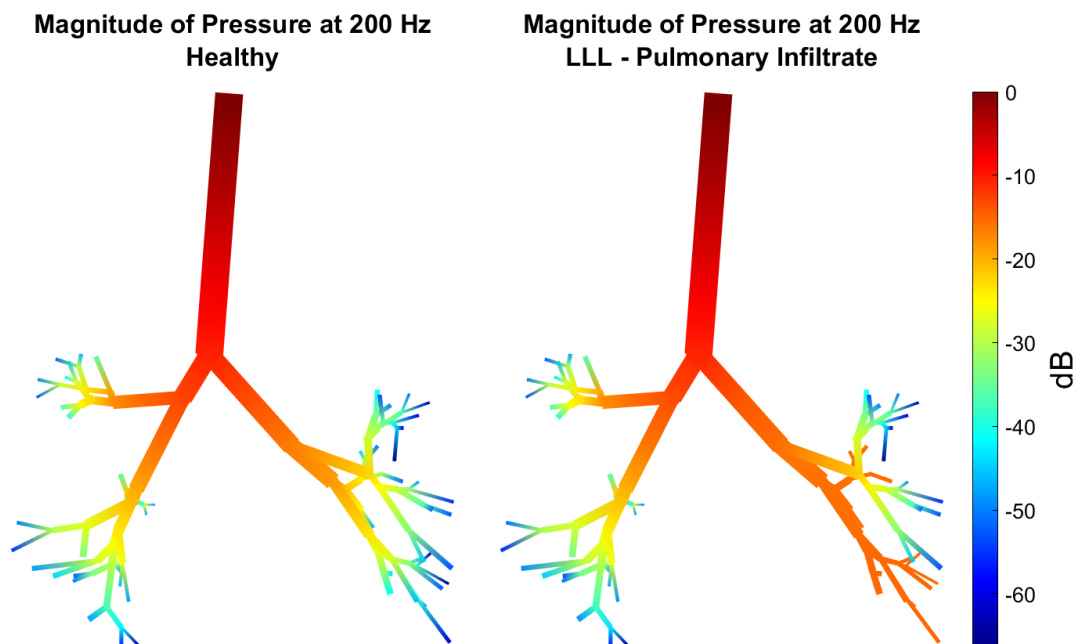
Figure 54: Magnitude of the acoustic pressure in logarithmic scale at 200 Hz. Comparison between healthy (left) and LLL Pulmonary Infiltrate (right)
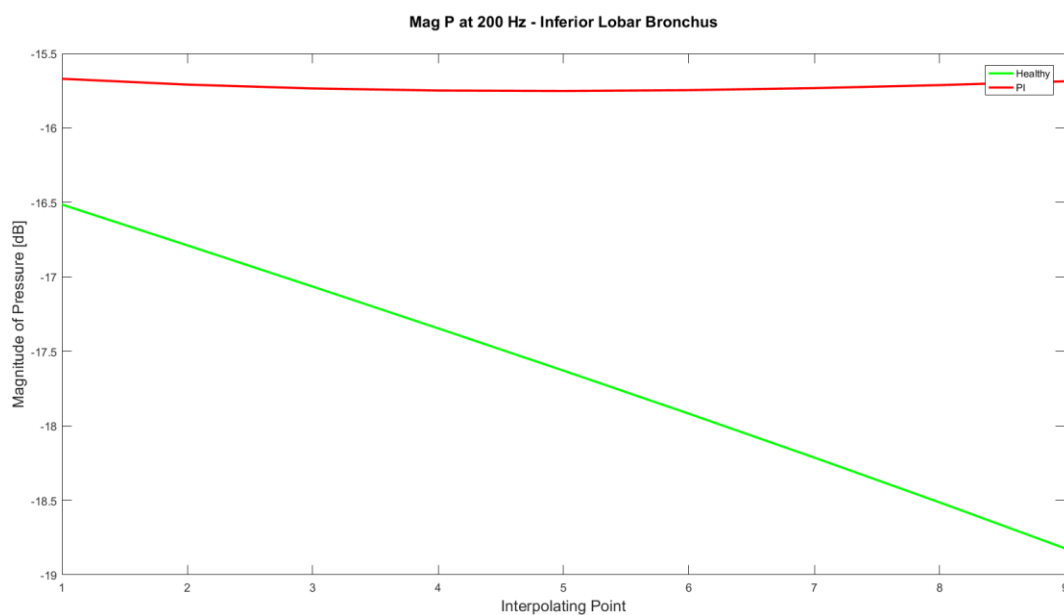
Figure 55: Trend of the magnitude of the acoustic pressure in logarithmic scale at 200 Hz in the inferior lobar bronchus for the healthy case (green) and pulmonary infiltration (red).

**Magnitude of Pressure at 800 Hz
Healthy**

**Magnitude of Pressure at 800 Hz
LLL - Pulmonary Infiltrate**
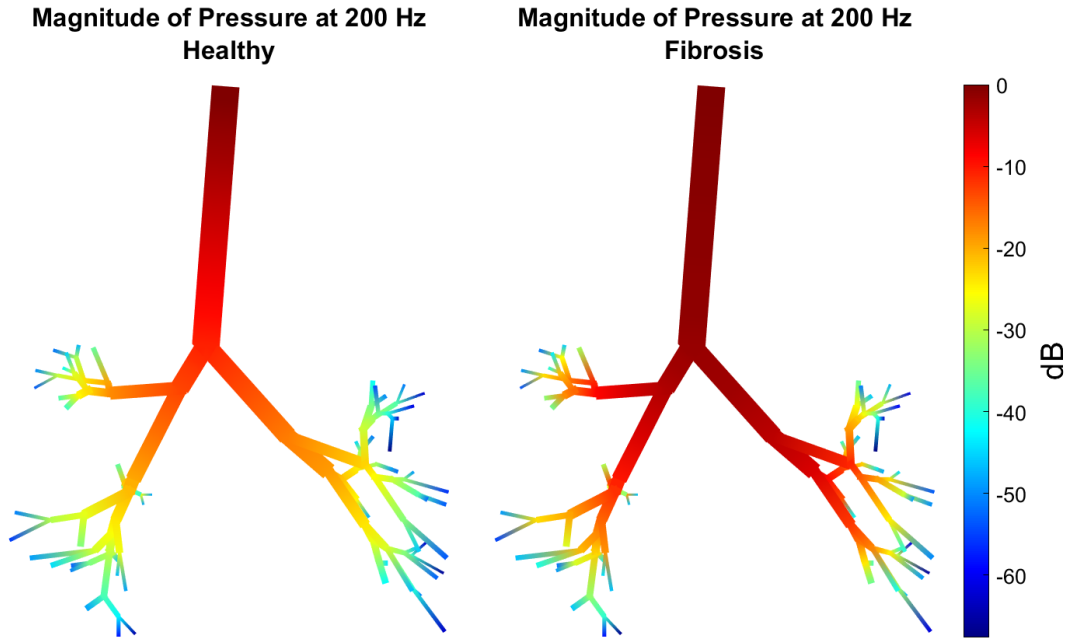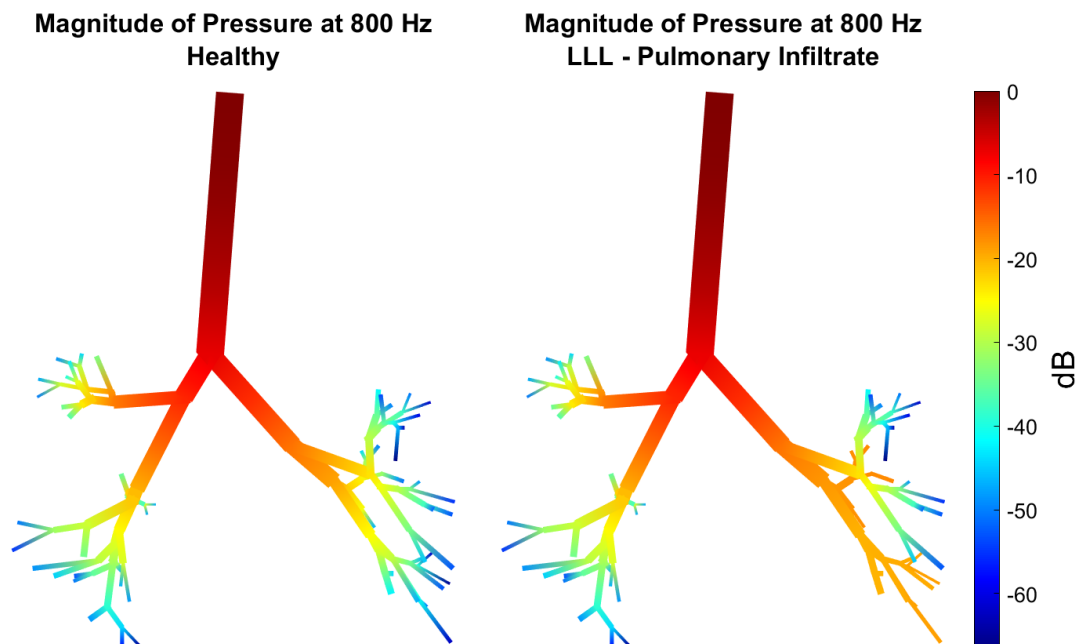

Figure 56: Magnitude of the acoustic pressure in logarithmic scale at 800 Hz. Comparison between healthy (left) and LLL Pulmonary Infiltrate (right)
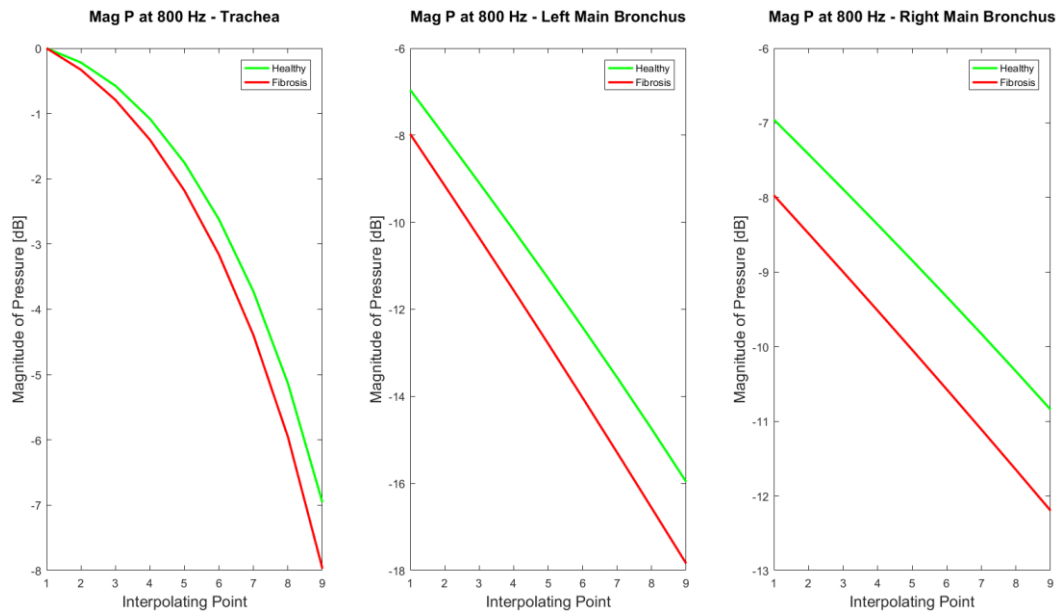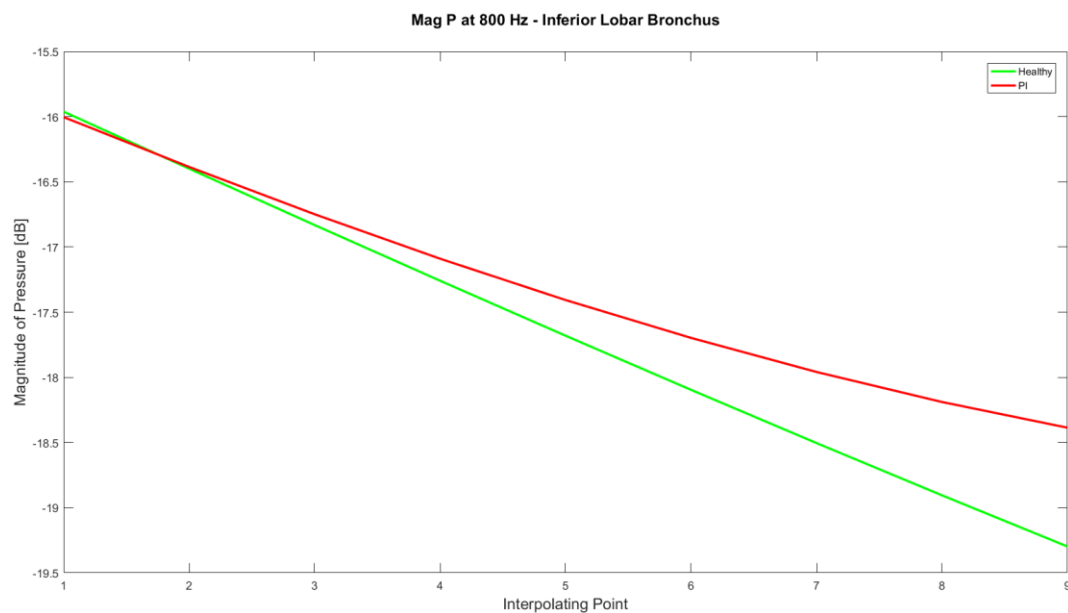

Figure 57: Trend of the magnitude of the acoustic pressure in logarithmic scale at 800 Hz in the inferior lobar bronchus for the healthy case (green) and pulmonary infiltration (red).

**Real part of Pressure at 200 Hz
Healthy**

**Real part of Pressure at 200 Hz
LLL - Pulmonary Infiltrate**
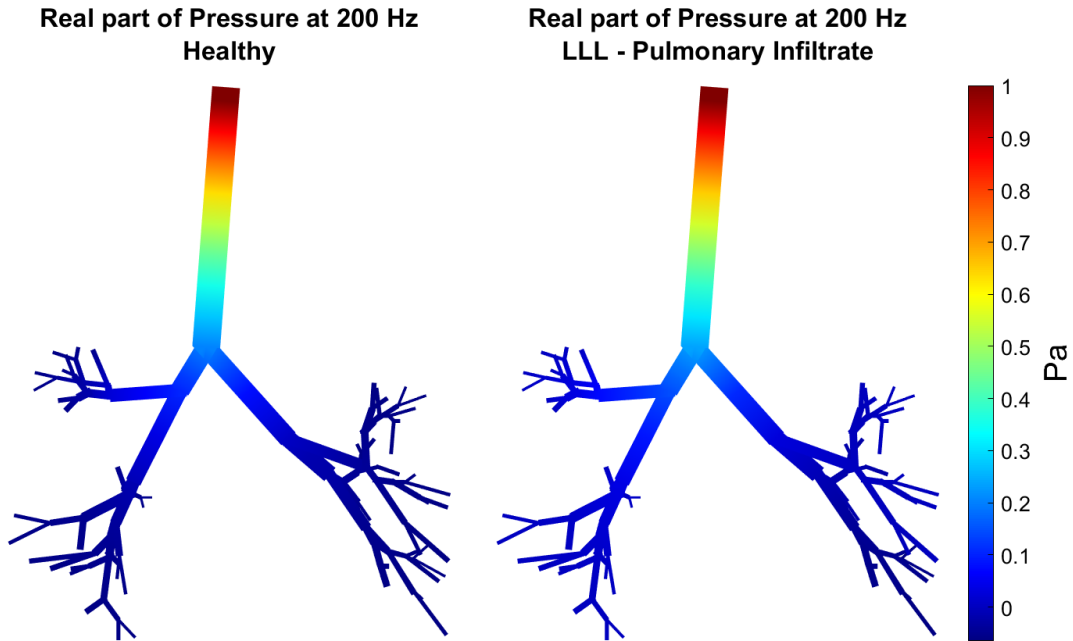
Figure 58: Real Part of the acoustic pressure in logarithmic scale at 200 Hz. Comparison between healthy (left) and LLL Pulmonary Infiltrate (right)
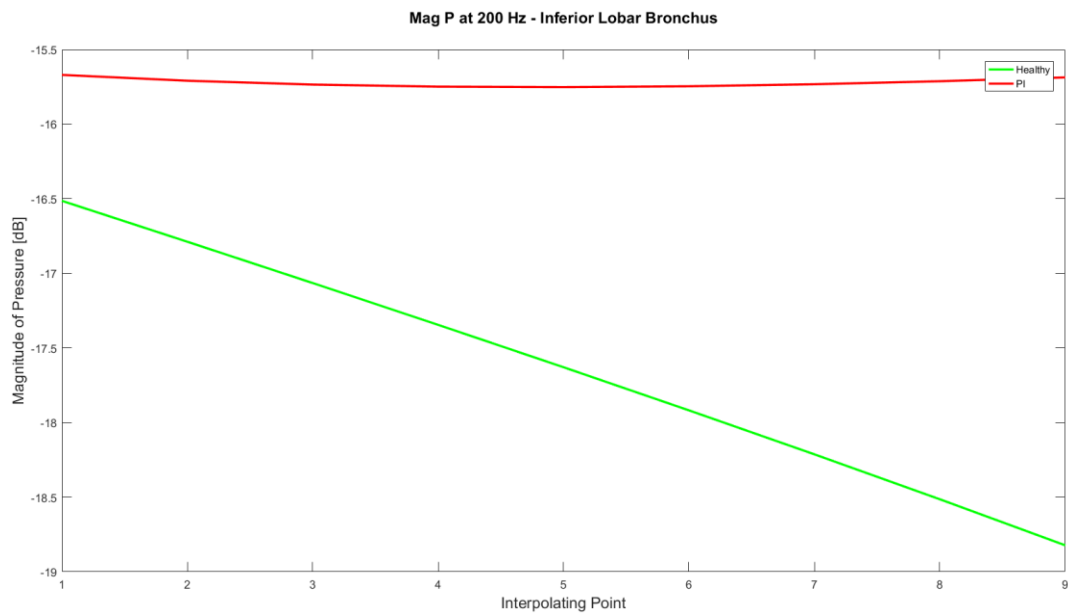
Figure 59: Trend of the real part of the acoustic pressure in logarithmic scale at 200 Hz in the inferior lobar bronchus for the healthy case (green) and pulmonary infiltration (red).
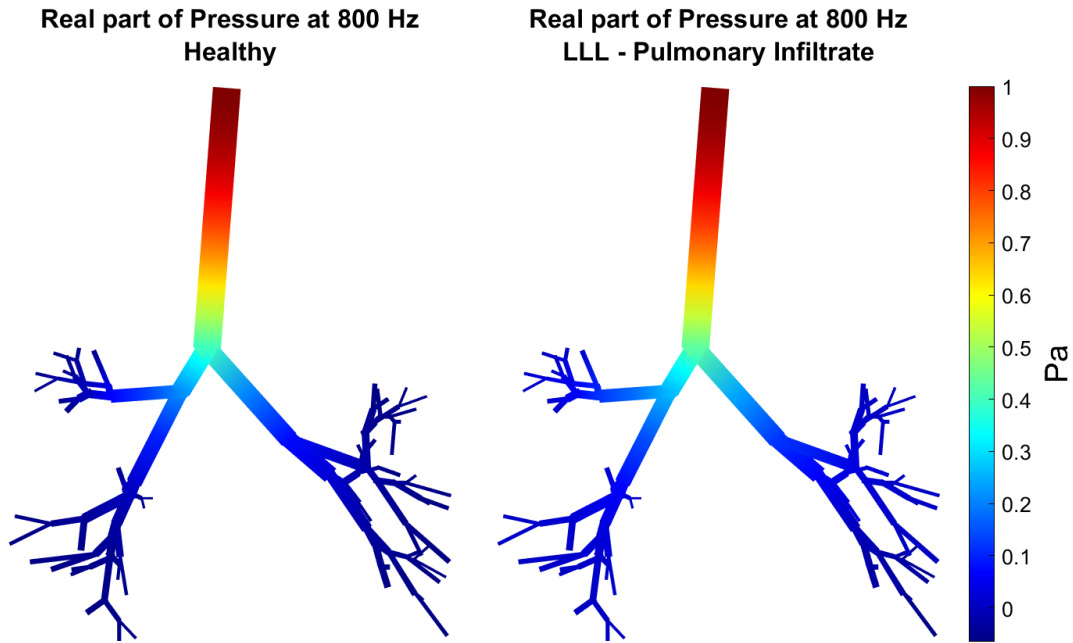
Figure 60: Real part of the acoustic pressure in logarithmic scale at 800 Hz. Comparison between healthy (left) and LLL Pulmonary Infiltrate (right)
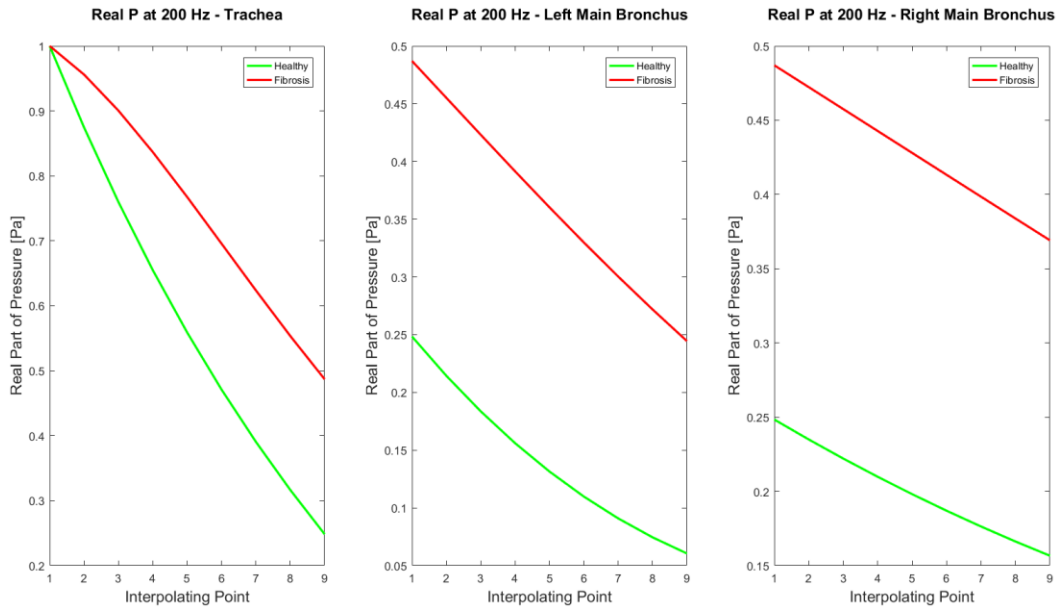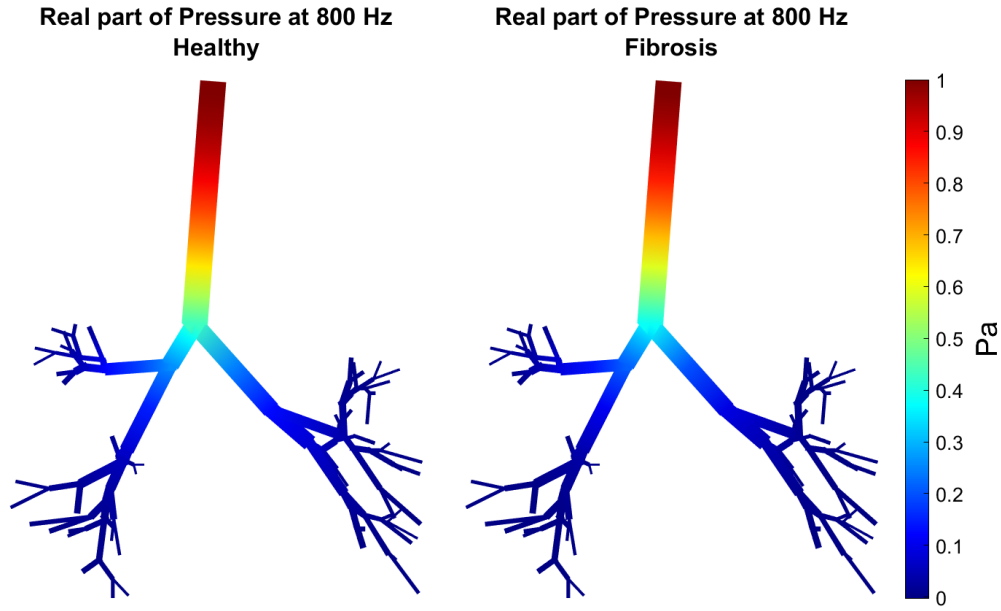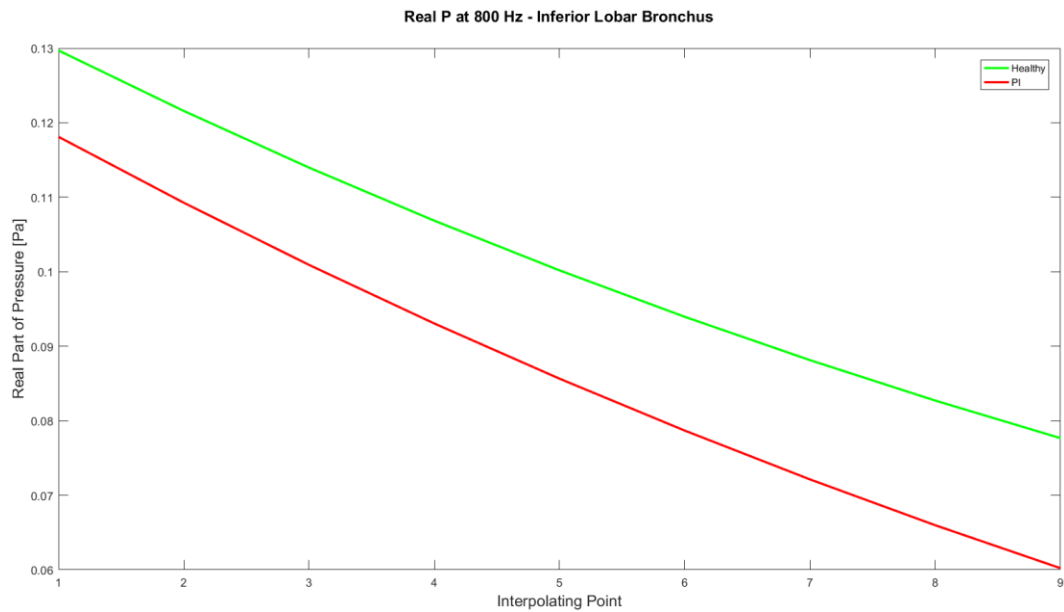

Figure 61: Trend of the real part of the acoustic pressure in logarithmic scale at 800 Hz in the inferior lobar bronchus for the healthy case (green) and pulmonary infiltration (red).

**Magnitude of Wall Rad Vel at 200 Hz
Healthy**

**Magnitude of Wall Rad Vel at 200 Hz
LLL - Pulmonary Infiltrate**
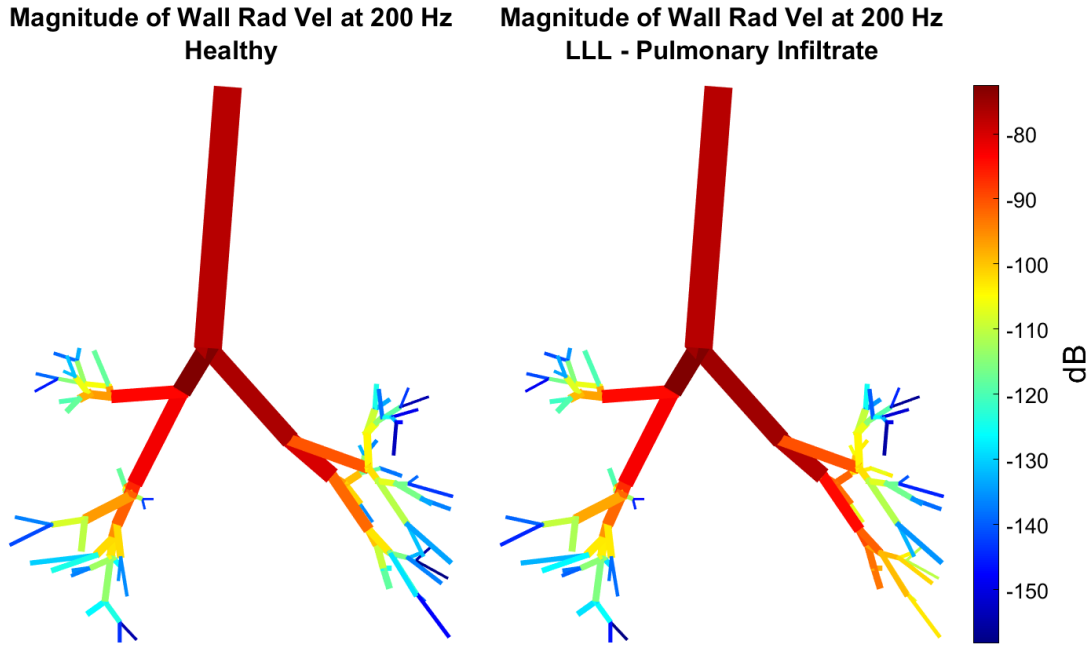
Figure 62: Magnitude of the wall radial velocity in logarithmic scale at 200 Hz. Comparison between healthy (left) and LLL Pulmonary Infiltrate (right)

**Magnitude of Wall Rad Vel at 800 Hz
Healthy**

**Magnitude of Wall Rad Vel at 800 Hz
LLL - Pulmonary Infiltrate**
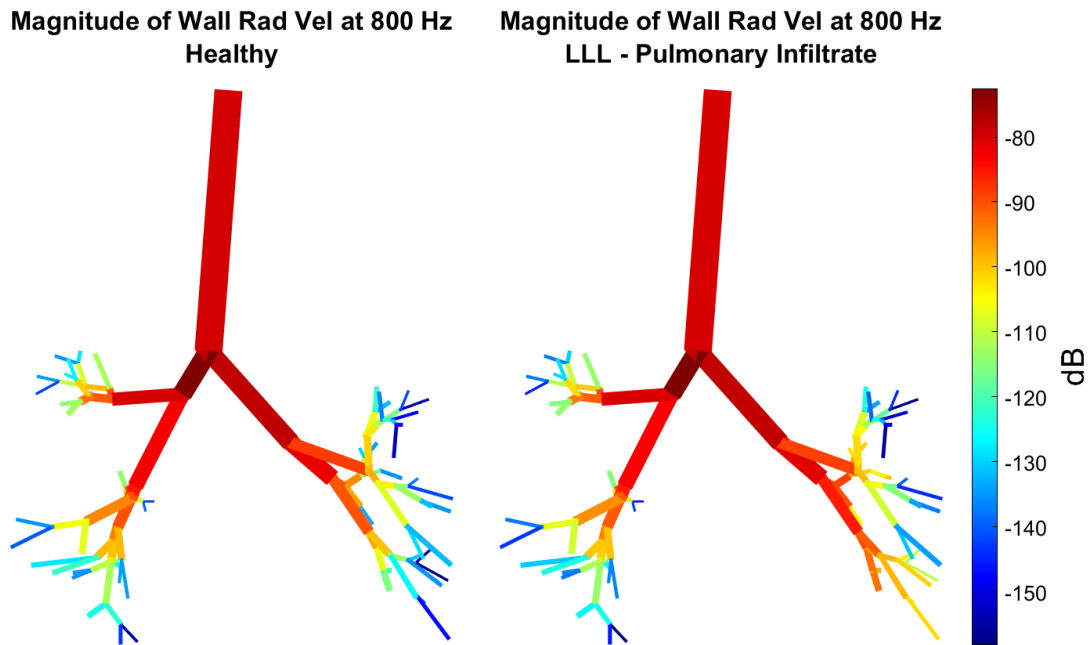
Figure 63: Magnitude of the wall radial velocity in logarithmic scale at 800 Hz. Comparison between healthy (left) and LLL Pulmonary Infiltrate (right)

CHAPTER 6

DISCUSSION

In this dissertation, frequency-domain response of a human tracheobronchial tree to an input acoustic wave of constant amplitude (1 Pa) and frequency ranging between 200 and 800 Hz was analyzed. The responses during two phases of the respiratory cycle have been evaluated: the beginning of the inspiratory phase and the beginning of the expiratory one. The system has been modeled with a one-dimensional waveguide considering a fluid (air) embedded in compliant viscoelastic airways wall made of soft tissue only. A Voigt model was used to simulate the frequency dependent response of the wall tissue of the airways. The analytical code developed in MATLAB was validated via COMSOL Multiphysics® numerical finite element analysis and successively used for the simulation of some specific pathological conditions such as asthma, fibrosis and pulmonary infiltrates.

The overall response of the system is highly dependent on the mutual interactions between the fluid and the airways walls especially in terms of energy transfer occurring at their interface. As a general statement, it can be inferred that a wave propagating in a medium is characterized by a certain energy. This energy can either dissipated because of the properties of the medium or transferred to the airways wall. The predominance of one phenomenon over the other is conditioned by impedance mismatch between the fluid and the wall of the airways. The transmission of energy is maximum when the two impedances have equal values and decreases in a monotonic way when the mismatch increases. In other words, a higher impedance mismatch causes the energy to be less likely transferred to the wall (and therefore to be stored in the fluid

longer) whereas a lower impedance mismatch determines a facilitated and more rapid energy transfer from the fluid to the wall.

After the energy is transferred to the wall, it starts being dissipated. The dynamics of the dissipation process, at this point, is dependent on the material properties of the wall. As already mentioned the wall viscoelastic behavior was approximated by a Voigt model, consequently the elastic modulus can be expressed by equation 3.2 here reported for sake of simplicity.

$$E = Y_s + i\omega\eta_s$$

According to the relation above, it can be observed that as the frequency increases there is an increase in the viscous term and consequently an increase in the damping effect. Given a certain amount of energy transferred to the wall, a higher energy dissipation is associated with higher frequencies.

As a final consideration, it should be recalled the impedance type analogy used in modelling the response of the system. This analogy is implicit in the expression of formula (2.41) and, at first approximation, allows to model each acoustic element (in other term each segment) as reported in Figure 64.
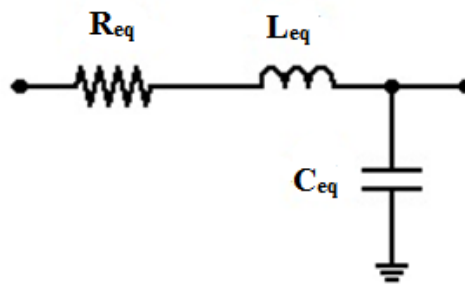
Figure 64: Transmission Line Analogy. Resulting circuit for each element

In such model, the voltage drop over the electrical element and the electrical current through that component represent the acoustic pressure drop over the acoustical component and the flux generated because of the pressure. The symbols L_{eq}, R_{eq}, C_{eq} correspond to the acoustic inertance, resistance and compliance respectively and consider both the properties of the walls and of the medium. The inertance represents the mass of the medium and of the walls, the compliance models the ability of these two components to expand and compress and finally the resistance is associated with the dissipation phenomena from the fluid to the walls. The appropriateness and the assumptions underlying this model are widely reported in literature [2], [42], [44] and won't be analyzed in this dissertation. What is of interest is the behavior of the response of such a system in the frequency domain. It is known that the value of impedance relative to the inertance is directly proportional to the frequency, whereas the value of the compliance relative to impedance shows an inverse proportionality with respect to the frequency. Consequently, at low frequencies and with a certain degree of approximation the inertance can be considered a short circuit and the compliance and open circuit. On the contrary, at high frequencies the inertance behaves like an open circuit and the compliance as a short circuit. In terms of pressure (voltage), a short circuit is always negligible as (for definition) it doesn't induce any modification. For this reason, it is possible to infer that at lower frequencies the effect of the compliance is predominant over the effect of the inertia whereas for high frequencies inertia plays a much more relevant role with respect to the compliance. This result will deeply affect the successive consideration in the comparisons between the pathological and the physiological cases (see paragraphs 6.3.1, 6.3.2, 6.3.3).

In the specific case of the tracheobronchial tree, the fluid to deal with is air. As reported in TABLE 5 and TABLE 6 the air properties are remarkably different than the one of the soft tissue

composing the wall structure. Consequently, the impedance mismatch is in general high even for relatively low frequencies. When the frequency is increased, because of relation (2.38) the impedance of the airways wall is increased, whereas the properties of the fluid are not modified. This causes the impedance mismatch to become further more evident as the frequency increases. Recalling what has been stated above, a higher impedance mismatch determines a lower energy transfer rate between the fluid and the wall. As more energy remains stored in fluid, the pressure tends to penetrate more deeply in the tree. This trend can be easily observed considering the trend of the real part of the acoustic pressure for different frequencies of both the analytical and numerical results reported in section 5.1.

6.1 <u>Validation of the Model</u>

The qualitative comparison of the results of the two parameters considered for the validation of the analytical model, namely the magnitude (in logarithmic scale) and the real part of the acoustic pressure clearly show a good agreement between the results obtained in MATLAB and the numerical simulations in COMSOL. The results are consistent all over the four frequencies of interest. The validity of the model was proved also via the analysis of the relative error between the analytical and numerical results.

For the inspiratory phase, this analysis shows an excellent matching of the results. The error slightly tends to increase at higher frequencies, but as reported in TABLE 10 the median errors are below the 10 %. The highest values of error are in the terminal branches with a peak value at 800 Hz of 36.14 %.

For the expiratory case the analysis of the error shows a slightly worse trend as the error, though reasonably low in terms of its median value (see TABLE 11), increases quite significantly

for the 800 Hz frequency, where it reaches relatively high values also in the left main bronchus of the tree. The maximum value of the error is reached for 800 Hz and is in the order of 63.48 %, although these value is reached for the terminal branches only.

Given the excellent results for the inspiratory phase and the acceptable matching in the case of the expiratory phase, the analytical model can be considered to be validated. The increased discrepancies between the analytical and numerical results at higher frequencies could be attributed to the choice of the nominal element size in the meshes used for the numerical simulations. This nominal dimension ought to be at least an order of magnitude smaller than the lowest wavelength and it is known that as frequency increases, wavelength gets shorter. Although it was verified that the meshes used in this dissertation meet the above-mentioned requirement in term of nominal element size, it is also true that, especially at 800 Hz, the margin of error increases.

6.2   Comparison Between the Beginning of Inspiratory and Expiratory Phases

The diameter of the airways varies according to the respiratory cycle. This is confirmed by the plot of the distribution of the diameters reported in Figure 5 and Figure 6. In general, during the inspiratory phase the airways exhibit an increment of the diameter and a reduction of the thickness, whereas in the expiratory phase the diameter is reduced and the thickness increased. In this dissertation, the very beginning of both phases was evaluated, consequently the morphometry of the airways at the beginning of each phase is still similar to the end of the previous one. In other words, it is possible to observe that at the beginning of the inspiratory phase the diameter of airways is relatively lower than the diameter at the beginning of the expiratory phase. Nonetheless, the variations of the geometry seem to have a negligible effect on the acoustic of the tracheobronchial tree in the two phases. This is confirmed both by the visual representation of the

three parameters presented in the result section and by the respective trend plots (see paragraph 5.2). On one hand, this similar response of the two phases can be ascribed to the fact the variations of the geometry themselves are relatively small and therefore hardly resolvable in term of acoustic analysis. This result is in line with the theoretical previsions. On the other hand, it should be considered that the creation of the geometry from the CT images by itself introduced a certain degree of approximation causing a mitigation of the differences between the two phases. Given the results obtained in paragraph 5.2 and the relative resemblance of the parameters of interest in the two respiratory phases considered it was decided to simulate the pathologic conditions only for the inspiratory case.

6.3 <u>Simulation of Pathological Conditions</u>

The results presented in section 5.3 supports the hypothesis that the pathology induced alterations of the airways in terms of mechanical and geometrical properties significantly affect the sound propagation throughout the tracheobronchial tree. The changes in sound propagation in turns are reflected on the distribution and the value of the acoustic parameters mentioned in this dissertation, namely the acoustic pressure and the wall radial velocity. The extrapolation of the differences in these parameters and especially of the wall radial velocity to the chest surface will allow the comparison with *in-vivo* measurements performed with Scanning Laser Doppler Vibrometry and possibly with MRE. This would lead not only to a better understanding of the effects of the pathologies themselves but could also in efficient and non-invasive method of detection for clinical purposes.

6.3.1 <u>Simulation of the Asthma Pathology</u>

The pathology of asthma was analytically simulated by increasing the thickness (h) of each segment of 1.5 times. The radius of the cross-section was reduced in proportionally to the new thickness values accordingly to equation (3.3). What can be observed by the analysis of the results, is that in the case of asthma pathology the pressure tends to penetrate more in the tree. This behavior is evident from both the qualitative evaluation of the color plots of the magnitude and (especially) the real part of the pressure and from the trend of those parameters in the trachea and the main bronchi. Indeed, it can be notice that the values of the pressure of the pathological condition (in red) are constantly higher than the ones in the physiological condition (in green). This consideration holds true for both the analysis at 200 Hz and the one at 800 Hz. The explanation of this trend is related to the acoustic impedance mismatch previously introduced. The increased thickness and the reduced diameter cause the wall impedance to increase in accordance with equation (2.38). The mismatch with the impedance of the fluid, consequently becomes more relevant. As the mismatch increases, the energy is transferred to wall later allowing the acoustic pressure to penetrate more deeply in the tree.

In terms of magnitude of the wall radial velocity, it can be noticed that in the big airways (trachea and main bronchi) there is not a substantial difference. The magnitude of the wall radial velocity tends to slightly increase in the pathological case, but this is evident mostly for the last generations and the terminal branches. A higher magnitude velocity implies that the wall is vibrating in a more significant way in the case of asthma rather than in the healthy one.

6.3.2   <u>Simulation of the Airways Fibrosis Condition</u>

The stiffening of the airways characteristic of pathological fibrosis was modeled by increasing the elastic modulus of the airways wall of a factor 5. This multiplicative factor causes the compliance of the wall to drastically reduce, which determines the wall impedance to increase significantly as outlined by equation (2.40). Once again the mismatch between the wall impedance and the fluid impedance becomes higher causing the pressure to penetrate the tree much more deeply in the pathological case then in the healthy one. This trend is clearly observable at 200 Hz. However, the results at 800 Hz does not seem to be affected as both the color plot and the trend in the trachea and main bronchi are negligibly modified. This behavior can be ascribed to the frequency dependency of the acoustical elements (compliance and inertance) used in of the model for the computation of the impedance. As it was previously stated, the compliance is predominant at lower frequencies, whereas at higher frequencies the role of the inertance is more relevant. By multiplying the elastic modulus by a factor 5, the compliance is deeply affected (namely reduced), whereas the inertance is left unaltered. At 200 Hz, which is a relatively low frequency, the modification in compliance are clearly represented by the different response of the system. At 800 Hz, the compliance still is higher that the physiological condition, but its effect in term of pressure alteration is minimal as it behaves like a short circuit: at this high frequency, the effect of the inertance is of first importance and, as already mentioned, the inertance itself was not altered. This determines the results at 800 Hz to be relatively similar in the comparison between the physiological and the pathological fibrotic case. This is reflected also in terms of wall radial velocity: at 200 Hz, it is possible to observe that the magnitude of the velocity is significantly higher in the fibrotic case than in the healthy case. This difference is substantial at the level of the trachea and the main bronchi whereas it tends to become less evident moving down the

tracheobronchial tree. Given that the magnitude of the velocity is a parameter directly proportional to the pressure, it is not surprising that at 800 Hz where there is not a significant variation of the distribution of the pressure (see above), also the magnitude wall radial velocity seems basically unaffected by the introduction of the pathology.

6.3.3 Simulation of the Pulmonary Infiltrate Condition

Pulmonary infiltrate localized in the lower lobe of the left lung was simulated. The increased resistance of the tree was modelled by multiplying the impedance of the left lower lobe terminal branches by a factor 10^5. For both the frequencies of interest it can be observed that the introduction of the occlusion on the lower left lobe causes the magnitude of the pressure to be significantly higher in the corresponding branches. This observation is even more evident considering the plot of the magnitude of the pressure for the healthy and the pathological cases. Not only the values but also the trends are significantly different. This is verified for both the frequencies of interest, although at 800 Hz this behavior seems slightly less marked. In addition to that the overall distribution of pressure in the rest of the tree does not seem to be affected in a significant way. The trend of the real part of the pressure is approximately equal in the physiological and in the pathological case. This is confirmed by the comparison between the plot of the real part of the pressure in the lower lobar bronchus for the healthy and pathological case. It is possible to notice that not only the trend is approximately the same but also the values are very close to each other. Because of the definition of magnitude of a complex variable, this implies that the main changes in terms of pressure distribution are related to the imaginary component of the pressure itself. In terms of magnitude of the wall radial velocity, once again the differences with respect to the physiological case are localized basically in the lower branches of the left lung. The alterations are

strikingly evident especially of the terminal branches where it can be noticed that the magnitude of the velocity is almost three orders of magnitude higher than the physiological case. The explanation of this trend can be found in the fact that the occlusion is acoustically correspondent to a hard sound boundary. When a propagating wave reaches a hard boundary, it doesn't further propagate downstream but is instead reflected upstream. In this way, air is forced to interact with the walls determining an increment of pressure which in turn causes a higher wall radial velocity.

6.4   <u>Limitations of the Model</u>

Although the work presented in this thesis tried to be as comprehensive and precise as possible, the nature itself of the process of modeling implies the introduction of some assumptions and simplifications. A model is generally a trade-off between the possibility to accurately describe the phenomena of interest and the necessity to obtain results in a reasonable computational time.

Two main categories of limitations can be recognized in the adopted model: one related to the generation of the geometry and one related to the acoustic simulations themselves. In terms of geometry, the tracheobronchial tree analyzed was composed of 108 segments only. This is obviously a relevant simplification as far as the complexity of the geometry is concerned. In MATLAB, every segment was approximated with a perfectly cylindrical tube without considering the physiological tempering of the airways. In COMSOL, to generate the cross-section of the branches, a gradual and constant reduction from the maximum proximal value to the minimum distal one was assumed. Although unavoidable to obtain a mesh for the successive computation, this generated geometry only partially resembling the physiological changes in cross-section of the human airways. Furthermore, in both the 1D geometry used in MATLAB and the 3D geometry in COMSOL, the segments modelling the airways were assumed to be completely straight. The

generation of more consistent geometries between MATLAB and COMSOL Multiphysics®
would have probably further reduced the error in the validation of the model. In addition to that,
the minimum value of the thickness was imposed to be relatively high (500 micrometers) to be
able to generate a mesh for the numerical simulation composed of reasonable number of elements.
The limitation on the minimum value of the thickness allowed also to avoid to have elements in
the numerical simulations which were too small, further reducing the time necessary for the
simulations.

As far as the analytic acoustic simulations are concerned, a main limitation is the
assumption regarding soft tissue and cartilage having the same material properties and
consequently considering the wall of the airways to be composed of soft tissue only. The
introduction of the cartilage is expected to have a significant impact on the magnitude of the wall
radial velocity, whereas the effect on the acoustic pressure itself could possibly be less pronounced.
One final remark should be done on the simulation of the pathologies. It is understood that in this
dissertation only some aspects of the mentioned disease or pathological conditions were
considered. This can barely simulate the complexity of the morphometrical, biological and
mechanical alterations generally associated with the clinical picture of a respiratory disease. In
addition to that, the quantification in terms of mechanical and structural chances induced by the
pathology is extremely poorly analyzed in literature and subjected to a remarkable inter-studies
variability.

6.5   <u>Conclusions</u>

The model validated and used in this thesis has been proven to effectively and accurately describe
the acoustic response of the human tracheobronchial tree to a known input acoustic pressure over

a defined frequency range (from 200 Hz to 800 Hz). Despite the limitations described in the previous section, this model provides a significant insight to the acoustic properties of the airways and to the alterations induced by some pathological conditions. In addition to that, it should be considered that the computational time of the analytical code in MATLAB is around 7.16 seconds, visualization included, for a multifrequency analysis. This value assumes even more significance if compared to the finite element method simulations where, to obtain result for frequencies ranged from 200 Hz to 800 Hz, more than one hour is required. The potential application of such a model are countless from both a clinical and a research point of view. In a long-term perspective, this model might eventually support clinicians in their everyday practice of diagnosis providing a useful and immediate comparison with the auscultation technique. As a more short-term goal, this model could be compared and used in association with elastography imaging techniques based on, for example, laser vibrometry and magnetic resonance elastography to provide quantitative information regarding both the physiological and pathological conditions of the respiratory system.

6.6 <u>Future Directions</u>

The analysis of the acoustics of the respiratory tract and the study of the pathology-induced alterations is still an open research field. In the first place, there is an impelling necessity of collecting data regarding the mechanical properties of the constituent materials of the airways wall tissue especially in terms of their modification in response to the pathology. Several experiments can be conducted with the goal of collecting this information such as Scanning Laser Doppler Vibrometry (SLDV) and *ex-vivo* mechanical characterization via tension/compression tests as well as creep/recovery simulations. In addition to that, the new emerging field of Magnetic Resonance Elastography (MRE) could be useful this first objective. Once the data regarding the tissue

mechanics have been collected, they can be easily introduced in the analytical model to enhance the precision of its predictions. This data must be coupled with the introduction of a more physiological based structure of the airways wall where also the cartilage content is considered: this should be done at least for the first 16 generations of the tracheobronchial tree where the cartilage fraction cannot be neglected. The new model should be than revalidated not only numerically but also experimentally via SLDV and MRE. One further step toward a possible and ambitious clinical application would be a radical change of perspective in terms of input of the model: the input is to be modified from a chosen pressure at the inlet of the trachea to the physiological (or pathological) breath sounds which generation occurs inside the tracheobronchial tree. Finally, to be comparable with the auscultation technique the model should extended to account for the surrounding lung structure and the coupling with the chest surface.

APPENDIX

<u>Comparison between the results of Royston et Al. [6] and Jackson et Al. [3]</u>.

The inversion and rearrangement of equation (2.45) leads to

$$Z_T^{(n)}[\omega]\frac{P_{in}^{(n)}[\omega]}{P_T^{(n)}[\omega]} = \frac{Z_{in}^{(n)}[\omega]\left(Z_T^{(n)}[\omega]sinh\left(\gamma_0^{(n)}[\omega]l^{(n)}\right) + Z_0^{(n)}[\omega]\cosh\left(\gamma_0^{(n)}[\omega]l^{(n)}\right)\right)}{Z_0^{(n)}[\omega]}$$

By introducing the definition of $Z_{in}^{(n)}[\omega]$ according to
(2.30) in the equation above the following system is obtained.

$$\begin{cases} Z_T^{(n)}[\omega]\dfrac{P_{in}^{(n)}[\omega]}{P_T^{(n)}[\omega]} = \dfrac{Z_{in}^{(n)}[\omega]\left(Z_T^{(n)}[\omega]sinh\left(\gamma_0^{(n)}[\omega]l^{(n)}\right) + Z_0^{(n)}[\omega]\cosh\left(\gamma_0^{(n)}[\omega]l^{(n)}\right)\right)}{Z_0^{(n)}[\omega]} \\ Z_{in}^{(n)}[\omega] = \dfrac{Z_T^{(n)}[\omega]cosh(\gamma_0^{(n)}[\omega]l^{(n)}) + Z_0^{(n)}[\omega]sinh(\gamma_0^{(n)}[\omega]l^{(n)})}{cosh(\gamma_0^{(n)}[\omega]l^{(n)}) + \left(Z_T^{(n)}[\omega]/Z_0^{(n)}[\omega]\right)sinh(\gamma_0^{(n)}[\omega]l^{(n)})} \end{cases}$$

By solving

$$Z_T^{(n)}[\omega]\frac{P_{in}^{(n)}[\omega]}{P_T^{(n)}[\omega]} = \frac{\left(\frac{Z_T^{(n)}[\omega]\cosh\left(\gamma_0^{(n)}[\omega]l^{(n)}\right)+Z_0^{(n)}[\omega]\sinh\left(\gamma_0^{(n)}[\omega]l^{(n)}\right)}{\cosh\left(\gamma_0^{(n)}[\omega]l^{(n)}\right)+\left(Z_T^{(n)}[\omega]/Z_0^{(n)}[\omega]\right)\sinh\left(\gamma_0^{(n)}[\omega]l^{(n)}\right)}\right)\left(Z_T^{(n)}[\omega]\sinh\left(\gamma_0^{(n)}[\omega]l^{(n)}\right)+Z_0^{(n)}[\omega]\cosh\left(\gamma_0^{(n)}[\omega]l^{(n)}\right)\right)}{Z_0^{(n)}[\omega]} =$$

$$\frac{Z_T^{2(n)}[\omega]\cosh\left(\gamma_0^{(n)}[\omega]l^{(n)}\right)\sinh\left(\gamma_0^{(n)}[\omega]l^{(n)}\right)+Z_T^{(n)}[\omega]Z_0^{(n)}[\omega]cosh^2\left(\gamma_0^{(n)}[\omega]l^{(n)}\right)+Z_T^{(n)}[\omega]Z_0^{(n)}[\omega]sinh^2\left(\gamma_0^{(n)}[\omega]l^{(n)}\right)+Z_0^{2(n)}[\omega]\cosh\left(\gamma_0^{(n)}[\omega]l^{(n)}\right)\sinh\left(\gamma_0^{(n)}[\omega]l^{(n)}\right)}{Z_0^{(n)}[\omega]\cosh\left(\gamma_0^{(n)}[\omega]l^{(n)}\right)+Z_T^{(n)}[\omega]\sinh\left(\gamma_0^{(n)}[\omega]l^{(n)}\right)} =$$

$$\frac{Z_T^{(n)}[\omega]\cosh\left(\gamma_0^{(n)}[\omega]l^{(n)}\right)\left(Z_0^{(n)}[\omega]\cosh\left(\gamma_0^{(n)}[\omega]l^{(n)}\right)+Z_T^{(n)}[\omega]\sinh\left(\gamma_0^{(n)}[\omega]l^{(n)}\right)\right)+Z_0^{(n)}[\omega]\sinh\left(\gamma_0^{(n)}[\omega]l^{(n)}\right)\left(Z_0^{(n)}[\omega]\cosh\left(\gamma_0^{(n)}[\omega]l^{(n)}\right)+Z_T^{(n)}[\omega]\sinh\left(\gamma_0^{(n)}[\omega]l^{(n)}\right)\right)}{\left(Z_0^{(n)}[\omega]\cosh\left(\gamma_0^{(n)}[\omega]l^{(n)}\right)+Z_T^{(n)}[\omega]\sinh\left(\gamma_0^{(n)}[\omega]l^{(n)}\right)\right)} =$$

$$Z_T^{(n)}[\omega]cosh(\gamma_0^{(n)}[\omega]l^{(n)}) + sinh(\gamma_0^{(n)}[\omega]l^{(n)})\,Z_0^{(n)}[\omega]$$

APPENDIX (continued)

The result is indeed the same of the rearranged equation for $P_{rat}^{(n)}[\omega]$ by Jackson and Al.

Analogous computation can be performed starting from equation (2.44) leading to the same solution.

CITED LITERATURE

[1]   K. Horsfield, "Morphometry of airways," *Handb. Physiol.*, no. 78, pp. 75–88.

[2]   G. R. Wodicka, K. N. Stevens, H. L. Golup, E. G. Cravalho, and D. C. Shannon, "A Model of Acoustic Transmission in the Respiratory System," vol. 36, no. 9, 1989.

[3]   A. C. Jackson, B. Suki, M. Ucar, and Hab, "Branching airway network models for analyzing high-frequency lung input impedance," *Am. Physiol. Soc.*, 1993.

[4]   A. C. Jackson, R. H. Habib, B. Suki, S. A. Wood, and W. Mitzner, "Serial distribution of airway diameters from input impedance and computed tomography," *Ann. Biomed. Eng.*, vol. 23, no. 6, pp. 740–749, 1995.

[5]   R. H. Habib, R. B. Chalker, B. Suki, and A. C. Jackson, "Airway Geometry and Wall Mechanical Properties Estimated from Subglottal Input Impedance in Humans," *J. Appl. Physiol.*, vol. 77, pp. 441–451, 1994.

[6]   T. J. Royston, S. Acikgoz, M. B. Ozer, H. a. Mansy, and R. H. Sandler, "Advances in Computational Modeling of Sound Propagation in the Lungs and Torso with Diagnostic Applications," *Biomed. Appl. Vib. Acoust. Ther. Bioeffect Model.*, p. 32, 2008.

[7]   Z. Dai, "The Audible Human Project: Modeling Sound Transmission in the Lungs and Torso," 2013.

[8]   Z. Dai, Y. Peng, H. A. Mansy, R. H. Sandler, and T. J. Royston, "Experimental and computational studies of sound transmission in a branching airway network embedded in a compliant viscoelastic medium," *J. Sound Vib.*, vol. 339, pp. 215–229, 2015.

[9]   B. Henry and T. J. Royston, "A Multiscale Image-Based Computational Model of Pulmonary Airway Acoustics," *J. Acoust. Soc. Am* .(in review).

[10]   D. U. Silverthorn, *Human Physiology - An integrated approach*. 2010.

[11]   M. Thiriet, *Anatomy and Physiology of the Circulatory and Ventilatory Systems*. 2013.

[12]   S. Standring, *Gray's Anatomy - 41st Edition*. 2015.

[13]   M. S. Kavuru, A. C. Mehta, and J. F. T. Jr, "Applied Anatomy of the Neck," no. February, pp. 1–4, 2012.

[14]   P. M. Boiselle and D. A. Lynch, *CT of the Airways*.

CITED LITERATURE (continued)

[15] B. T. Finucane, B. C. H. Tsui, and A. H. Santora, *Principles of Airway Management, 4th Ed*, vol. 82, no. 6. 1996.

[16] J.A Verschakelen, *Computed Tomography of the Lung*. 2010.

[17] E. A. Gabriel and T. Salerno, *Principles of Pulmonary Protection in Heart Surgery*. .

[18] J. H. Bates, *Lungs Mechanics*. 2009.

[19] S. Yim Yeh and R. Schwartzstein, "Asthma: Pathophysiology and Diagnosis," in *Asthma, Health and Society A Public Health Perspective*, 2010.

[20] T. R. Bai and D. A. Knight, "Structural changes in the airways in asthma: observations and consequences.," *Clin. Sci. (Lond).*, vol. 108, no. 6, pp. 463–77, 2005.

[21] T. R. Bai, J. Cooper, T. I. M. Koelmeyer, P. D. Paré, and T. D. Weir, "The Effect of Age and Duration of Disease on Airway Structure in Fatal Asthma," vol. 162, pp. 663–669, 2000.

[22] S. Godfrey, "Asthma and COPD," *Asthma COPD*, pp. 699–711, 2002.

[23] A. Cancellieri, G. Dalpiaz, M. Maffessanti, A. Pesci, R. Polverosi, and M. Zompatori, *Diffuse Lung Disease: Clinical Features, Pathology, HRCT*. 2006.

[24] G. Maloney, E. Anderson, and D. M. Yealy, "Pneumonia and Pulmonary Infiltrates," in *Tintinalli's Emergency Medicine: A Comprehensive Study Guide, 8e*, J. E. Tintinalli, J. S. Stapczynski, O. J. Ma, D. M. Yealy, G. D. Meckler, and D. M. Cline, Eds. New York, NY: McGraw-Hill Education, 2016.

[25] J. Ribeiro and B. Fisher, "Eosinophilic Lung Desease," *Pediatr. Respir. Rev.*, vol. 3, pp. 278–284, 2002.

[26] a Siddiqui and S. Ahmed, "Pulmonary manifestations of sickle cell disease," *Postgrad. Med. J.*, vol. 79, no. 933, pp. 384–390, 2003.

[27] M. Bahoura, "Pattern recognition methods applied to respiratory sounds classification into normal and wheeze classes," *Comput. Biol. Med.*, vol. 39, no. 9, pp. 824–843, 2009.

[28] S. Reichert, R. Gass, C. Brandt, and E. Andrès, "Analysis of respiratory sounds: state of the art.," *Clin. Med. Circ. Respirat. Pulm. Med.*, vol. 2, pp. 45–58, 2008.

CITED LITERATURE (continued)

[29] P. Piirila and A. R. A. Sovijarvi, "Crackles: Recording, analysis and clinical significance," *Eur. Respir. J.*, vol. 8, no. 12, pp. 2139–2148, 1995.

[30] J. Fredberg and S. Holford, "Discrete lung sounds: crackles (rales) as stress-relaxation quadrupoles.," *J. Acoust. Soc. Am.*, vol. 73, pp. 1036–1046, 1983.

[31] B. A. Reyes, S. Charleston-Villalobos, R. Gonzalez-Camarena, and T. Aljama-Corrales, "Analysis of discontinuous adventitious lung sounds by Hilbert-Huang spectrum.," *Annu. Int. Conf. IEEE Eng. Med. Biol. Soc.*, vol. 2008, pp. 3620–3, 2008.

[32] A. Bohadana, G. Izbicki, and S. S. Kraman, "Fundamentals of lung auscultation.," *N. Engl. J. Med.*, vol. 370, no. 8, pp. 744–51, 2014.

[33] Z. Wang, S. Jean, and T. Bartter, "Lung sound analysis in the diagnosis of obstructive airway disease," *Respiration*, vol. 77, no. 2, pp. 134–138, 2009.

[34] H. Pasterkamp, S. S. Kraman, and G. R. Wodicka, "State of the Art Advances Beyond the Stethoscope," *Am. J. Respir. Crit. Care Med.*, vol. 156, no. 3, pp. 974–987, 1997.

[35] S. A. Taplidou and L. J. Hadjileontiadis, "Wheeze detection based on time-frequency analysis of breath sounds," *Comput. Biol. Med.*, vol. 37, no. 8, pp. 1073–1083, 2007.

[36] P. Forgacs, *Lung Sounds*. 1978.

[37] A. H. Benade, "On the propagation of sound waves in a cylindrical conduit," *J. Acoust. Soc. Am.*, vol. 44, no. 2, pp. 616–623, 1968.

[38] R. H. Habib, B. Suki, J. H. Bates, and A. C. Jackson, "Serial Distribution of Airway Mechanical Properties in Dogs: Effects of Histamine," *J. Appl. Physiol.*, vol. 77, pp. 554–566, 1994.

[39] A. B. Dubois, A. W. Brody, D. H. Lewis, and B. F. J. Burgess, "Oscillation mechanics of lungs and chest in man," *J. Appl. Physiol.*, vol. 8, pp. 587–594, 1956.

[40] J. J. Fredberg and J. A. Moore, "Distributed Response of Complex Branching Networks," *J. Acoust. Soc. Am.*, vol. 63, pp. 954–961, 1978.

[41] S. Miyawaki, M. H. Tawhai, E. A. Hoffman, S. E. Wenzel, and C.-L. Lin, "Automatic construction of subject-specific human airway geometry including trifurcations based on a CT-segmented airway skeleton and surface," *Biomech. Model. Mechanobiol.*, 2016.

[42] P. Harper, S. S. Kraman, H. Pasterkamp, and G. R. Wodicka, "An acoustic model of the respiratory tract.," *IEEE Trans. Biomed. Eng.*, vol. 48, no. 5, pp. 543–550, 2001.

CITED LITERATURE (continued)

[43] C. M. Ionescu, P. Segers, and R. De Keyser, "Mechanical properties of the respiratory system derived from morphologic insight," *IEEE Trans. Biomed. Eng.*, vol. 56, no. 4, pp. 949–959, 2009.

[44] R. W. Guelke and A. E. Bunn, "Trasmission Line Theory applied to Sound Wave Propagation in Tubes with Compliant Walls," *Acustica*, vol. 48, pp. 101–107, 1981.

VITA

NAME   Lorenzo Aliboni

EDUCATION   B.S. in Biomedical Engineering, Politecnico di Milano, Milan, Italy, 2015

                             Secondary School Degree, Liceo Scientifico Leonardo da Vinci, Milan, Italy, 2012

RESEARCH EXPERIENCE   01/2017-05/2017 Research Assistant in the Acoustics and Vibrations Laboratory at University of Illinois at Chicago

                             02/2015-08/2015 Activity in the Laboratory of Biomechanics and Biomaterials at Politecnico di Milano

                             02/2014-09/2014 Activity in the Novel, Emerging Computing System Technologies Laboratory (NECST) at Politecnico di Milano